Technische Universität Berlin

Open-Source Modeling of Flow Based Market Coupling:

Methods, Parametrization, and Analysis for Sustainable Power Systems

vorgelegt von
M. Sc.
Richard Weinhold
ORCID: 0000-0001-8741-2830

an der Fakultät VII – Wirtschaft und Management
der Technischen Universität Berlin
zur Erlangung des akademischen Grades

Doktor der Ingenieurwissenschaften
— Dr. Ing. —

genehmigte Dissertation

Promotionsausschuss:

Vorsitzender:	Prof. Dr. Georg Meran (TU Berlin)
Gutachter:	Prof. Dr. Christian von Hirschhausen (TU Berlin)
Gutachter:	Prof. Dr. Yury Dvorkin (New York University)
Gutachter:	Prof. Dr. Hannes Weigt (Universität Basel)

Tag der wissenschaftlichen Aussprache: 3. Dezember 2021

Berlin 2022

Abstract

In modern electricity systems the provision of electricity goes far beyond the mandatory electrical engineering, but instead means providing equivalent reliability and affordability while making the electricity system sustainable. The pathway to a fully decarbonized electricity system requires continuous improvement in market design to accommodate this transformation. Within the European internal energy market for electricity, methods for capacity allocation and congestion management coordinate transmission system operators, power exchanges, generators and consumers for efficient use of transmission infrastructure. As part of the transformation, these methods have to meet high standards defined by the large system size and increasing complexity and dynamic of the generation infrastructure. Flow-based market coupling represents a more dynamic and accurate method for capacity allocation, that is based on network models and forecasted market data, and promises to satisfy the requirements for future electricity markets.

This thesis provides a comprehensive analysis of flow-based market coupling and proposes an open-source electricity market model to facilitate numerical experiments on market design effectiveness.

Part I covers the origin of the European internal market for electricity and highlights the main drivers and considerations that lead to the inauguration of flow-based market coupling and the current market structure. The methods used in this thesis and the academic context are introduced and discussed.

Part II describes the methods that are developed as part of this thesis to model flow-based market coupling. The proposed open-source power market tool (POMATO) is based on fundamental methods of Operations Research and electrical engineering and provide a transparent and accessible tool for research on electricity markets and flow-based market coupling.

Part III includes three applications that enhance the understanding of flow-based market coupling, by evaluating parameter choices and methods, and investigate its efficiency with high shares of intermittent renewable generation. Particularly, the ability of flow-based market coupling to accommodate policy relevant consideration in order to better

integrate renewable energy sources in the system are discussed.

Flow-based market coupling represents an improvement over static methods for capacity allocation in different ways. The process's ability to implicitly consider all transactions simultaneously based on detailed network and generation forecasts provides measurable improvements to the market design. While the process is inherently more transparent it is also more complex and therefore requires careful parametrization. The applications in this thesis follow a proposed nominal parametrization that in combination with the open-data principles can provide a sustainable basis for future research.

Keywords: Flow-based market coupling; renewable energy sources; electricity market design; congestion management; capacity allocation; power systems modeling; optimal power flow; security constrained optimal power flow; uncertainty; open source

Zusammenfassung

In modernen Stromsystemen gehen die Herausforderungen beim Bereitstellen von Strom weit über elektrotechnische Fertigkeiten hinaus – vielmehr müssen höhere Nachhaltigkeitsstandards bei gleicher Preisgünstigkeit und Versorgungssicherheit erreicht werden. Der Weg zu einem vollständig dekarbonisierten Stromsystem erfordert eine kontinuierliche Weiterentwicklung des Marktdesigns, das diese Transformation abbilden muss.
Kern des europäischen Energiebinnenmarkts für Elektrizität sind Methoden für Kapazitätsvergabe und Engpassmanagement. Diese haben den Zweck, Übertragungsnetzbetreiber, Strombörsen, Erzeuger und Verbraucher im Hinblick auf eine effiziente Nutzung der Übertragungsinfrastruktur zu koordinieren. Als Teil der Energiewende müssen diese Methoden hohen Standards genügen, die vor allem durch die Größe des Systems und die zunehmende Komplexität und Dynamik der Erzeugungsinfrastruktur definiert sind. Die flow-based market coupling (zu deutsch (last-) flussbasierte Marktkopplung) stellt gegenüber bestehenden Methoden eine dynamischere und genauere Methode für die Kapazitätszuweisung dar, da sie auf Netzmodellen und prognostizierten Marktdaten basiert und dadurch den stetig steigenden Anforderungen entspricht. Diese Arbeit bietet eine umfassende Behandlung von flow-based market coupling und stellt ein Open-Source-Strommarktmodell vor, das die Komplexität des Prozesses adäquat abbildet und quantitative Forschung zur Effektivität des Marktdesigns gemäß Open-Source-Grundsätzen ermöglicht.
Teil I gibt einen Überblick über die Entstehung des europäischen Energiebinnenmarkts für Elektrizität. Die Umstände und die Motivation werden dargestellt, die zur Einführung von flow-based market coupling und der aktuellen Marktstruktur geführt haben. Außerdem beinhaltet dieser Teil eine Einführung und Beschreibung der in dieser Arbeit verwendeten Methoden und der akademische Zusammenhang mit weiteren Publikationen im Rahmen des Forschungsbereichs werden dargestellt und diskutiert.
Teil II beschreibt die Methoden, die im Rahmen dieser Arbeit zur Modellierung der flow-based market coupling entwickelt werden. Hierbei handelt es sich um Methoden zur Berücksichtigung von Stromflüssen unter ungeplanten Leitungsausfällen und der Model-

lierung von Strommärkten. Diese – auf Basis der Forschungsbereiche Operations Research und Elektrotechnik entwickelten – Methoden sind Teil des unter Open-Source-Lizenz veröffentlichten Strommarktmodells "POMATO". POMATO stellt ein transparentes und zugängliches Werkzeug für die Forschung und die Evaluierung von Strommärkten dar und erlaubt eine detaillierte Abbildung von flow-based market coupling.
Teil III enthält drei Anwendungen, die zum Verständnis der flow-based market coupling beitragen. In den drei Publikationen dieses Teils wird die Wahl von Parametern und Methoden im Hinblick auf die Effizienz von flow-based market coupling bewertet und die Kompatibilität des Prozesses mit hohen Anteilen erneuerbarer Energien überprüft. Insbesondere die Aspekte in der Parametrisierung von flow-based market coupling, die die Berücksichtigung von regulatorischen Überlegungen zur Integration von erneuerbaren Energien erlauben, werden dargelegt und diskutiert.
Flow-based market coupling stellt in verschiedener Hinsicht eine Verbesserung gegenüber statischen Methoden der Kapazitätszuweisung dar. Die Fähigkeit des Prozesses, implizit alle Transaktionen gleichzeitig auf der Grundlage detaillierter Netz- und Erzeugungsprognosen zu berücksichtigen, stellt quantifizierbare Verbesserungen für das Marktdesign dar. Obwohl der Prozess inhärent transparent ist, erfordert jedoch die erhöhte Komplexität eine sorgfältige Parametrisierung. Die Anwendungen in dieser Arbeit bieten neben den entwickelten Methoden eine nominale Parametrisierung, die als Grundlage für folgende Arbeiten dienen kann und die Vergleichbarkeit gewährleistet. In Kombination mit der Veröffentlichung sowohl der Methoden als auch der Daten nach Open-Source-Grundsätzen kann diese Arbeit eine nachhaltige Basis für zukünftige Forschung bieten.

Acknowledgments

This dissertation would not have been possible without the many friends and colleagues and their input, feedback, encouragement and support. I want to thank my supervisor Prof. Christian von Hirschhausen who has not only introduced me to the field but always encouraged me to explore the topics on my own terms. It was a pretty amazing journey from one of the first *EW2a* lectures, where Prof. von Hirschhausen explained Kirchhoff's Laws by walking up and down the stairs in the classroom, to panel discussions with the Green Party and excursions into the *Asse II* mine.

While Prof. von Hirschhausen certainly enabled my academic journey, I shared most, if no all, of it with Robert Mieth. Robert has contributed to my research and this dissertation as a fantastic colleague and to my mental well being as good friend. His disregard for my physical well-being during risky explorations in the Arizona desert can be excused as I am very grateful for his company. I want to thank my colleagues at the Workgroup for Infrastructure Policy Christoph, Jens, Leonard and Mario for their insights, feedback and friendship. I really miss the our office H3144, while its a messy chaos for some – I think its a (modelling) palace and we will hopefully return soon.

Research on flow-based market coupling presented many challenges to me and I faced a steep learning curve. Thankfully, I had the opportunity to work with David Schönheit and Constantin Dierstein who have helped me to better understand the topic at hand. I also had the pleasure to supervise Richard Hauschild in his thesis that has actively contributed to this dissertation. I want to thank the Danish Energy Agency and my fantastic colleagues Thorbjørn, Ulrik, Matteo, Morten and Jonatan. It was Thorbjørn who has started me on the topic of flow-based market coupling and I am grateful for the arrangement that allowed me to pursue my PhD.

Lastly, I am eternally grateful for the incredible patience and amazing support and assistance I received from Maja over the past years, keeping me sane and happy which is all anybody would ever need.

Overview

Contents

List of Figures

List of Tables

List of Acronyms

AC . . . . . alternating current

ACER . . . . . European Agency for the Cooperation of Energy Regulators

ADMM . . . . . Alternating Direction Method of Multipliers

ANOVA . . . . . analysis of variance

ATC . . . . . available transfer capacity

CA . . . . . capacity allocation

CACM . . . . . capacity allocation and congestion management

CB . . . . . critical branch

CBCO . . . . . critical branch under critical outage

CEE . . . . . Central Eastern Europe

CM . . . . . congestion management

CNE . . . . . critical network element

CNEC . . . . . critical network element and contingency

CO . . . . . critical outage

CORE . . . . . CORE region

CWE . . . . . Central Western Europe

D2CF . . . . . 2-days ahead congestion forecast

DCPF . . . . . linear power flow

DSK . . . . . demand shift key

ED . . . . . economic dispatch

EUPHEMIA . . Pan-European Hybrid Electricity Market Integration Algorithm

FAV . . . . . final adjustment value

FBA . . . . . flow-based allocation

FBMC . . . . . flow-based market coupling

FfE . . . . . Forschungsstelle für Energie

FRM . . . . . flow reliability margin

GSK . . . . . generation shift key

HVDC . . . . . high-voltage direct-current

IEM . . . . . internal energy market

ISK . . . . . injection shift key

JAO . . . . . Joint Allocation Office

LODF . . . . . load outage distribution factor

LP . . . . . linear program

minRAM . . . . minimum remaining available margin

NTC . . . . . net transfer capacity

NUTS . . . . . Nomenclature of Territorial Units for Statistics

OPF . . . . . optimal power flow

OR . . . . . Operations Research

OTC . . . . . over-the-counter

PCR . . . . . Price Coupling of Regions

POMATO . . . . Power Market Tool

PTDF . . . . . power transmission distribution factor

PV . . . . . photovoltaik

PX . . . . . power exchange

RAM . . . . . remaining available margin

RES . . . . . renewable energy sources

SCOPF . . . . . security-constrained optimal power flow

TSO . . . . . transmission system operator

Part I

Introduction

Chapter 1

Zonal Electricity Markets and Flow-Based Market Coupling

"To crush your enemies, to see them driven before you, and to hear the lamentations about inefficiencies in zonal market coupling".

(Conan the Barbarian)

1.1 Motivation

This dissertation is a product of my years working at the Workgroup for Infrastructure Policy (WIP) and the ability to explore, understand, and work on different topics with many interesting people. Much of the motivation to contribute to the field of electricity economics stems from this, for me, productive environment. My first research efforts, together with my colleague Robert Mieth, were fueled by obscure panel discussions in the Bavarian hinterland and its Ministry for Economy, resulted in a publication (Mieth et al. 2015) and a snappy blog entry[1] that made the rudimentary point that when planning with more than 10 GW of lignite in the 2030 German electricity system, you are really getting the transmission system you deserve rather than the one you want. From the experience of participating in public, political, and academic discussions I learned that the transformation of the electricity system that is required in order to reach climate targets cannot be treated as a one-dimensional discipline. While technology plays a crucial role, reaching the goals of national and international climate agreements is not solely an engineering problem. In fact, in many studies we argue that a largely renewable-based energy system is not only possible but also efficient, using technologies that we have available today (Hainsch et al. 2020; Kendziorski et al. 2021). By that standard, the energy transformation is mostly an organizational effort instead of an engineering problem. A solution lies in the connection of politics, economy, technical ingenuity, and the application in everyday social life. Among many important means of communication, that form the interface between these components are quantitative methods that aim to *"serve to help answer questions on energy policy, decarbonization, and transitions towards renewable energy sources".*[2]

The beauty of conveying issues of energy markets with optimization problems is that the formulation is inherently transparent by using a general mathematical formalism. An example that we use in our lectures on modeling energy markets is Ehrenmann and Smeers (2005) that by a very simple model setup illustrates complex consideration of electricity market design.

However, more recent model applications are significantly more complex due to more meticulous formulations or larger scopes. Both inhibit transparency since the modeled causalities are less immediate, recalculation requires complex data-sets or significant computational power. Overall, the required work to turn a formal description into a

[1] See: https://energie-klimaschutz.de/neue-praemissen-netzplanung/

[2] See: Manifesto of the Open Energy Modelling Initiative https://openmod-initiative.org/manifesto.html

running model has increased significantly.

Therefore, to maintain the usefulness of research applying quantitative methods and conserve the utility it provides to transforming the energy sector, it does not suffice anymore to simply write down the mathematical formulation of the solved problem. Additional effort is required to enable other researchers or stakeholders to re-run and re-use the analyses and make the methods transparent by accessibility.

In this thesis, I aim to do just that and provide a way to model flow-based market coupling using open methods and open data, in the spirit of the *GNU General Public Licence*, "in the hope that it will be useful".

1.2 Zonal Electricity Markets

The European electricity system is organized as a collection of mostly national bidding zones that are coupled in what is denoted as the internal energy market (IEM) for electricity. The current market design represents over 20 years of development, that aims to actively contribute to the creation of a sustainable energy system while ensuring affordable and secure provision of electricity. The organizational effort to integrate each member state into the IEM is substantial but integral to guarantee fair market access for consumers and generators. A core component is the process of coupling markets, which requires a high level of coordination in terms of the available capacity for the coupling process (capacity allocation) and the operation of infrastructure (congestion management). The current method of flow-based market coupling (FBMC) aims to facilitate the coupling of markets in a transparent and efficient manner and is subject of this thesis. This introduction highlights the general development of the European IEM, illustrates the significance of cross-zonal exchange and introduces the involved parties. I want to highlight the motivation of these parties to propose FBMC as the target method for capacity allocation and congestion management and how recently, as part of the Clean Energy Package (Directorate General for Energy 2019), the regulatory process started to engage more directly with these methods.

Before the market liberalisation, electricity supply was characterized as a service that was provided by regulated regional monopolies, often vertically integrated utilities. The introduction of the IEM defined electricity as an economic good, and therefore the IEM should, as any other market, be open for generators and consumers. For consumers, this meant an open choice of supplier and for generators, this meant guaranteed access to the network. One immediate requirement was the unbundling of generation and network.

Generally, the directives define, in what is often denoted as a "top-down" process (Meeus, Purchala, and Belmans 2005; Weigt 2009), the conditions that the IEM has to suffice, but do not design the market itself. The heterogeneous characteristics of the existing electricity markets required the directives to leave member states a large degree of freedom on the implementation, as they posed significant changes to existing market structures. Therefore, the market liberalization is an iterative process over multiple years, mainly the first three energy packages 1996, 2003, and 2009, in which the process was monitored and evaluated according to the core principles of the IEM and the energy policy triangle of security of supply, sustainability, and affordability. While the first iterations only consisted of basic rules and guidelines, the regulation process would quickly define more specific solutions based on regional implementations that proved to be efficient. This is sometimes described as "experimentalist policymaking" that actively encourages developments from the involved parties (Rangoni 2016) or as a "funnel concept" (Consentec 2007) that converges to a target model based on iterative improvements to the IEM. Ultimately, this process spawned power exchanges (PXs) in most member states, providing a means to balance market participant's positions in a short term market alongside one or multiple dedicated transmission system operators (TSOs) accommodating the market outcome in the network and European Agency for the Cooperation of Energy Regulators (ACER) as an independent institution to coordinate and foster the development of the IEM.

For this thesis two things are of great importance. First, the position of each member state is very pronounced, defining the IEM as a decentralized collection of national markets rather than a single, centralized market for electricity (Glachant 2010). Second, due to the pre-liberalized market structure, national networks were much stronger than cross-border connections, which were mainly created to achieve higher levels of reliability and security (Consentec and Institute of Power Systems and Power Economics of Aachen University of Technology 2001), resulting in a market design that mostly disregards intra-zonal connections and where inter-zonal connections were very limited. While commercial exchange was not explicitly part of the first energy package (European Commission 1997) and therefore no harmonized process was in place, the negative impact on IEM's efficiency from insufficient cross-border capacities and inefficient capacity allocation was quickly identified (Meeus and Belmans 2008). Therefore, the inefficiencies do not only result from limited infrastructure but also are problems of institutional and organizational nature that are of importance to the topic of this thesis.

The process of capacity allocation describes how transmission capacities are made

available to the markets. In the early stages of the IEM capacity allocation was considered a form of congestion management, as constraining exchange prevented overuse of the transmission system. Later the two terms are more explicitly separated and congestion management is understood as methods to remedy overloaded transmission infrastructure. For capacity allocation, the system's transport capacity is subsumed for each border as so-called available transfer capacities (ATCs) from which the net transfer capacities (NTCs) is derived, aiming to describe the bi-directional exchange capacities between two market areas (ETSO 2000). It is important to also differentiate the type of trades affected by this, which can be categorized in long-term, non-standardized bilateral contracts denoted as over-the-counter (OTC) transactions and standardized long- and short-term trades facilitated by PXs. Cross-border exchange was procured solely by TSOs and required explicitly allocated capacities for any cross-border transactions, which means that cross-border exchange of energy needs to explicitly acquire or reserve the corresponding transmission capacity. Most transactions were traded OTC and due to the long-term nature of these contracts, the capacity was often allocated inefficiently, meaning reserved for transactions that did not reflect the economic sensible direction (Glachant and Lévêque 2006) or maintained an arbitrage between market areas even in unconstrained cases (De Jonghe, Meeus, and Belmans 2008). Secondly, the static nature of NTCs — at the early stages NTC values were updated bi-annually — meant that capacity was often not reflecting the actual system state. And finally, allocating capacity to long-term contracts could prevent capacity allocation to pooled short-term markets (Glachant and Lévêque 2006) that usually set and broadcast prices (Boisseleau 2004). To address these shortcomings, both the way capacity is allocated to the markets and the way this capacity was calculated or set were targets of improvements.

To address the "allocation", implicit allocation of transmission capacities can be introduced to allocate cross-border exchange energy and transmission capacity simultaneously. This does however require coupling of the affected markets, which means the involvement of PXs in the capacity allocation process in an important role to communicate prices and quantities (Meeus et al. 2009). While providing the necessary benefits for short-term markets, the additional organizational aspects, especially in a decentralized market structure were identified as challenges (Consentec and Frontier Economics 2004).

Among market coupling with implicit auctions, nodal markets and zonal market with market splitting, as practiced in Scandinavia, were avidly discussed as methods for congestion management. Nodal pricing integrates the transmission system into the market clearing process and is the economic first best solution (Ehrenmann and Smeers 2005),

as it co-optimizes transmission- and generation resources and does not solely rely on congestion management to ensure operability of the transmission system. In addition to the economic efficiency, locational marginal pricing can provide efficient investment incentives (Brunekreeft, Neuhoff, and Newbery 2005). For the IEM, nodal pricing would require market clearing utilities integrating TSOs and PXs in either a centralized form, including all European bidding zones, or similar to the independent system operators in the United States, as individual market areas that are coupled along their "seams" (Neuhoff, Hobbs, and Newbery 2011).

The model of the Scandinavian spot market *NordPool*, often denoted as market splitting was considered. The *NordPool* market is organized in a single central PX and countries that are organized in multiple bidding zones. The ability to split a large bidding zone along congestions and specific structure of the Scandinavian transmission system with low interdependency between commercial exchanges ETSO (2001b) made market splitting very effective in the Scandinavian market, but less applicable for the continental European system that is highly mashed. Additionally, the actual reconfiguration proves to be difficult (Bjørndal and Jørnsten 2001).

While many aspects affect the development of the IEM, both alternatives do require a more centralized IEM organization that was not politically feasible or wanted. Brunekreeft, Neuhoff, and Newbery (2005) therefore argue that due to its compatibility with the European system structure a market coupling with implicit auctions should be iteratively introduced. In 2006 under the Trilateral Coupling, the three markets of France, Belgium and the Netherlands were coupled with implicit auctions under common market rules as an initiative of the responsible PXs. Only after the Trilateral Coupling proved to be an improvement to the IEM, implicit capacity allocation was encouraged as part of the regulation (European Commission 2009b) of the third energy package (European Commission 2009a) and the Trilateral Coupling was extended to the Central Western Europe (CWE) region including the German, Austrian, and Luxembourgian bidding zones.

Over the next years, more countries joined the common market under the proposed name Price Coupling of Regions (PCR), which in the 2015 iteration of the energy directive was set the nominal form of market coupling in the IEM. Notably, the process of market coupling remains a mostly decentralized form of market clearing, with member states' ability to individually set regulation, facilitated by national TSOs and PXs and a coordinated form of market coupling in form of the central coupling algorithm Pan-European Hybrid Electricity Market Integration Algorithm (EUPHEMIA) and harmonized rules

for capacity allocation and congestion management.

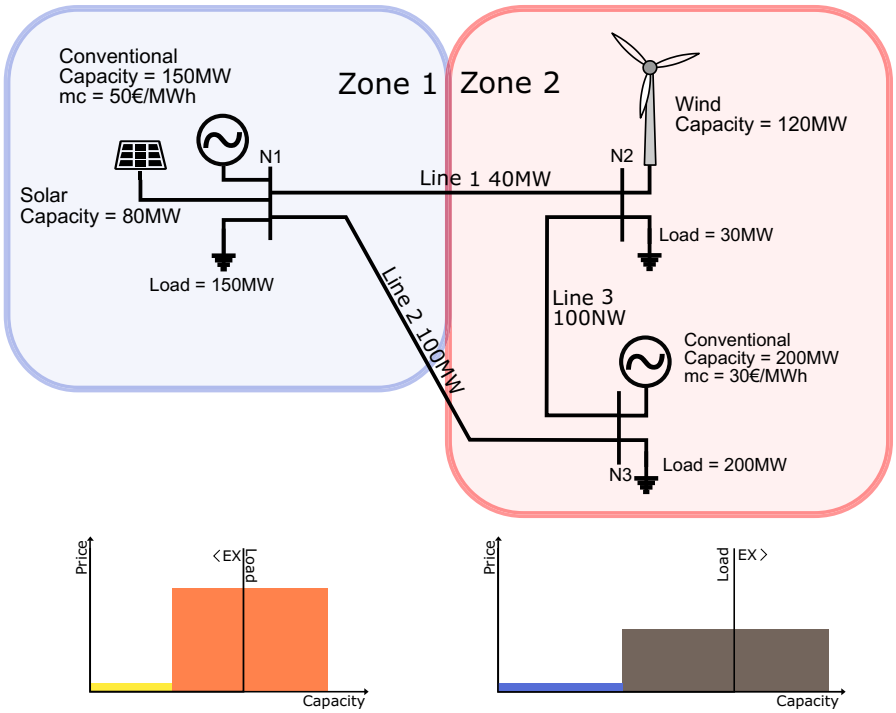

Figure 1.1: Exemplary three-node system with two market areas

Figure 1.1 illustrates the price coupling with implicit auctions. The system is composed of two zones with constant load and the markets are cleared by matching demand and supply bids. Here, two zones are coupled via the PXs in each zone exchanging information about the prices and then coupling the markets based on the available transfer capacity derived by the TSOs. In this case, demand bids in *Zone 1* would be matched by supply bids in *Zone 2*, resulting in a commercial flow from *Zone 1* to *Zone 2*, until no price difference exists or the transfer capacity is fully utilized.

The coupling process through PXs requires transparent communication of available capacities, however, the process of defining exchange capacities has been identified as inefficient very early in the development of the IEM. While NTCs have been updated more frequently and using more complex methods, it was still apparent that a single bilateral value cannot adequately depict the actual cross-border capacity that is in fact dependant on the current system state, other transactions, and the resulting power flows (Consentec 2007). These aspects were addressed by new methods for capacity allocation based on actual power flows and denoted as flow-based allocation (FBA). FBA was first

developed early in the liberalization process (ETSO 2001c; Consentec and Frontier Economics 2004) based on linear power flow considerations in meshed transmission networks and proposed as a target model for market coupling in Consentec (2007) and Vattenfall Europe Transmission GmbH (2009). Renamed as flow-based market coupling (FBMC), the process was further developed in a "dry run" — meaning a non-operational context — in 2008 (Amprion et al. 2011) and validated in a parallel run in 2013 (Rte et al. 2015) as an efficient method for capacity allocation. FBMC and the market coupling process PCR were implemented as the target model for capacity allocation and congestion management in the 2015 iteration of the regulation and has been used in CWE since.

By 2021, most of Europe's day-ahead markets are coupled with the described price-coupling process. With the market structure defined, the regulatory focus moved to the process itself and specifically to its compatibility with environmental policy. While environmental aspects are part of the first energy package (European Commission 1997), establishing market structure remained a priority in the initial iterations. With the Clean Energy Package (Directorate General for Energy 2019) and the accompanying update to the regulation on capacity allocation and congestion management, sustainability became more of a focus with direct regulation of market rules to ensure better integration of renewable energy sources (RES) by enforcing TSOs to attribute more capacity to the markets.

This thesis aims to contribute in three ways: First, representing the process of FBMC in fundamental electricity market models is required to evaluate its efficiency in systems that will change from the status quo—both in terms of installed capacities and transmission infrastructure. This thesis contributes to the field by providing the means of analysis with the creation of an open-source and accessible electricity market model Power Market Tool (POMATO) including new and improved methods to model the technical specifics of the process. Second, model applications evaluate the efficiency of the process itself by establishing analysis on the core parameters and comparing different methods of capacity allocation and congestion management. And third, the compatibility of the process in systems with high shares of intermittent renewable generation is evaluated and discussed in large-scale applications.

The methods derived and applied in this thesis are based on fundamentals of Operations Research (OR) and electrical engineering, specifically, the economic dispatch problem, that is introduced in Section 1.3, and its extension by power flow constrains, denoted as optimal power flow (OPF), described in Section 1.4. The considerations for modeling FBMC are described in Section 1.5, based on the preliminaries on optimization

and power flow.

Section 1.6 enumerates existing literature on FBMC and their contributions to the field to give context to this thesis's contributions. This includes academic publications as well as documentations, reports or white papers of the regulatory body and the involved parties.

The contents of the thesis and the specific contributions to research on zonal electricity markets and FBMC are described in Chapter 1.7, which also discusses the requirement of open methods and open data in the context of quantitative research in this field.

Section 1.8 summarizes the findings and provides avenues for future research.

1.3 Preliminaries on the Economic Dispatch Problem

Modeling electricity markets, such as the spot market component of the IEM in which demand and supply bids are matched, align well with methods of OR. Electricity spot markets are commonly cleared using the merit-order process, in which supply bids are accepted until demand is satisfied and the last accepted bid defines the market price.

Figure 1.2: Combined merit order of exemplary three-node system

Given the example merit-order, collecting generation capacities and loads from both zones of the three-node example in Figure 1.1, shown in Figure 1.2, we can find the most cost-efficient dispatch graphically by accepting bids until the load is satisfied.

This problem can also be solved by formulating a cost-minimizing optimization problem (following the formal description of Luenberger and Ye (2008))

$$\begin{aligned}
\min \quad & f(\boldsymbol{x}) && && \text{(1.1a)}\\
\text{s.t.} \quad & h_i(\boldsymbol{x}) = 0 && \forall i \in \mathcal{I} && \text{(1.1b)}\\
& g_j(\boldsymbol{x}) && \forall j \in \mathcal{J} && \text{(1.1c)}\\
& \boldsymbol{x} \in \mathcal{S} && && \text{(1.1d)}
\end{aligned}$$

where $\boldsymbol{x}$ is an n-dimensional vector of decisions variables that are within a real-valued set $\mathcal{S}$ subject to a set $\mathcal{I}$ of equality- and set $\mathcal{J}$ of inequality constraints that define the feasible region for $\boldsymbol{x}$. The problem finds the optimal solution x^* at which the objective function $f(\boldsymbol{x})$ is minimized within the feasible region.

If all constraints and objective functions remain linear the model can be solved by various solution techniques, for example the simplex algorithm (Dantzig 1963).

Generators $\mathcal{G}$	Cost mc [€/MWh]	Capacity g^{max} [MW]
Solar	0	80
Conventional 1	50	150
Wind	0	120
Conventional 2	30	200

Table 1.1: Capacity and bid data exemplary three-node system

Given the data of the merit-order of Figure 1.2, shown in Table 1.1 and the demand d of 380MW we can formulate the economic dispatch problem analogous to Equation (1.1) as follows:

$$\begin{aligned}
\min \quad & \sum_i mc_i \cdot G_i && && \text{(1.2a)}\\
\text{s.t.} \quad & \sum G = d && && \text{(1.2b)}\\
& G_i \leq g_i^{max} && \forall i \in \mathcal{G} && \text{(1.2c)}\\
& G_i \geq 0 && \forall i \in \mathcal{G} && \text{(1.2d)}
\end{aligned}$$

The problem minimizes the total generation cost such that the sum of generation covers demand and no generator is dispatched above its capacity. Problem (1.2) results in the optimal solution $G^* = \begin{pmatrix} 80 & 0 & 120 & 180 \end{pmatrix}^T$ denoting the cost-optimal dispatch of available generators to cover demand. With no transport constraints present, problem

(1.2) corresponds to a *uniform pricing* market clearing with unrestricted market access for all nodes or zones in the system, resulting in a single market price.

Problem (1.2) can be generalized to model an entire system by including not one but many demand snapshots, adding constraints that model generation or demand in more detail, include uncertainty, differentiate between different market areas or include transport. Note, that in this example it is assumed that generators bid at their true cost, no market power is exerted, and demand is inelastic. Also, the economic dispatch model is a one-shot optimization that implicitly includes futures or OTC transactions in the dispatch decision. These assumptions are common in large-scale model applications as in this thesis or in Leuthold, Weigt, and von Hirschhausen (2012), however, more general model classes allow to model these aspects as well Ventosa et al. (2005).

1.4 Preliminaries on Power Flow

For a system of nodes of set $\mathcal{N}$ that are connected by a set of lines or transformers of set $\mathcal{L}$, the apparent power S injected at node i can be described in relation to the voltage V and voltage-angle difference ϕ to connected nodes $k \in \mathcal{N}$ and the connections' conductance g_{ik} and susceptance b_{ik} as per Equation (1.3) or as per the components of active power (1.4) and reactive power (1.5) (Mieth 2021).

$$S_i = \sum_{k \in \mathcal{N}} V_i V_k (\cos(\phi_i - \phi_k) + j \sin(\phi_i - \phi_k))(g_{ik} - j b_{ik}) \tag{1.3}$$

$$P_i = \sum_{k \in \mathcal{N}} V_i V_k (g_{ik} \cos(\phi_i - \phi_k) + b_{ik} \sin(\phi_i - \phi_k)) \tag{1.4}$$

$$Q_i = \sum_{k \in \mathcal{N}} V_i V_k (g_{ik} \sin(\phi_i - \phi_k) + b_{ik} \cos(\phi_i - \phi_k)). \tag{1.5}$$

These equations, defining alternating current (AC) power flow, are hard to solve as part of optimization problems like (1.2) because of the four decision variables voltage angle, voltage magnitude, active and reactive power injections and their non-linear relation. For techno-economic studies, a linear approximation of the AC power flow equations are often employed to maintain a computationally tractable formulation that remains accurate enough (Van Hertem 2006; Overbye, Cheng, and Sun 2004). These assumptions are:

1. For high voltage transmission lines, resistance is typically much lower than the

reactance ($r \ll x$) and can therefore be neglected: $r \approx 0$ and thus $g \approx 0$.

2. Voltage angle differences $\phi_{ik} = \phi_i - \phi_k$ are typically very small which means $\sin \phi_{ik} \approx \phi_{ik}$.

3. Under normal operation, all voltage magnitudes are close to the nominal system voltage. This can be expressed as $V_i \approx 1$ p.u. (per unit) as a form of standardization of nodal voltages to the respective system voltage (Mieth 2021) and thus $V_i V_k \approx 1$.

Based on these assumptions reactive power is neglected, Equation (1.4) simplifies to (1.6), and the power flow on a line $l \in \mathcal{L}$ between nodes $i, k \in \mathcal{N}$ becomes (1.7).

$$P_i = \sum_{k \in \mathcal{N}} b_{ik}(\phi_i - \phi_k) \tag{1.6}$$

$$P_l = b_{ik}(\phi_i - \phi_k) \tag{1.7}$$

Both can be written in matrix form with $\boldsymbol{B_d}$ being a $\mathcal{L} \times \mathcal{L}$-diagonal matrix with the line susceptances on the diagonal, a column vector of nodal voltage angles $\boldsymbol{\phi}$ and the incidence matrix $\boldsymbol{A}$, which is a $\mathcal{N} \times \mathcal{L}$ matrix where for all $l \in \mathcal{L}$ and $k \in \mathcal{N}$, capturing the topology of the grid:

$$A_{lk} = \begin{cases} 1 & \text{if } k \text{ is start-node of } l \\ -1 & \text{if } k \text{ is end-node of } l \\ 0 & \text{else} \end{cases} \tag{1.8}$$

$$\boldsymbol{P_l} = \boldsymbol{B_d} \cdot \boldsymbol{A} \cdot \boldsymbol{\phi} = \boldsymbol{B_l} \cdot \boldsymbol{\phi} \tag{1.9}$$

$$\boldsymbol{P_n} = \boldsymbol{A^T B_d} \cdot \boldsymbol{A} \cdot \boldsymbol{\phi} = \boldsymbol{B_n} \cdot \boldsymbol{\phi} \tag{1.10}$$

We can derive a node-to-line sensitivity as the ratio between power flow $\boldsymbol{P_l}$ on a line $l \in \mathcal{L}$ and power injection $\boldsymbol{P_n}$ at each node $n \in \mathcal{N}$ and write it in terms of the node susceptance matrix $\boldsymbol{B_n}$ and line susceptance matrix $\boldsymbol{B_l}$. Because power flow is defined by angle differences, we choose a reference node with fixed voltage angle and derive the node-to-line sensitivity for this slack node as

$$\mathbf{PTDF} = \boldsymbol{B_l} \begin{pmatrix} 0 & 0 \\ 0 & \tilde{\boldsymbol{B}}_{\boldsymbol{n}}^{-\mathbf{1}} \end{pmatrix} \tag{1.11}$$

where $\tilde{\boldsymbol{B}}_{\boldsymbol{n}}$ is the node susceptance matrix without the row and column associated with the slack node (first row and first column in this case).

The result is the so-called $\mathcal{N} \times \mathcal{L}$ power transmission distribution factor (PTDF) matrix that linearly connects nodal power injections INJ with line flows F such that $\text{PTDF} \cdot INJ = F$.

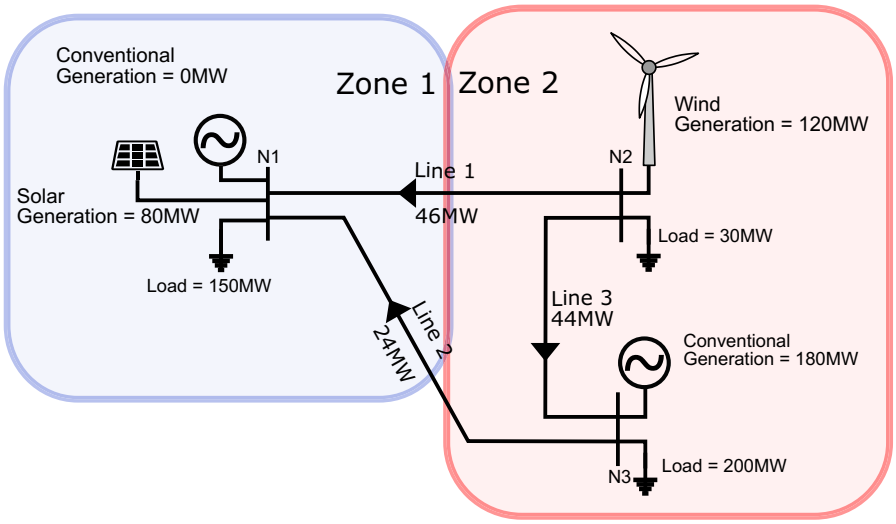

Figure 1.3: Dispatch and power flows for uniform pricing market clearing.

We can derive the PTDF matrix for the previously introduced example three node system of Figure 1.3, with assumed impedances of 1 for *Line 1* and *Line 2* and 0.5 for *Line 3*, the incidence matrix $\boldsymbol{A}$ and line capacity $\overline{f}$:

$$\boldsymbol{A} = \begin{pmatrix} -1 & 1 & 0 \\ 1 & 0 & -1 \\ 0 & 1 & -1 \end{pmatrix} \quad \text{PTDF}^n = \begin{pmatrix} 0 & 0.6 & 0.4 \\ 0 & -0.4 & -0.6 \\ 0 & 0.4 & -0.4 \end{pmatrix} \quad \overline{f} = \begin{pmatrix} 40 \\ 100 \\ 100 \end{pmatrix} \tag{1.12}$$

The previously obtained optimal solution $G^* = \begin{pmatrix} 80 & 0 & 120 & 180 \end{pmatrix}^T$ to the economic dispatch problem (1.2) and resulting nodal injections result in the following power flows that are also shown in Figure 1.3.

$$\begin{pmatrix} 0 & 0.6 & 0.4 \\ 0 & -0.4 & -0.6 \\ 0 & 0.4 & -0.4 \end{pmatrix} \begin{pmatrix} -70 \\ 90 \\ -20 \end{pmatrix} = \begin{pmatrix} 46 \\ -24 \\ 44 \end{pmatrix} \tag{1.13}$$

Notably, the power flow in *Line 1* exceeds its capacity. To include the power flow in the optimization we can formulate the so-called optimal power flow (OPF) problem, co-optimizing dispatch and network resources, as an extension to Problem (1.2) as follows:

$$\min \quad \sum_i mc_i \cdot G_i \tag{1.14a}$$

$$\text{s.t.} \sum_{i \in \mathcal{G}_n} G_i - d_n = INJ_n \qquad \forall n \in \mathcal{N} \tag{1.14b}$$

$$G_i \leq g_i^{max} \qquad \forall i \in \mathcal{G} \tag{1.14c}$$

$$-\overline{f} \leq \text{PTDF} \cdot INJ \leq \overline{f} \tag{1.14d}$$

$$G_i \geq 0 \qquad \forall i \in \mathcal{G} \tag{1.14e}$$

The energy balance (1.14b) is defined for each node by balancing nodal demand d_n and generators located at each node. The resulting nodal injections result in line flows $\text{PTDF} \cdot INJ$ that are bound by the line capacity $\overline{f}$. The optimal solution of (1.14) results in $G^* = \begin{pmatrix} 80 & 15 & 120 & 165 \end{pmatrix}^T$ and feasible power flows.

1.5 Modeling Flow-Based Market Coupling

The process of FBMC aims to provide a transparent methodology for capacity allocation, including information about the current system state, individual network components, and other transactions in the system. The fundamental process was first described in ETSO (2001a) as a method to efficiently allocate "scarce transmission capacity in highly meshed networks" and to define a method to "alleviate [...] the complexity of independent auctions".

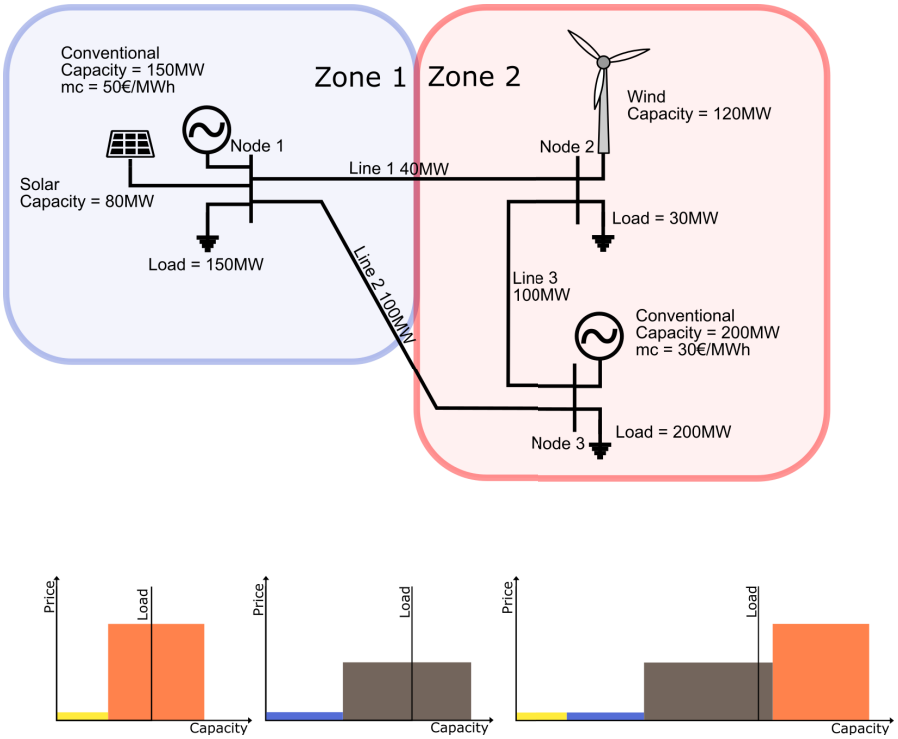

Figure 1.4: Exemplary three-node system: Individual market clearing (left) and uniform pricing (right)

Using the aforementioned example in Figure 1.4 we can extend Problem (1.2) to model market coupling via static NTCs with a new decision variable $EX_{z,zz}$ capturing directed commercial exchange from zone z to zone zz that are part of set $\mathcal{Z}$. The energy balance (1.15b) balances zonal demand d_z, generation within a zone and its net-position, that is, a zone's net-export.

$$\min \quad \sum_i mc_i \cdot G_i \tag{1.15a}$$

$$\text{s.t.} \quad \sum_{i \in \mathcal{G}_z} G_i + \sum_{zz} EX_{z,zz} - EX_{zz,z} = d_z \qquad \forall z \in \mathcal{Z} \tag{1.15b}$$

$$G_i \leq g_i^{max} \qquad \forall i \in \mathcal{G} \tag{1.15c}$$

$$EX_{z,zz} \leq ntc_{z,zz} \qquad \forall z, zz \in \mathcal{Z} \tag{1.15d}$$

$$G_i \geq 0 \qquad \forall i \in \mathcal{G} \tag{1.15e}$$

$$EX_{z,zz} \geq 0 \qquad \forall z, zz \in \mathcal{Z} \tag{1.15f}$$

With (1.15) exchange between the two zones is limited by the parameter *ntc* and solutions can be placed in-between the two extremes depicted in Figure 1.4: individual market clearing with no exchange and uniform pricing with infinite exchange. In this example the problems of the NTC/ATC methods become apparent. It is difficult to set appropriate values and it is quite clear that the available capacity highly depends on the current load, the availability of intermittent generation, and the resulting power flows.

Following the continuously updated "Documentation of the CWE FB MC solution" (50Hertz et al. 2020) that is currently available in version 5, the available capacity can be derived using the flow-based methods for the exemplary system: First, define a basecase. Second, derive remaining transfer capacity available for commercial exchange. Third, use the available capacity to constrain commercial exchange in the market clearing.

The basecase reflects the expected system state and includes information about load and availability of intermittent generation. A basecase dispatch yields a generation schedule g^{bc} and the resulting net-positions np^{bc}, meaning the zonal system balance. As described in Chapter 1.4 a transmission system can be modeled by a PTDF matrix that maps nodal power injections to power flows on transmission lines. Therefore, the power flow in the example system can be described with the following PTDF matrix and line capacities $\overline{f}$ as per (1.12).

To connect line flow and commercial exchange, we can use the information about which plants will serve changes in net-position. In this example these are the conventional generators located at *Node 1* for *Zone 1* and *Node 3* for *Zone 2*. This information is commonly denoted as generation shift key (GSK) and generally describes the participation factor of generators towards the net-position. Typically, the GSK is only defined by conventional generators since RES are considered must-take and are therefore always part of the dispatch and the basecase calculation. The GSK can be used to derive a zonal PTDF^z that describes the relation between zonal net-positions and power flows on transmission lines:

$$GSK = \begin{pmatrix} 1 & 0 \\ 0 & 0 \\ 0 & 1 \end{pmatrix} \qquad \text{PTDF}^z = \text{PTDF}^n \cdot GSK = \begin{pmatrix} 0 & 0.4 \\ 0 & -0.6 \\ 0 & -0.4 \end{pmatrix} \tag{1.16}$$

We can formulate the intuition that the available transfer capacity from basecase power flows should be made available to the changes in net-positions between the basecase np^{bc}

and the net-position of the market result np^m as follows:

$$\text{PTDF}^z(np^m - np^{bc}) \leq \overline{f} - f^{bc} \tag{1.17}$$

$$\text{PTDF}^z\, np^m \leq \overline{f} - (f^{bc} - \text{PTDF}^z\, np^{bc}) = RAM \tag{1.18}$$

The resulting Equation (1.18) describes bounds on the net-position based on line capacities, basecase flows, and basecase exchange. The term $f^{bc} - \text{PTDF}^z\, np^{bc}$ is often denoted as reference flow f^{ref} capturing power flows from nodal injections and commercial transactions in the basecase. The term $\overline{f} - f^{ref}$ describes the remaining available capacity that bounds net-positions in the market coupling.

The combination of zonal PTDF and remaining available margin (RAM) is commonly described as flow-based parameters as they can be directly used in an economic dispatch problem where the they are used to constrain the zonal net-position:

$$\min \quad \sum_{i \in \mathcal{G}} mc_i \cdot G_i \tag{1.19a}$$

$$\text{s.t.} \quad \sum_{i \in \mathcal{G}_z} G_i - d_z = NP_z \qquad \forall z \in \mathcal{Z} \tag{1.19b}$$

$$NP_z = \sum_{zz} EX_{z,zz} - EX_{zz,z} \qquad \forall z \in \mathcal{Z} \tag{1.19c}$$

$$G_i \leq g_i^{max} \qquad \forall i \in \mathcal{G} \tag{1.19d}$$

$$\text{PTDF}^Z\, NP \leq RAM \tag{1.19e}$$

$$G_i \geq 0 \qquad \forall i \in \mathcal{G} \tag{1.19f}$$

$$EX_{z,zz} \geq 0 \qquad \forall z, zz \in \mathcal{Z} \tag{1.19g}$$

For the exemplary three-node system we can derive these flow-based parameters by starting with the individual market clearing as the basecase, that is, solving (1.15) with $ntc = 0$ yielding power flows and net-positions, which can be used to calculate the RAM:

$$f^{bc} = \begin{pmatrix} 18 \\ 18 \\ 72 \end{pmatrix} \quad np^{bc} = \begin{pmatrix} 0 \\ 0 \end{pmatrix} \quad \text{RAM} = \begin{pmatrix} 22 \\ 32 \\ 28 \end{pmatrix}$$

The resulting flow-based parameters can be used to constrain the net-positions for each region and result in the cost-optimal allocation of generation capacities subject to network constraints, as depicted in Table 1.2.

Specifically, for the designated congestion of *Line 1* Equation (1.19e) yields

$$\begin{pmatrix} 0 & 0.4 \end{pmatrix} NP \leq 22$$

limiting the net-position of *Zone 2* — and subsequently of *Zone 1* — to 55 MW and results in a market result that reflects the physical infrastructure.

Table 1.2: Resulting dispatch and cost for clearing *Zone 1* and *Zone 2* individually, Uniform, or with flow-based parameters.

Generation (MW)	Individual	Uniform	Flow-Based
Solar (Node 1)	80	80	80
Conventional (Node 1)	70	0	15
Wind (Node 2)	120	120	120
Conventional (Node 3)	110	180	165
Net-Positions (Zone 1, Zone 2)	(0,0)	(-70,70)	(-55,55)
Power Flow (Line 1)	18	46	40
Total Cost	6800	5400	5700

In comparison with dispatch without commercial exchange, the cost are lower, as more low-cost generation is part of the market. The lowest cost result from a *Uniform Pricing* without limits on exchange, but result in power flows on *Line 1* that exceed its capacity and therefore would require redispatch.

This example highlights the main components of FBMC: the basecase and its power flows and net-positions, GSKs, zonal PTDF, reference flows and the resulting flow-based parameters. Compared to a zonal market coupling via the NTC/ATC method, the capacity is allocated towards the net-position and not bilaterally. While for this example solving Problem (1.15) with an NTC of 55 MW would result in the same solution, for larger, highly mashed, systems with more bidding zones the flow-based parameters become more faceted and define a common solution space for all considered market zones. Note, in this example the GSK perfectly describes how generators participate in net-position changes and provides no loss in information. This also means that the solution is equivalent to an OPF, that is, the solution to Problem (1.14) and that the resulting

flow-based parameters are independent of the basecase configuration.

The simplicity of the example embezzles other relevant components that are highly important in the real process. In most real-life scenarios the GSKs are inherently imperfect, therefore there are different strategies to parametrize GSKs based on power plant schedule or direction of net-position changes. The basecase includes forecast characteristics, with all pitfalls that come with imperfect information. The network representation via PTDF needs to be carefully assembled. Including too many lines, especially lines that are insensitive to cross-border exchange, will unnecessarily limit commercial exchange. TSOs therefore limit the line selections to critical network element (CNE) and in extension to critical network element and contingency (CNEC) in order to consider contingencies. The process also involves security and market considerations that are covered in reliability margins, commonly denoted as flow reliability margins (FRMs), or minimum capacities that have to be attributed to markets in form of the minimum remaining available margin (minRAM) criterion that was introduced as part of the Clean Energy Package. Additionally, since FBMC constrains power flows indirectly via the net-positions, power flow from the market result can exceed line capacities and require ex-post congestion management. These topics become especially relevant for large-scale applications and are addressed within this thesis.

1.6 Literature on FBMC

The process of FBMC originates from the effort of TSOs to find a better way for capacity allocation in meshed transmission systems (ETSO 2001a). As part of the early developments, different publications from different stakeholders exist that generally describe the market coupling process and its components. Examples are publications Klaar and Panciatici (2004), Schavemaker et al. (2008), Aguado et al. (2012), and Marien et al. (2013) and the master thesis of Dufour (2007) that originate from a inter-TSO research and working groups or co-operations between TSOs and PXs as in ETSO and EuroPEX (2004). The goal with these publications was to establish and improve the process as well as to move it closer to implementation.

With the implementation of FBMC, first as a dry-run during 2008 and parallel run in 2013, publications by directly involved parties commonly follow their duties to transparently document FBMC (Vattenfall Europe Transmission GmbH 2009; Amprion et al. 2011; Amprion et al. 2014; 50Hertz et al. 2017), document the accompanying publication process (Joint Allocation Office 2017), and monitor the implementation (Rte et

al. 2015). Such documentary publications are also available from the Scandinavian TSOs to document the process and describe the effects on the coupling process for potential implementation at the respective bidding zones (Energinet et al. 2014). The purpose of those types of publications focuses on broadcasting the required information to market parties.

In addition to the descriptive literature of the involved parties, the regulatory side publishes, besides the regulation itself, monitoring reports and inquiries, commission staff working documents, white papers, etc. Publishing institutions would be the European Commission itself or its directorates general, national regulatory bodies, ACER or the internal research institutions like the Joint Research Centre or the European Parliamentary Research Service. Besides the broadcasting function of the publications to convey regulatory decisions, e.g. ACER (2011), the publications also aim to inform members of the commission of upcoming decisions, e.g. European Parliamentary Research Service (2019), or summarizing current positions on policy options (European Commission 2016, 2018). These publications are usually based on the previously mentioned reports by TSOs or PXs or commissioned research. Examples are Consentec and Institute of Power Systems and Power Economics of Aachen University of Technology (2001), Consentec and Frontier Economics (2004), and Consentec (2007) that provided quantitative foundation for the current market design with implicit allocation using FBMC and price coupling, Logarithmo and E-Bridge (2017) that investigates welfare effects of FBMC or Antonopoulos et al. (2020) from the Joint Research Centre of the European Commission that investigate the comparability of nodal market designs and the European IEM. The listed reports by the regulatory body and market parties only cover a small subset of available information, however sufficient to generally describe the process.

Academic publications on FBMC, with the exception of master thesis's in cooperation with TSOs, start to appear with the implementation of FBMC in the CWE region. Publications can be grouped by scale, method and focus. Most publications model FBMC using methods of OR as described in Section 1.3 and 1.5.

To highlight specific interaction between it can be useful to stick with a simple example network or simplified representation of a real system, similar to Section 1.5. Boury (2015) and Van den Bergh, Boury, and Delarue (2016) provide a comprehensive overview of the relevant parameters, similarly to the publications that originate from TSO work-groups, however describing the process from the perspective of quantitative research by extending analytic expressions for GSK accuracy and loop flows. Van den Bergh and Delarue (2016) focuses on improvements to GSKs. Poplavskaya et al. (2020) compares FBMC to nodal

market clearing in a 6-node setup similar to Ehrenmann and Smeers (2005). Plancke et al. (2016) utilizes a simplified network of the CWE region to illustrate the effective of FBMC over the ATC method on the one hand, but also the importance of parameter choice regarding basecase. Felten et al. (2019) and Felten et al. (2021) describe the impact of GSK in a simplified 4-node system and the inclusion of intra-zonal lines in FBMC against a nodal benchmark case. Lang, Dallinger, and Lettner (2020) utilizes a simplified network for the European electricity system and investigates the effusiveness of FBMC with an extended flow-based region of 13 countries with focus on the Austrian bidding zone.

While small-scale experiments can illustrate the direct relation of parameter choices, the inherent inaccuracies of the process, similarly to the example of Section 1.5, often remain uncovered. Since large-scale applications often require significant computation resources, slightly increasing the complexity model can help to better simulate the real-world process. Two examples for medium-sized application are Byers and Hug (2020) that is based on a 96 bus network and Schönheit et al. (2021b) and Schönheit et al. (2021a) based on the 118 bus network. Byers and Hug (2020) focus on the basecase formulation and describes the modeling or parameter choices that influence results. Schönheit et al. (2021b) argues that the parameter choices of involved TSOs are substantial and Schönheit et al. (2021a) identifies improvements for CNEC selection process based on changed bidding zone configurations. Both studies are conducted using an open modeling approach that does not involve commercial software.

For large-scale applications different publications exist that utilize closed-source model frameworks for studies on FBMC that focus on different result metrics. Matthes, Spieker, and Rehtanz (2017) propose the simulation framework MILES (Spieker et al. 2016) and in Matthes et al. (2019) evaluate the impact of minimum RAMs on overloaded network elements. Marjanovic et al. (2018) investigates the extension to the CORE region (CORE) region and its impact on net-position, critical network elements and prices. Wyrwoll et al. (2018) describes the impact of less restrictive choice of critical network elements on commercial exchange and conventional generation schedules and in extension investigates different basecase configurations in Wyrwoll et al. (2019). Finck, Ardone, and Fichtner (2018) use a Matpower (Zimmerman, Murillo-Sánchez, and Thomas 2011) based power flow implementation to determine the impact of GSKs on generation schedules. Based on the formulation of Boury (2015), Hauschild (2019) provides an analysis of loop and reference flows in an application of the CWE region. Voswinkel et al. (2019) distinguishes between perfect foresight and different sources of "process-induced uncertainty". Felling

et al. (2019) cover an in-depth description of the FBMC process and an application on the CWE with an endogenous method to find an efficient bidding zone configuration. The study also distinguishes between different scenarios regarding the choice of critical network elements and basecase calculation under imperfect information. Schönheit, Dierstein, and Möst (2021) investigates the impact of the minimum RAM criterion that was introduced as part of the Clean Energy Package and proposes a specific way to model this policy engagement with FBMC. This research uses an updated version of *ELMOD*, originally developed by Leuthold, Weigt, and von Hirschhausen (2008, 2012), that is openly documented (Schönheit et al. 2020a), but requires commercial software to run. Aravena and Papavasiliou (2016) generally investigate zonal market design and evaluate the role of market design in integrating RES. This work is extended in Aravena et al. (2021) where the authors propose a cutting plane technique to solve FBMC instances by iteratively adding constraints. Additionally, the publication discusses the effectiveness of FBMC and ATC in comparison to the first-best market clearing via nodal pricing.

Research on the integration of intermittent renewable generation, similar to Neuhoff et al. (2013), in the context of FBMC has not been thoroughly covered. Schönheit et al. (2021b) include scenarios with moderate shares of RES but the analysis does not focus on this aspect.

Research on FBMC with methods other than optimization exist and utilize market data to evaluate the process or further the methods. Morin (2016) uses data of the parallel run between 2014 and 2015 to statically link line constraints to load or weather conditions. Schönheit and Sikora (2018) and Schönheit (2019) improve the choice of GSK by statistically choosing generators to participate in net-position changes based on non-public market data. van Stiphout (2016) uses the geometric properties of the flow-based domain to approximate it based on market data. The way flow-based parameters constrain commercial exchange is often visualized in so-called flow-based domains. Fundamentally, flow-based domains are polytopes with the dimensionality of number of bidding zones (Fuchs, Scherer, and Andersson 2015) and their composition is part of multiple publications (Felten et al. 2019; Schönheit, Dierstein, and Möst 2021). Zad et al. (2021) describes adequacy assessments using flow-based domains in that process discusses and evaluates their geometric attributes.

Those publications all contribute to a better understanding of FBMC and describe the process and modeling approaches in detail. Generally, most contributions agree on the modeling process of a basecase, day-ahead market stage and physical delivery with congestion management. The main components of FBMC, as described in Section 1.5,

are the basecase parametrization, CNEC selection, GSK strategy and the employment of the minRAM criterion and reliability margins, denoted as FRM.

1.7 Outline and Contributions of this Dissertation

This dissertation is structured in three parts:

- **Part I Introduction** includes an overview over the the European electricity market and preliminaries on the methods used in this thesis as Chapter 1.
- **Part II Methods** describes methods to model FBMC. The first contribution in Chapter 2 presents an open-source electricity market model by the name Power Market Tool (POMATO) that aims to facilitate open research and discussion on FBMC. Chapter 3 complements the modeling efforts by a method that allows to consider unplanned outages within the economic dispatch problem using an algorithm to efficiently create a non-redundant set of power flow constraints. This algorithm is used in the following applications in different ways: To create computationally tractable problem, to provide the ability to solve the OPF including contingencies and to pre-solve the flow-based domains, i.e. the day-ahead solution space for cross-zonal exchange.
- **Part III Applications** The methods described in Part II are applied to different case studies that compose Part III. First, as part of describing the process and the effect of core parameters, Chapter 4 investigates the impact of GSKs on the day-ahead trading domains. The case study is performed on the CWE region and represents a large-scale application. Chapter 5 takes a step back and aims to describe the complete process, including congestion management which was explicitly not analyzed in Chapter 4, and the impact of high shares of intermittent generation and the resulting uncertainty from forecast errors. The case study is based on the Pena, Martinez-Anido, and Hodge (2017) version of the well-known IEEE 118 bus network. Chapter 6 combines both applications and provides a comprehensive study of the CWE region for the target year 2030. In contrast to the previous case study, that described the impact of different GSKs, this study includes both capacity allocation and congestion management that allows to numerically evaluate different parametrizations of the capacity allocation process and the impact of higher RES shares in the mid-term.

A large part of this thesis revolves around quantitative methods to evaluate different configurations of capacity allocation and congestion management in electricity markets. To create lasting contributions, the methods have to be open and transparent. Open can mean very different things in different contexts. A mathematical formulation is inherently open, however the additional steps to a working model can be substantial.

In line with Weibezahn and Kendziorski (2019) and the manifest of the Open Energy Modeling Initiative[3] the contributions aim to be open, i.e. are published under an open license, and accessible. The aspect of accessibility covers many aspects of a publication and ensures its usefulness to the community. Weibezahn and Kendziorski (2019) describes many dimensions that are part of open science, which extends to input- and output data as well as data-processing. Additionally, accessibility implies that contributions are documented, tested and maintained (Hirth, Schlecht, and Mühlenpfordt 2018). All these aspects are covered with the publication of the electricity market model POMATO. Beyond the fundamental aspects of publishing the code under open license (Weinhold 2020b), the code is fully documented (Weinhold 2020a) and continuously tested with a code-coverage of over 90%. POMATO is version controlled, so that functionality is preserved for different analyses. Additionally, for the analysis in Chapter 6 all data is published in a comprehensive tool that allows to follow each step of the pre-processing (Weinhold 2021) from raw data to the processed POMATO-compatible data-sets.

1.7.1 Chapter 2: Power Market Tool (POMATO)

The proposed open-source *Power Market Tool* (POMATO) aims to enable research on interconnected modern and future electricity markets in the context of the physical transmission system and its secure operation. POMATO has been designed to study capacity allocation and congestion management (CACM) policies of European zonal electricity markets, especially FBMC. For this purpose, POMATO implements methods for the analysis of simultaneous zonal market clearing, nodal (N-k secure) power flow computation for capacity allocation, and multi-stage market clearing with adaptive grid representation and redispatch. The computationally demanding N-k secure power flow is enabled via an efficient constraint reduction algorithm. POMATO provides an integrated environment for data read-in, pre- and post-processing and interactive result visualization. Comprehensive data sets of European electricity systems compiled from Open Power System Data and Matpower Cases are part of the distribution. POMATO is implemented in Python

[3] See: www.openmod-initiative.org/manifesto.html

and Julia, leveraging Python's easily maintainable data processing and user interaction features and Julia's well-readable algebraic modeling language, superior computational performance and interfaces to open-source and commercial solvers.

1.7.2 Chapter 3: Fast Security-Constrained Optimal Power Flow

Determining contingency aware dispatch decisions by solving a security-constrained optimal power flow (SCOPF) is challenging for real-world power systems, as the high problem dimensionality often leads to impractical computational requirements. This problem becomes more severe when the SCOPF has to be solved not only for a single instance, but for multiple periods, e.g. in the context of electricity market analyses. This paper proposes an algorithm that identifies the minimal set of constraints that exactly define the space of feasible nodal injections for a given network and contingency scenarios. By internalizing the technical limits of the nodal injections and enforcing a minimal worst-case impact of contingencies to line flows, computational effort can be further improved. The case study applies and analyzes the methods on the IEEE 118 and A&M 2000 bus systems, as well as the German and European transmission systems. In all tested cases the proposed algorithm identifies at least 95 % of the network and security constraints as redundant, leading to significant SCOPF solve time reductions. Scalability and practical implementation are explicitly discussed. The code and input data of the case study is published supplementary to the paper under an open-source license.

1.7.3 Chapter 4: The Impact of Different Generation Shift Key Strategies

The trading of electricity across zones relies on cross-border capacities, provided by transmission system operators. The target design of the European Union for capacity calculations is flow-based market coupling, a method that provides trading domains while taking into account grid restrictions. Flow-based market coupling heavily relies on GSKs, an essential predictive parameter, translating zonal balance changes that originate from market coupling into nodal injections and consequent line flow changes. This analysis quantifies the effect of different GSKs strategies on the market coupling domains and individual network elements. A strategy entails suppositions regarding which generating units partake in market changes and to what extent. For this, a novel method for base case computations is proposed that relies on matching historical reference flows of network elements. The results show that different strategies substantially alter the shape and size of flow-based market coupling domains and have a statistically significant im-

pact on individual network elements. For many lines, the average line flow sensitivity to market changes differs between 1-5% across strategies and up to 10% for a few lines. Furthermore, the analysis details how the n-1 security criterion influences the composition of domain constraints and to what extent network elements are affected by it. Particularly with regard to the planned geographical expansion of flow-based market coupling and changing regulatory demands for transmission system operators, this work attests to the importance of developing accurate and transparent flow-based market coupling parameters and model-based representations.

1.7.4 Chapter 5: Uncertainty-Aware Capacity Allocation for Flow-Based Market Coupling

The effective allocation of cross-border trading capacities is one of the central challenges in implementation of a pan-European internal energy market. flow-based market coupling (FBMC) has shown promising results for to achieve better price convergence between market areas, while, at the same time, improving congestion management effectiveness by explicitly internalizing power flows on critical network elements in the capacity allocation routine. While academic publications that synthesize FBMC in model frameworks agree on a general process that aligns with the real market coupling process, they differ greatly in some core assumptions. However, the question of FBMC effectiveness for a future power system with a very high share of intermittent renewable generation is often overlooked in the current literature. This paper provides a comprehensive summary on FBMC modeling assumptions, discusses implications of external policy considerations and explicitly discusses the impact of high-shares of intermittent generation on the effectiveness of FBMC as a method of capacity allocation and congestion management in zonal electricity markets. We propose to use an RES uncertainty model and probabilistic security margins on the FBMC parameterization to effectively assess the impact of forecast errors in renewable dominant power systems. Numerical experiments on the well-studied IEEE 118 bus test system demonstrate the mechanics of the studied FBMC simulation. Our data and implementation are published through the open-source Power Market Tool (POMATO).

1.7.5 Chapter 6: Evaluating Policy Implications on the Restrictiveness of FBMC

The current stage in the evolution of the European internal energy market for electricity is defined by the transformation towards a renewable energy system. The Clean Energy Package aims to ensure that methods for capacity allocation and congestion management, that are at the center of the European internal market for electricity, align with this transformation.

Flow-based market coupling, the preferred method for capacity allocation, is first and foremost a formal process to allocate exchange capacities to the markets. The process itself builds on network models in combination with forecasts for dispatch, renewable in-feed and load. However, the process also allows for many considerations of the involved parties that impact the resulting capacities. As part of the Clear Energy Package, the regulatory body enacted their ambition to increase exchange capacities by enforcing transmission system operators to allocate a minimum margin of physical line capacity with the goal of providing a higher level of competition and better integration of renewable energy sources. This study investigates this and other policy relevant consideration of flow-based market coupling and numerically evaluates their effect on capacity allocation and congestion management for the central western European region. The numerical experiments are conducted for the status quo and the target year 2030 using open methods and open data. This includes a high spacial and temporal resolution on transmission, generation, renewable feed-in and load data, as well as performant economic dispatch and network models. The model results quantify the trade-off between permissive capacity allocation and increased congestion management for the status quo. For high shares of intermittent renewable generation, less constrained exchange capacities are favourable, however also highlight the importance of the markets ability to integrate high shares of intermittent generation.

Table 1.3: Chapter origins and own contribution.

Chapter	Pre-publications & Own Contribution
2	**Power Market Tool (POMATO) for the Analysis of Zonal Electricity Markets**
	This chapter is the accepted version of the following publication: Richard Weinhold and Robert Mieth. 2021. "Power Market Tool (POMATO) for the Analysis of Zonal Electricity Markets." *SoftwareX* 16:100870.
	Joint work with Robert Mieth. Both authors contributed equally to the article. Software implementation done by me.
3	**Fast Security-Constrained Optimal Power Flow through Low-Impact and Redundancy Screening**
	This chapter is the accepted version of the following publication: Richard Weinhold and Robert Mieth. 2020a. "Fast Security-Constrained Optimal Power Flow Through Low-Impact and Redundancy Screening." *IEEE Transactions on Power Systems* 35 (6): 4574–4584.
	Joint work with Robert Mieth. Both authors contributed equally to the article. Implementation of the model and algorithm done by me.
4	**The Impact of Different Generation Shift Key Strategies on the Flow-based Market Coupling Domain: A Model-based Analysis of Central Western Europe**
	This chapter is the accepted version of the following publication: David Schönheit, Richard Weinhold, and Constantin Dierstein. 2020. "The Impact of Different Strategies for Generation Shift Keys (GSKs) on the Flow-Based Market Coupling Domain: A Model-Based Analysis of Central Western Europe." *Applied Energy* 258:114067.
	Joint work with David Schönheit and Constantin Dierstein. Together with the first author, I coordinated the creation of this article. All authors shared the conceptualization of the article. My main contributions were the computation of the market model results based on historical power flows and, implementation of the network representation and writing the corresponding sections in the final publication.
5	**Uncertainty-Aware Capacity Allocation in Flow-Based Market Coupling**
	This chapter is the submitted to *Applied Energy*.
	Joint work with Robert Mieth. Both authors contributed equally to the article. Model implementation done by me.

Chapter origins and own contribution (continued).

Chapter	Pre-publications & Own Contribution
6	**Evaluating Policy Implications on the Restrictiveness of Flow-based Market Coupling with High Shares of Intermittent Generation: A Case Study for Central Western Europe**
	This chapter is the submitted to *Energy Policy*.
	Single-author original research article.

1.8 Conclusions and further research

This dissertation contributes to the field in different ways. First, the development of an open-source model that allows to synthesize the FBMC process offers a transparent and accessible way to research zonal market design. The implemented methods contribute to modeling power flow in techno-economic models. Second, this dissertation provides valuable insights into how FBMC allocates capacity to the markets and the impact of specific parameter choices. The papers of this dissertation contribute to the existing literature, as discussed in Section 1.6, to better describe the relations of parameter choices and the resulting capacity that is made available to the market. And third, this dissertation delivers valuable insights into the effectiveness of FBMC in systems with high shares of RES.

Specifically, the numerical experiments show that the proposed methods provide improvements to both performance and model accuracy. Studies on the effectiveness of market design and integration of intermittent generation prove the effectiveness of FBMC for small synthetic case studies and large-scale applications.

This dissertation also contributes to the comparability of these results. Given that parameterizations differ greatly between academic publications, it can be challenging to derive general conclusions from the results. To alleviate this problem, data collection and processing is explicitly part of the numerical experiments, to provide the additional transparency required for large-scale applications. The contributions in Chapter 5 and 6 propose a nominal parametrization of FBMC in electricity market models and introduce the notion that chances in parameters will increase/decrease the available capacity allocated to the markets. This explicitly includes policy relevant considerations that are part of the process's parametrization.

FBMC, in its operational state, is still new and this comparability is crucial moving

forward as it continues to evolve. Conceptually, the process offers great benefits in its inherently more general way to allocate capacity and include the system state more explicitly. While these benefits can be numerically shown, the process offers many more avenues to further improvements. First and foremost this would be the extension to the CORE region, which will allow for better use of transmission capacities as more bidding zones' net-position are part of the allocation process. Additionally, methods to better include operational considerations, like remedial actions or the operation of active network elements, in the capacity allocation process will greatly impact FBMC's efficiency. Both are not yet, or only partially, included in academic contributions and will, hopefully based on the groundwork provided in this dissertation, become future contributions to the field.

Part II

Methods

Chapter 2

Power Market Tool (POMATO) for the Analysis of Zonal Electricity Markets

"Optimization, then, should be regarded as a tool of conceptualization and analysis rather than as a principle yielding the philosophically correct solution."

(From the Introduction in Luenberger and Ye (2008))

The contents of this chapter have been published in SoftwareX 16 (Weinhold and Mieth 2021). Available Online: https://doi.org/10.1016/j.softx.2021.100870. For this dissertation the original article has been adapted to ensure consistent notation and format.

2.1 Motivation and Significance

Europe's increasing electricity production from renewable energy resources in combination with a significant decline of conventional generation capacity, has spawned political and academic interest in the transmission system's ability to accommodate this transition (Amprion 2019). Specifically, higher levels of coordination in a pan-European electricity market to facilitate meeting emission targets, while ensuring reliable power supply at acceptable cost (European Parliament 2020), require the internalization of the power transmission capabilities into trading processes.

Central to this discussion is the efficiency of capacity allocation and congestion management (CACM) policies between and within electricity market areas that share transmission infrastructure (European Commission 2015). Capacity allocation (CA) summarizes regulatory and market mechanisms that constrain electricity trading volumes between two adjacent market areas with respect to the expected available cross-border transmission capacity at time of delivery. Congestion management (CM), on the other hand, refers to methods ensuring that the physical system state at time of delivery indeed remains within its security margins, e.g., does not cause transmission line overloads. Noticeably, well defined CA based on suitable forecasts can reduce CM measures, such as out-of-market generator redispatch coordinated by the transmission system operator (TSO). Previously implemented CA policies based on static net transfer capacities (NTCs) consider tie-line capacities between markets, but neglect restricting transmission assets within market zones, thus leading to often non-feasible market outcomes, increased CM (redispatch) or overly conservative market results (Amprion et al. 2011; European Commission 2015). To overcome these deficiencies and in an effort to "*move towards a genuinely integrated [European] electricity market*" (European Commission 2015, Article 3), the Central Western European (CWE) countries inaugurated flow-based market coupling (FBMC) (Van den Bergh, Boury, and Delarue 2016), a more complex CA policy that aims to increase the potential volume of cross-border electricity trading while decreasing CM requirements by explicitly accounting for cross-border and zone-internal transmission limits.

The proposed *Power Market Tool (POMATO)* has been designed to enable further research on the status-quo and future policies of practical zonal electricity markets, especially FBMC. While the theory of a centrally coordinated zonal electricity market is somewhat mature, see e.g. Ehrenmann and Smeers (2005), practical implementation with imperfect coordination between market and system operators requires ongoing analyses.

The current European FBMC is a multi-stage process coordinated by multiple TSO and involves detailed zone-specific load and generation forecasts and network models, which are typically not, or only partially, disclosed by the TSOs (Schönheit, Weinhold, and Dierstein 2020). However, the medium- and long-term evolution of the FBMC design requires an informed public decision based on independent FBMC analyses that study the impact of, e.g., more countries joining the coupled market or bidding zone layouts (which have been declared inefficient by a recent TSOs study (ENTSO-E 2018)). Notably, the yearly federal report on the future of the grid in Germany (*"Netzentwicklungsplan"*), included a rudimentary FBMC representation for the first time in its 2018 edition (Bundesnetzagentur 2018), three years after FBMC implementation.

There are few model implementations of the FBMC process available to the academic community (Aravena and Papavasiliou 2016; Matthes et al. 2019; Schönheit et al. 2020a). Aravena and Papavasiliou (2016) compare various CA policies and demonstrate the benefits of FBMC traditional approaches using real-world data sets. Also, this study proposes an iterative approach to meet the practical requirement that any dispatch has to be robust against unplanned transmission equipment outage (*N-1 security*). However, datasets and model implementation are not published along the paper. Similarly, Matthes et al. (2019) present a FBMC formulation for estimating future FBMC parameters and studying the impact of regulations that require additional security margins on critical transmission lines. This model uses an external convex hull reduction for a N-1 secure FBMC solution and is implemented in the MILES framework (Spieker et al. 2016), which, to our knowledge, is also not publicly available. Schönheit et al. (2020a) extend the classic GAMS[1] model ELMOD (Leuthold, Weigt, and von Hirschhausen 2012) to facilitate FBMC analyses and study the impact of regulations requiring a minimum availability of interzonal trading volumes (Schönheit, Dierstein, and Möst 2021). Here, N-1 security is approximated through static security margins and despite comprehensive documentation in (Schönheit et al. 2020a) the code extension itself is undisclosed.

POMATO aims to overcome some of the caveats of Aravena and Papavasiliou (2016), Matthes et al. (2019), and Schönheit et al. (2020a) by providing a documented and open-source framework that is easy to use and goes beyond the implementation of an academic optimization model. Some main features and contributions are:

1. Separation of data processing (implemented in Python[2]) and optimization (imple-

[1] www.gams.com
[2] www.python.org

mented in Julia[3]) to achieve a flexible Python-based user interface that is familiar to many users, while creating a lean implementation of the central optimization model in the well-readable JuMP algebraic modeling language (Dunning, Huchette, and Lubin 2017).

2. Open-source available and documented on GitHub[4] (Weinhold 2020b, 2020a).

3. Comprehensive data set of the European electricity market and transmission infrastructure based on Open Power Systems Data[5] and Matpower[6] data sets.

4. Electricity market model with zonal and nodal market clearing and a module to synthesize the FBMC process, including heat sector coupling.

5. Exact N-1 secure dispatch implementation suitable for large-scale networks and multi-period analyses. The used algorithm removes redundant constraints, similar to the convex hull approach in Matthes et al. (2019), but has been optimized for optimal power flow (OPF) analyses, yielding improved computation times.

6. Stochastic OPF using chance-constraints to analyse the impact of forecast errors from renewable energy sources.

2.2 Software Description

POMATO's architecture is structured in three layers as shown in Figure 2.1. The *model core* collects the mathematical formulations of the necessary optimization problems and provides an interface to the required solvers. To ensure a lean model implementation and efficient re-runs without re-calculating large parameter sets, the model core is encapsulated in a *data processing* layer. This layer automates parameter calculation and validation, provides parameters to the model core, and validates and processes the resulting model output. Finally, all functionality of POMATO is collected in the outer *user interface* layer via readable API-like commands.

[3] www.julialang.org
[4] github.com/richard-weinhold/pomato
[5] open-power-system-data.org/
[6] matpower.org/

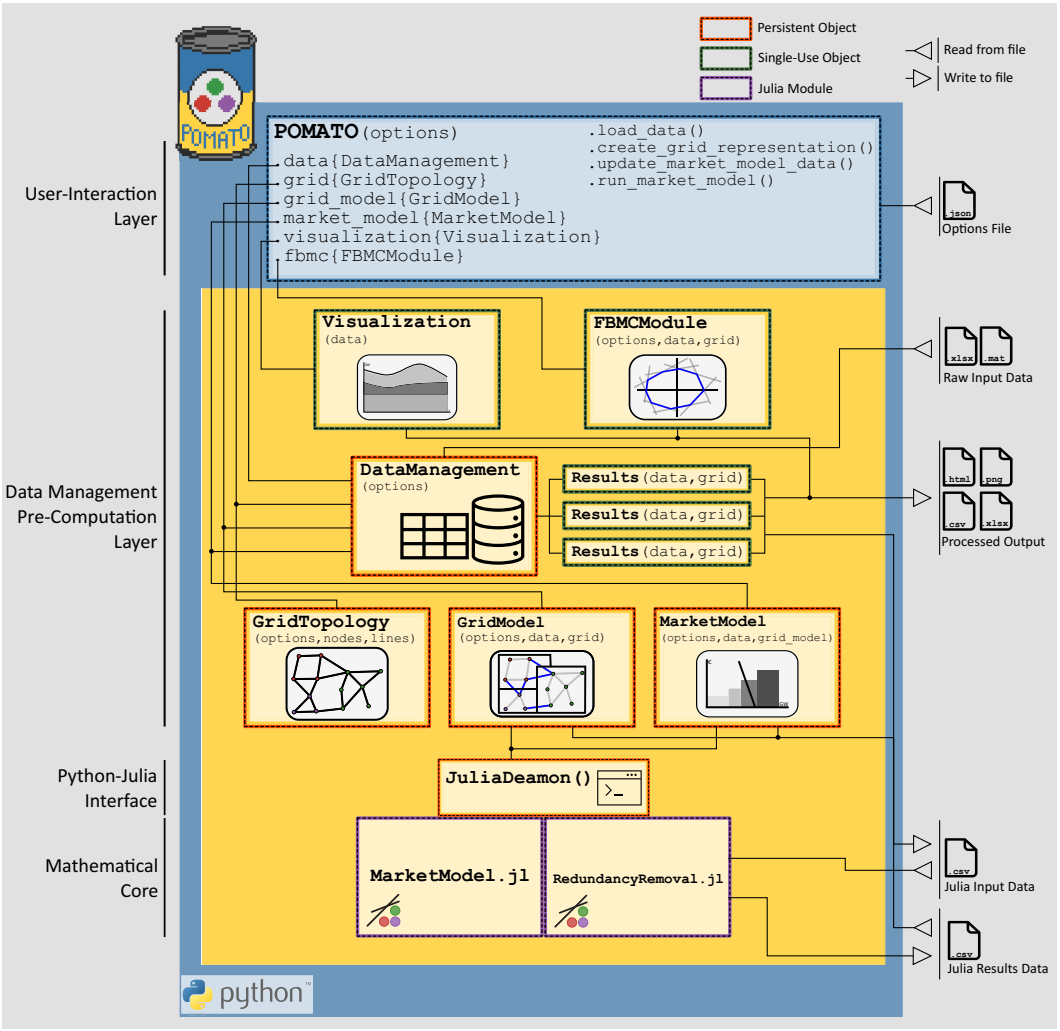

Figure 2.1: POMATO's layered architecture. The inner model core is colored purple, the data processing layer is colored yellow, and the outer user interface is colored blue.

2.2.1 Model Core

The core of POMATO is an electricity market model. This model is a linear optimization problem that finds the least cost generation schedule that matches system demand with respect to all technical constraints. Equation (2.1) shows the general structure of such a

model[7]. See also our previous work in Schönheit, Weinhold, and Dierstein (2020):

$$\min \ \text{OBJ} = \sum COST\_G + COST\_H + COST\_CURT + OOM\_PEN \tag{2.1a}$$

s.t.

Cost Definition (2.1b)

Generation Constraints (2.1c)

Heat Constraints (2.1d)

Storage Constraints (2.1e)

Energy Balances (2.1f)

Network Constraints. (2.1g)

Objective (2.1a) minimizes the cost of electricity generation ($COST\_G$), heat generation ($COST\_H$), load curtailment ($COST\_CURT$) and out-of market penalties (OOM_PEN, e.g. cost of redispatch) over all units and time steps. Constraints in (2.1b) define these cost components as sets of linear functions. Depending on the modeled market framework, some cost may be zero. Constraints (2.1c) and (2.1d) enforce limits on the available electricity and heat generation, respectively. Constraints (2.1e) enforce the time-coupled energy constraints for storages and limit their efficiency-corrected charging and discharging power. Equations (2.1f) ensure that for all market areas generation equals demand plus net export (export minus import) at all times. Network constraints (2.1g) capture the transmission system topology as nodes (buses) and lines and enforce exchange capacity limits. Physical flows are modeled using the linearized (DC) power flow equations so that nodal net injections can be mapped to power flows either directly using power transfer distribution factor power transmission distribution factor (PTDF) matrix or implicitly via auxiliary voltage angle variable, see e.g. Weinhold and Mieth (2020a) and Hörsch et al. (2018).

The specific definitions of constraints (2.1b)-(2.1g) are activated and parametrized by POMATO "on the fly" based on user-defined options. For example, nodal market clearing enforces an energy balance in (2.1f) for each *node* and exchanges are limited by the physical power flow and the thermal transmission system capacities. Zonal markets, on the other hand, ensure an aggregated energy balance for an entire *zone* (i.e. multiple connected nodes). Exchanges with neighboring zones are limited either explicitly

[7]The exact mathematical equations can be found in the POMATO documentation under pomato.readthedocs.io/en/latest/model_formulation.html

by NTCs, which constrain individual cross-border exchanges, or implicitly through constraints on the net positions (total net export) of each zone. The latter is used to model FBMC by calculating zonal PTDFs, see e.g. Schönheit, Weinhold, and Dierstein (2020), that map zonal net positions to power flows on (critical) lines. Additionally, constraints to model CM (redispatch) and external security requirements (contingency robustness) can be included. For redispatch models, a nodal market is solved subject to additional out-of-market penalties based on results of a previously solved zonal market. Specifically, the optimal redispatch is the least-cost change from a given generation schedule with predefined out-of-market penalties and fixed *zonal* balances so that the resulting *nodal* balances are feasible for the given transmission network. Preventive system security requirements based on contingency (N-1) analyses, are enforced through a suitable extensions of zonal and nodal PTDF matrices.

Optimal dispatch with preventive robustness against all contingencies (unplanned outages) is computationally demanding and requires preliminary solution heuristics (Weinhold and Mieth 2020a). Otherwise, because the number of constraints grows exponentially with the network size, typical multi-period dispatch problems for real-world economic analyses cannot be solved in reasonable time or with commonly available computation resources. However, it has been shown that many (in fact most) of these constraints are *redundant*, i.e. never binding in the optimal solution due to the existence of more restrictive constraints (Bouffard, Galiana, and Arroyo 2005). To ensure feasible solution times for real-world networks over longer time horizons (e.g. weeks to years), POMATO's model core includes additional functionality to identify these redundant constraints. Implementation and performance of this redundancy-removal algorithm has been presented in our previous work (Weinhold and Mieth 2020a), where we showed that for most of the studied transmission networks over 99% of the constraints can be removed from the optimization problem, allowing to solve previously infeasible larger market models and significantly reducing the solve time of smaller problems.

The methods and algorithms implemented in the model core require a suitable framework that enables fast robust computations and facilitates the use of interchangeable solver back-ends. The open-source Julia Language provides a competitive combination of performance and readability (Bezanson et al. 2017), as well as suitable libraries for implementing the required mathematical programming (electricity market model and redundancy removal). Here, we opted for the popular, well-readable and flexible JuMP package (Dunning, Huchette, and Lubin 2017). POMATO's Julia modules (`MarketModel.jl` and `RedundancyRemoval.jl`) are parametrized and called automatically by the higher PO-

MATO layers, as indicated in Figure 2.1.

Remark 1 (Risk-Aware Economic Dispatch). When modeling systems with high shares of stochastic renewable generation, feed-in uncertainty with respect to capacity reserve, network constraints and risk-perception of the system operator can be internalized in the marker clearing using *chance constraints* (Dvorkin 2020; Mieth, Kim, and Dvorkin 2020). This capability is released with POMATO as an experimental feature. Further analysis will be provided in a future publication.

Remark 2 (Solvers). JuMP allows to easily communicate with a wide range of solvers. Per default, POMATO will install and use the open CLP solver[8]. However, if available on the user's system, POMATO can be configured to use commercial solvers like Mosek[9] or Gurobi[10]. Other solvers can be implemented as outlined in the documentation[11].

2.2.2 Data Management and Pre-Processing

POMATO's central Data-Management layer, see Figure 2.1, manages the functionality of the model core by providing data and model parametrizations, calling and monitoring the Julia processes, and validating their results. To enable flexible data-handling that avoids redundant calculations, we leverage Python and its object-oriented programming paradigm which resolves issues typically related to static scripts. In such linear approaches, e.g. in GAMS, all parameters are handled in the global scope of the program so that any desired conditional functionality renders the code overly complex and hard to maintain. Alternatively, encapsulating the required functionally in different objects (modules), ensures data consistency and compatible methods.

The data-management layer consists of four main modules, `DataManagement`, `GridTopology`, `GridModel` and `MarketModel`. These modules are created once in every instance of POMATO and each provides specific methods to the user-interface and other modules. Additionally, single-use modules are used for result processing, e.g. FBMC calculations and result visualization. `DataManagement` is the central module to handle all data and their corresponding options. All input data is validated with respect to predefined data structures that are required to run the desired market model and are made available to other modules. Due to the persistence of `DataManagement`, changes in data, e.g. from user manipulations or model results, are propagated throughout POMATO.

[8] github.com/jump-dev/Clp.jl
[9] github.com/MOSEK/Mosek.jl
[10] github.com/jump-dev/Gurobi.jl
[11] pomato.readthedocs.io/en/lastest/installation.html/#solvers

Pre-processing and validation of data related to the transmission network topology requires specific methods that are collected in the `GridTopology` module. It uses network data (bus/node and line/branch information) and provides the parameters for subsequent power flow calculations. Additionally, `GridTopology` verifies the properties of the network graph, sets reference nodes for multiple disconnected networks, creates contingency scenarios and manages settings of phase shifting transformers.

The verified and pre-processed data is then used by the `GridModel` and `MarketModel` modules to provide the input data for the model core. Based on the market model that is desired from the user (and that is feasible given the available data), `GridModel` uses the data provided from `GridTopology` and `DataManagement` to compile the correct grid representation with all physical properties. This includes the parametrization of the network constraints, as discussed in Section 2.2.1 above, as well as generator locations, cost models, and zonal configurations. Also, `GridModel` calls `RedundancyRemoval` in the process of compiling the set of parameters for a N-1 secure dispatch. If this algorithm has been performed in previous runs, `GridModel` loads available parameters to avoid time-consuming re-runs. These parameters define the constraints under which the market has to be cleared. Finally, `MarketModel` collects these constraints and manages the required model runs. After the optimization in the model core has obtained an optimal solution, `MarketModel` instantiates a new `Results` object in the `DataManagement` module. Communication between the POMATO instance and the mathematical core is achieved via a threaded process within the `JuliaDaemon` module, see Remark 4.

The decoupling of model runs and data processing allows to efficiently solve multi-stage market clearing processes that iterate between different market model configurations. Two relevant examples are itemized below.

Ex. 1 - *Redispatch Analysis:* Zonal electricity markets are cleared as a single price zone without any internal network constraints. In a second stage, potential transmission line overloads are rectified by out-of-market CM measures, i.e., redispatch. For this purpose, a second model run with nodal resolution is required.

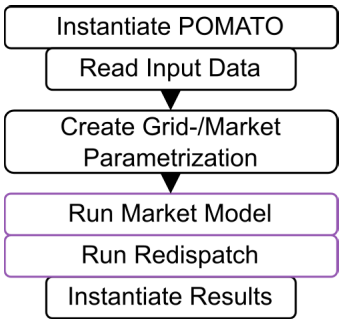

Ex. 2 - *FBMC:* FBMC uses a forecasted nodal dispatch (base case) to derive zonal PTDF matrices that establish the relation between zonal net-positions and flows on critical network elements, critical network elements and contingencies (CNECs). The resulting feasible region of net-positions with respect to the technical limits of the CNECs are called *FBMC domains*. These domains are used to solve the zonal market clearing that is then corrected by subsequent CM measures. The supplementary `FBMCModule` automatizes the necessary re-parametrization of parts of the model data, including the generation of the *FBMC domains* depicted in Figure 2.2, and facilitates the necessary re-runs of the optimization model.

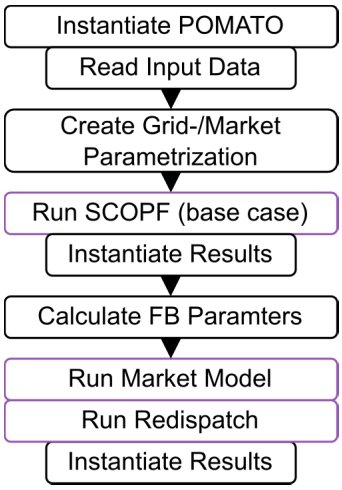

Remark 3 (Contingency Scenarios). Alternatively to a strict N-1 contingency analyses, i.e., protecting the system against the outage of every single transmission line, the user can specify customized contingency scenarios. Such scenarios can either ignore certain lines as potential contingencies or define contingency groups of outages that are likely to occur simultaneously, e.g., parallel lines.

Remark 4 (Python-Julia Interface). Communication between the Julia language and Python is implemented by a `JuliaDaemon` class that maintains a threaded Julia program

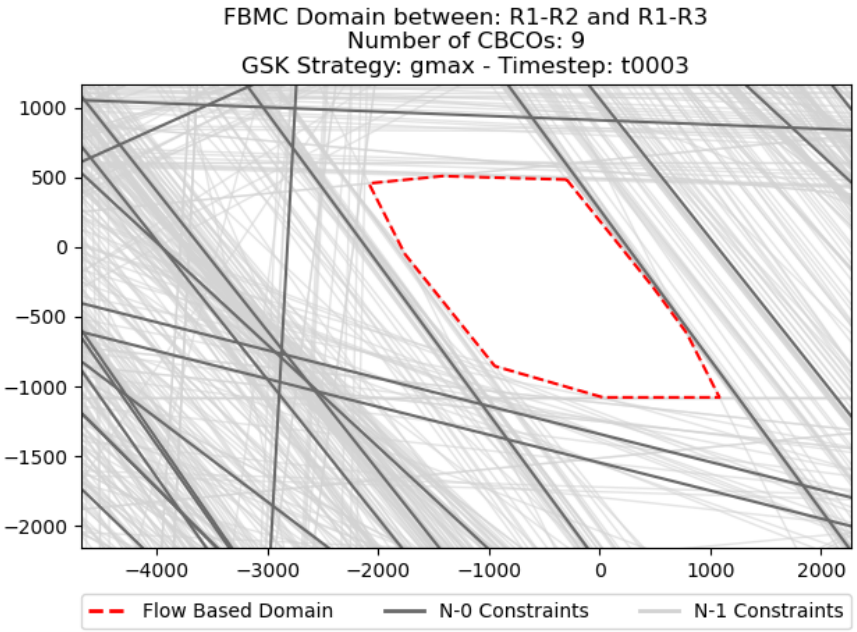

Figure 2.2: Exemplary Flow Based Domain

and executes its functions when requested by `MarketModel` or `GridModel`. Instructions are transferred via *json* files that are written to the POMATO package folder. This way, the Julia process has to be started only once and remains alive after a model is completed, which allows fast re-solving of a model with different parameters.

2.2.3 User Interface

All modules of the data processing layer presented in previous Section 2.2.2 are attributed to the overall POMATO object, which provides a comprehensive set of functions to the user. Although the methods of the lower level modules are accessible to the user, the POMATO module provides predefined methods for the typical use cases of this program. A brief overview is presented in the illustrative application in Section 2.3. Additionally, POMATO provides a collection of visualization features. Its `create_geo_plot` method shows market and redispatch results including prices on an interactive map using the *Ploty*[12] library. Many results, such as the FBMC domains or generation schedules, can be automatically plotted as a collection of interactive 2D diagrams. In addition, POMATO

[12] plotly.com

can start a *Dash*[13] server, featuring a curated view of interactive plots and visualisations. See documentation[14] or www.pomato.io/dashboard.html for a live online demo.

2.2.4 Publication

POMATO is available under the *LGPLv3* license on GitHub including a comprehensive documentation (Weinhold 2020b, 2020a). To facilitate testing, maintenance and readability, POMATO's Python and Julia components are stored in separate repositories. However, all installation is handled by the central Python module in Weinhold (2020b). See also Remark 5.

The repository also includes exemplary data-sets that cover the core functionality. These include a data-set for the German power system, that has been compiled to showcase POMATO's functionality, as well as the NREL 118 bus network (Pena, Martinez-Anido, and Hodge 2017), and Matpower case files. More details on how to create custom data-sets can be found in the accompanying documentation[15].

Remark 5. (Installation) POMATO requires Python and Julia to be installed. When both are available on the user's system the installation of POMATO is managed through Python via pip[16]. The Python installer will detect the Julia distribution on the system and automatically pull the two Julia packages, `MarketModel` and `RedundancyRemoval` from their separate repositories. They will be installed in a Julia virtual environment to isolate any dependencies from possible user installed Julia packages.

2.3 Illustrative Application

This section illustrates the application of POMATO and the corresponding example code is shown below and its line numbers are referenced in the subsequent description.

```
1 from pomato import POMATO
2
3 mato = POMATO(wdir=wdir, options_file="options/de.json")
4 mato.load_data('data_input/DE_2020.zip')
5
6 mato.create_grid_representation()
7 mato.run_market_model()
```

[13] plotly.com/dash/
[14] pomato.readthedocs.io/en/latest/model_functionality.html#the-dashboard
[15] pomato.readthedocs.io/en/latest/input_model_data.html
[16] pip.pypa.io

```
8
9  market_result, redispatch_result = mato.data.return_results()
10
11 # Check for Overloaded lines N-0
12 n0_m, _ = market_result.overloaded_lines_n_0()
13 print("Number of N-0 Overloads: ", len(n0_m))
14 n0_r, _  = redispatch_result.overloaded_lines_n_0()
15 print("Number of N-0 Overloads: ", len(n0_r))
16 n1_r, _  = redispatch_result.overloaded_lines_n_1()
17 print("Number of N-1 Overloads: ", len(n1_r))
18
19 gen = redispatch_result.redispatch()
20 print("Total Redispatch in MWh: ", gen.delta_abs. sum())
21
22 mato.visualization.create_geo_plot(redispatch_result,
23                                    show_prices=True,
24                                    show_redispatch=True)
```

After importing the POMATO module in line `1`, a new POMATO class is instantiated in line `3` with the requested working directory (`wdir`) and an options file in the JSON[17] format that configures the model run. In this example the options file specifies a zonal market clearing, subject to NTCs, and subsequent redispatch with redispatch-cost and model horizon:

```
1  {"optimization": {
2    "type": "ntc",
3    "model_horizon": [0, 168],
4    "redispatch": {
5      "include": true,
6      "cost": 50}}
```

A comprehensive list and descriptions of possible configurations can be found in the online documentation[18]. In line `4` the POMATO object loads the required data, which automatically instantiates the data management objects as described in Section 2.2.2 above. The command in line `6` creates the grid representation for the specified model run and line `7` starts the actual model run. After successful completion, two `Results` are instantiated into `DataManagement` and are available to the user (see line `9`) for further

[17] www.json.org
[18] pomato.readthedocs.io/en/latest/options.html

analysis, e.g., to check for overloaded lines with and without contingencies (see lines 11–20). Finally a geo-plot is created in line 22, which yields Figure 2.3.

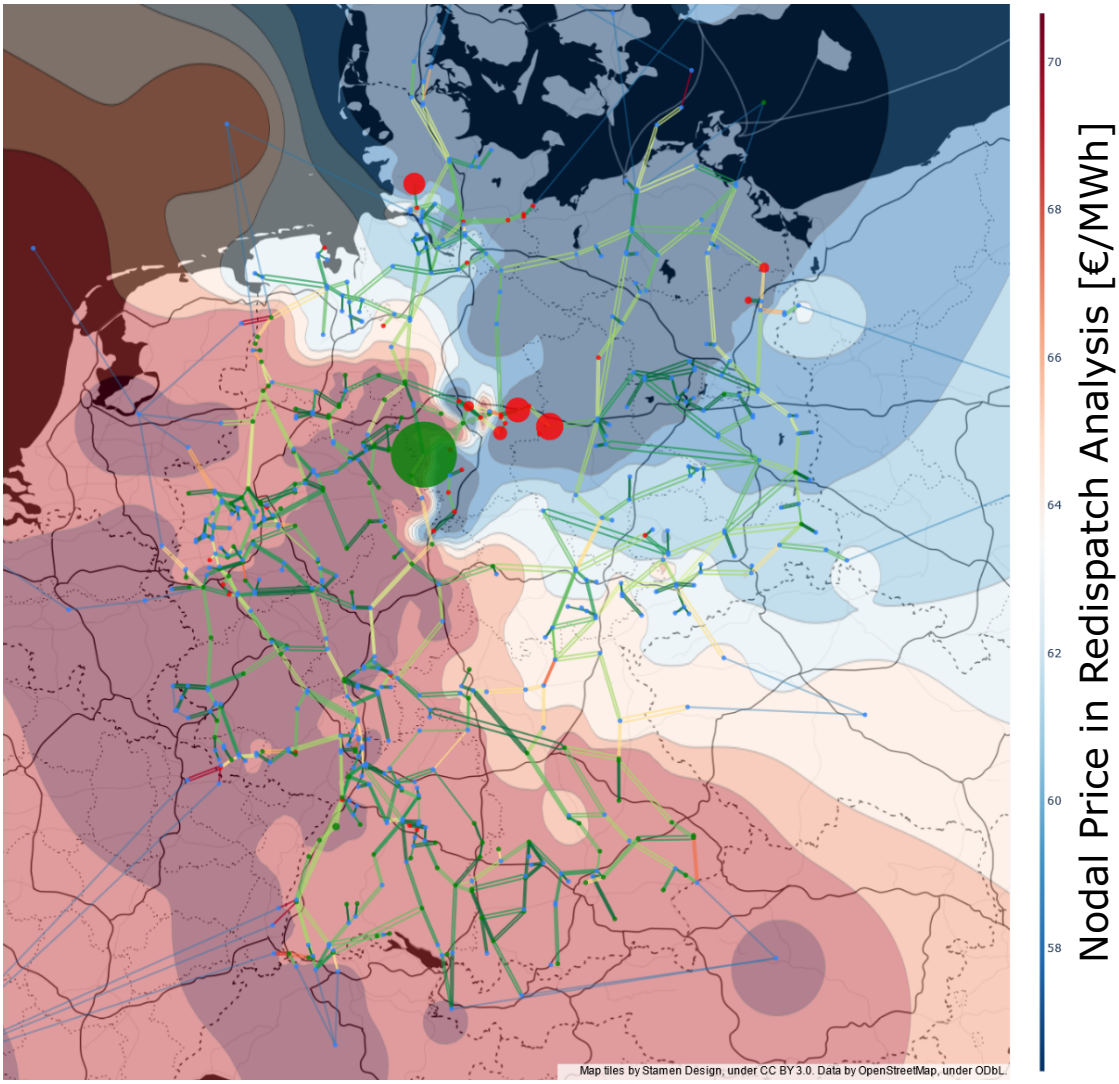

Figure 2.3: Geo-plot of market- and redispatch result for Germany. Red and green circles indicate negative and positive changes in generation schedules, respectively, due to redispatch. Change magnitude are proportional to the circles' radius. Line colors indicate average line load where green is low loads and red is high load. Prices as dual multipliers on the nodal power balances of the redispatch run are indicated by the contour plot overlay.

Execution time of this example is around 7.5 minutes, including data read-in, Julia start-up, solving both the market- and the redispatch problem, as well as the final result

analysis and plotting. Subsequent runs benefit from already active Julia processes, which saves 2 to 4 minutes of computation time.

2.4 Impact

POMATO offers features that may be of interest for practitioners, researchers and students alike, all of which benefit from POMATO's open-source availability.

- The high-level API-like functionality of the top-layer POMATO class (see Section 2.2.3) facilitates the use of POMATO without a detailed understanding of power engineering and economics. With minimal understanding of the required data structure, POMATO offers a low barrier for users to obtain relevant results from their own data sets and to produce insightful visualizations of these results.
- By separating the model core from the user interface, more advanced users will be able to extend or modify the mathematical formulations for their needs, which we hope to enable new research in the area of zonal market clearing.
- Advanced interactive visualizations can support educators to convey some concepts of power system operations and electricity markets.

2.5 Conclusion and further development

This paper presents a tool that aims to enable the broad analyses of zonal electricity markets. The proposed Power Market Tool POMATO is open-source, provides essential data-sets and comprehensive online documentation. Central to POMATO's functionality is its ability to synthesize the flow-based market-coupling (FBMC) process. Further POMATO includes a redundancy removal algorithm that enables security constrained (N-k) dispatch with feasible computation times. While the current version of POMATO already includes prototypical options for the analyses of stochastic (chance-constrained) market clearing, extensions to stochastic and risk-aware markets and power flow analyses along the lines of Dvorkin (2020) and Mieth, Kim, and Dvorkin (2020) are subject to ongoing development.

Chapter 3

Fast Security-Constrained Optimal Power Flow through Low-Impact and Redundancy Screening

"Take me to the power plant.
I'm on a mission for fission."

(Homer Simpson)

The contents of this chapter have been published in IEEE Transactions on Power Systems (Volume: 35, Issue: 6), Weinhold and Mieth (2020a).
 Appendix A contains the original appendix to this publication. For this dissertation the original article has been adapted to ensure consistent notation and format.

3.1 Introduction

Power flow physics and transmission limits constrain electricity market transactions. With increasing uncertainty, mainly driven by the proliferation of intermittent renewable generation, a precise calculation of securely available transmission capacity can improve market efficiency and system reliability, (ENTSO-E 2019). For example, in 2015 the transmission system operators (TSOs) of Central Western European (CWE) inaugurated flow-based market coupling (FBMC) to manage cross-border electricity trading on the shared transmission infrastructure, "*bringing commercial transactions closer to the physical reality*", (Amprion 2019). As a result, FBMC introduces operative security considerations into the market clearing process by identifying critical network elements and outage scenarios (contingencies), so called critical branch under critical outages (CBCOs), (Van den Bergh, Boury, and Delarue 2016). The identification of these CBCOs requires power flow optimization with contingency scenarios and is therefore closely related to solving a security-constrained optimal power flow (SCOPF). As FBMC represents a significant part of the market clearing in Europe (Schönheit, Weinhold, and Dierstein 2020), studies on its interconnected markets need some means of accommodating a representation of the security constrained transmission infrastructure. To enable multiperiod market simulations that internalize physical network constraints with contingency scenarios, this paper proposes a method that identifies the minimal set of constraints that defines the solution space spanned by the transmission and contingency constraints. Once acquired, this set can be used to significantly reduce the computational effort of solving SCOPF problems on this network.

3.1.1 Related literature

Since its introduction in Alsac and Stott (1974), SCOPF and its solution has been studied extensively. Solving a full SCOPF problem in practice is typically obstructed by the dimensions of the resulting numerical problem and its computational complexity, (Capitanescu et al. 2011). However, it is well known that only a limited subset of credible contingencies will eventually be active at the optimal solution (Bouffard, Galiana, and Arroyo 2005). Leveraging the fact that a candidate solution can easily be checked for feasibility, standard state-of-the-art approaches rely on iteratively adding contingency scenarios to a reduced base problem. This method was proposed in Alsac and Stott (1974) and Stott and Hobson (1978) and has since been improved and extended, e.g. by more efficient constraint selection methods based on line loading (Wood and Wollenberg

1996), impact bounds (Brandwajn 1988), or a ranking of corrective actions (Fliscounakis et al. 2013). Further extensions towards corrective control actions have been proposed, e.g. in Capitanescu and Wehenkel (2008) and Karangelos and Wehenkel (2019) include the risk of failure of these actions. To decrease solution time, decomposition techniques based on Bender's Decomposition, (Li and McCalley 2008; Phan and Kalagnanam 2013; Dvorkin et al. 2016a; Velloso, Van Hentenryck, and Johnson 2019), or decentralized optimization based on the Alternating Direction Method of Multipliers (ADMM) (Phan and Kalagnanam 2013; Chakrabarti et al. 2014), have been proposed. Departing from the iterative solution approach, recent work in Thams et al. (2017) and Halilbašić et al. (2018) use data-driven decision making trees to map contingencies to conditional line transfer capacities that ensure secure and stable post-contingency operation.

The methods in Stott and Hobson (1978), Wood and Wollenberg (1996), Brandwajn (1988), Fliscounakis et al. (2013), Capitanescu and Wehenkel (2008), Li and McCalley (2008), Dvorkin et al. (2016a), Velloso, Van Hentenryck, and Johnson (2019), Phan and Kalagnanam (2013), Chakrabarti et al. (2014), Chakrabarti and Baldick (2020), Thams et al. (2017), and Halilbašić et al. (2018) are concerned with the solution of a specific instance of the SCOPF problem. As such, they can be feasible in the context of day-to-day operational computations, but might be too complex for simulations that require solving an SCOPF for multiple time steps, even under the DC power flow assumption. Alternatively, the SCOPF can be simplified by identifying constraints that are never active (redundant). Respective methods haven been proposed in the context of network-constrained unit commitment without contingencies, e.g. in (Zhai et al. 2010; Hua et al. 2013; Roald and Molzahn 2019; Pineda, Morales, and Jimenez-Cordero 2020). In the context of a mixed-integer security constrained unit commitment problem, (Madani, Lavaei, and Baldick 2016) define bounds on the decision variables and then identify constraints that are redundant given these bounds. A two step method combining a data-driven pre-screening and an iterative reintroduction of previously discarded constraints was proposed in (Zhang et al. 2019).

Our approach in this paper is closest related to the notion of "umbrella contingencies", which have been introduced in Bouffard, Galiana, and Arroyo (2005). This contingency (sub)set contains the most restrictive outages that cover for all other possible outages implicitly and is independent from case-specific objective functions and uncertain parameters, such as load profiles or renewable generation. While computing the SCOPF with this subset of contingencies has been shown to significantly reduce its solve time, identifying this set, on the other hand, is itself obstructed by impractically high computational

effort. To improve umbrella constraint discovery, network partitioning to enable parallel computation (Ardakani and François Bouffard 2013), and approximate pre-processing (Ardakani and Francois Bouffard 2015), has been proposed. However, these approaches require an additional layer of implementation and the results are sensitive to the partitioning method. In Ardakani and François Bouffard (2018) neural networks are proposed to predict umbrella constraints if system conditions change, but this requires previous identification of training sets.

3.1.2 Contributions

Similar to Ardakani and Francois Bouffard (2015) and Ardakani and François Bouffard (2013), this paper proposes a method to identify a minimal set of constraints that exactly represent the space of feasible nodal injections defined by the transmission system and its contingency scenarios. Relative to Ardakani and Francois Bouffard (2015) and Ardakani and François Bouffard (2013) we improve the discovery of this minimal set by leveraging a geometric algorithm based on Clarkson (1994) that scales better and avoids additional preprocessing. Also, no pre-generated or historical samples are required. The resulting minimal set directly relates to the CBCOs, as it collects constraints of transmission lines that are critical under some critical outages.

Additionally, we demonstrate two methods that further reduce the number of necessary constraints, such that the time needed to identify these constraints and the solve time of the subsequent SCOPFs is further decreased. First, we propose to only include constraints that are non-redundant under the condition that the nodal injection at each node does not exceed predefined technical limits. In geometric terms, these technical nodal injection limits add additional cuts to the SCOPFs solution space and generally remove more than one of the CBCO-related constraints. Second, we show how a large number of constraints can be ignored, if the impact of contingencies on line flows is below a certain threshold and relate this approach to the common operational practice of security margins. The threshold choice is discussed in terms on its impact on the SCOPFs solution.

The proposed methods have been implemented in an open-source framework, which is tailored to enable comprehensive analyses of the European power system and markets with flow-based market coupling (FBMC) market clearing (Weinhold and Mieth 2020b). To showcase the performance of the proposed methods, we conduct numerical experiments on the illustrative IEEE 118 bus system, on two real-world data-sets of the German and European power system, and on the A&M synthetic 2000 bus network.

Finally, we discuss scalability and practical implementation.

3.2 Problem Formulation

In this paper we consider a preventive SCOPFs problem on multiple time steps $t \in \mathcal{T}$. As common for this type of analyses we leverage the DC power flow approximation (Capitanescu et al. 2011; Ardakani and François Bouffard 2013), to derive a linear relationship between nodal active power injections, contingencies and line flows.

3.2.1 Power flow preliminaries

The physical network is represented by the set of nodes $\mathcal{N}$ with $N = |\mathcal{N}|$, the set of generators $\mathcal{G}$ with $G = |\mathcal{G}|$ and the set of lines $\mathcal{L}$ with $L = |\mathcal{L}|$. Vector g_t indexed by $g_{t,i} \geq 0$ denotes the active power generation of each generator i and vector d_t indexed by $d_{t,n} \leq 0$ denotes the aggregated active demand at each node $n \in \mathcal{N}$ at time t. At every time t the vector of nodal injections is given by

$$x_t = d_t + M g_t \tag{3.1}$$

indexed by $x_{t,n}$ where M is a mapping of generators to nodes. Upper and lower generation limits are given by $\overline{g}_t$ and $\underline{g}_t$ indexed by $\overline{g}_{t,i}$ and $\underline{g}_{t,i}$ respectively. Each line $l \in \mathcal{L}$ is a directed connection with arbitrary but fixed orientation between one sending node s and one receiving node r. At each time t positive flow $f_{t,l} \geq 0$ indicates active power flow from s to r and negative flow $f_{t,l} \leq 0$ indicates active power flow from r to s over line l. For all $l \in \mathcal{L}$ the power flows are collected in the vector f_t indexed by $f_{t,l}$ and the line capacities are given by vector $\overline{f}$ indexed by $\overline{f}_l$. The physical power flow equations are approximated by power transmission distribution factors (PTDFs) where the PTDF matrix $B^0 \in \mathbb{R}^{L \times N}$ is a linear mapping of nodal injections x_t to power flows f_t such that:

$$f_t = B^0 x_t. \tag{3.2}$$

We refer the interested reader to Appendix A.1.1 for a derivation of the PTDF matrix. Superscript 0 denotes the base-case PTDF, i.e. the pre-contingency case with no unplanned outage

3.2.2 Contingency preliminaries

Consider a contingency scenario c such that $\mathcal{L}_c \subseteq \mathcal{L}$ is the set of one or multiple lines that experience an unplanned outage. The post-contingency flow along any line $l \notin \mathcal{L}_c$ is determined by line outage distribution factor $\text{LODF}_{l\mathcal{L}_c} \in \mathbb{R}^{1\times|\mathcal{L}_c|}$ such that:

$$f^c_{t,l} = f^0_{t,l} + \text{LODF}_{l\mathcal{L}_c} f^0_{t,\mathcal{L}_c}, \tag{3.3}$$

where $f^c_{t,l}$ is the flow on line l in outage scenario c, and $f^0_{t,l}$ is the pre-contingency flow on line l and $f^0_{t,\mathcal{L}_c}$ is the vector of pre-contingency line flows of lines $\mathcal{L}_c$ at time t. Note that any entry in $\text{LODF}_{l\mathcal{L}_c}$ can be either positive or negative. For the derivations of the load outage distribution factors (LODFs) we refer the interested reader to Appendix A.1.2. For every possible contingency $c \in \mathcal{C}$ indexed by $c = \{1, ..., C\}$ we use these sensitivity factors to define contingency-PTDF matrices B^c as:

$$B^c = B^0 + \begin{bmatrix} \text{LODF}_{1\mathcal{L}_c} B^0_{\mathcal{L}_c} \\ \text{LODF}_{2\mathcal{L}_c} B^0_{\mathcal{L}_c} \\ \vdots \\ \text{LODF}_{L\mathcal{L}_c} B^0_{\mathcal{L}_c} \end{bmatrix}, \quad \forall c \in \mathcal{C}, \tag{3.4}$$

where $B^0_{\mathcal{L}_c}$ is the $|\mathcal{L}_c| \times N$ matrix collecting the rows of B^0 corresponding to the outages in c. Given a vector of nodal injections x_t the resulting post-contingency power flows after outage c can be computed as:

$$f^c_t = B^c x_t. \tag{3.5}$$

Note that the formulations and methodologies in this paper can be extended to accommodate generator contingencies, if they allow a linear representation, e.g. as shown in Madani, Lavaei, and Baldick (2016).

3.2.3 Security constrained optimal power flow

We consider a multi-period preventive OPF as:

$$\min_{g,x} \sum_{t\in\mathcal{T}} C(g_t) \tag{3.6a}$$

$$\text{s.t.} \quad d_t + Mg_t = x_t \qquad \forall t \in \mathcal{T} \tag{3.6b}$$

$$e^\top x_t = 0 \qquad \forall t \in \mathcal{T} \tag{3.6c}$$

$$\underline{g}_t \leq g_t \leq \overline{g}_t \qquad \forall t \in \mathcal{T} \tag{3.6d}$$

$$-\overline{f}^0 \leq B^0 x_t \leq \overline{f}^0 \qquad \forall t \in \mathcal{T} \tag{3.6e}$$

$$-\overline{f}^c \leq B^c x_t \leq \overline{f}^c \qquad \forall t \in \mathcal{T}, \forall c \in \mathcal{C}. \tag{3.6f}$$

Objective (3.6a) minimizes the cost of generation given by cost-function $C(g_t)$. Eqs. (3.6b) and (3.6c) enforce the nodal and global power balances. Eq. (3.6d) imposes limits on the active power output of the generators. Eqs. (3.6e) and (3.6f) enforce that no line is overloaded due to the resulting power flow for the base case and every contingency. Thus, (3.6e) and (3.6f) define the feasible region of nodal injections given base and contingency PTDFs, and the thermal line flow limits:

$$\mathcal{F}(B, \overline{f}) = \{x : -\overline{f} \leq Bx \leq \overline{f}\}, \tag{3.7}$$

where

$$B = \begin{bmatrix} B^0 \\ B^1 \\ \vdots \\ B^C \end{bmatrix}, \quad \bar{f} = \begin{bmatrix} \bar{f}^0 \\ \bar{f}^1 \\ \vdots \\ \bar{f}^C \end{bmatrix}. \tag{3.8}$$

Using (3.7), (3.8) the following formulation is equivalent to (3.6):

$$\min \sum_{t \in \mathcal{T}} C(g_t) \tag{3.9a}$$

$$\text{s.t.} \quad \text{(3.6b)–(3.6d)} \tag{3.9b}$$

$$x_t \in \mathcal{F}(B, \overline{f}) \qquad \forall t \in \mathcal{T}. \tag{3.9c}$$

Remark 6. As (3.9c) constrains the vector of nodal injections x_t to be within the feasible region defined by the network capacity and its contingency scenarios, it is independent from both the objective function and other constraints on x_t. Here the constraints in (3.9b) only capture the power balances and the technical generator constraints. However, other constraints e.g. inter-temporal constraints (e.g. to model storages) or generation related binary variables (e.g. to model unit-commitment) can be included without af-

fecting (3.9c).

To reflect the upper and lower bounds of feasible region $\mathcal{F}(B, \overline{f})$, each PTDF matrix $B^0, \ldots, B^C$ introduces $2L$ linear inequalities to the problem. Thus, even the least complex set of N-1 contingencies, i.e. only one simultaneous outage, requires $2L(L+1)$ inequalities to define feasible region $\mathcal{F}(B, \overline{f})$. Furthermore, this set of inequalities has to be evaluated for every time step t to solve (3.6). Therefore, the resulting problem size quickly becomes computationally intractable with increasing system size and more complex contingency scenarios. However, it has been shown that only a subset of these inequalities is necessary to sufficiently define $\mathcal{F}(B, \overline{f})$ (Bouffard, Galiana, and Arroyo 2005), thus reducing computational complexity. In the following section we propose a procedure that discovers the minimal set of inequalities (constraints) based on endogenous model parameters and exogenous data characteristics.

3.3 Redundancy Screening

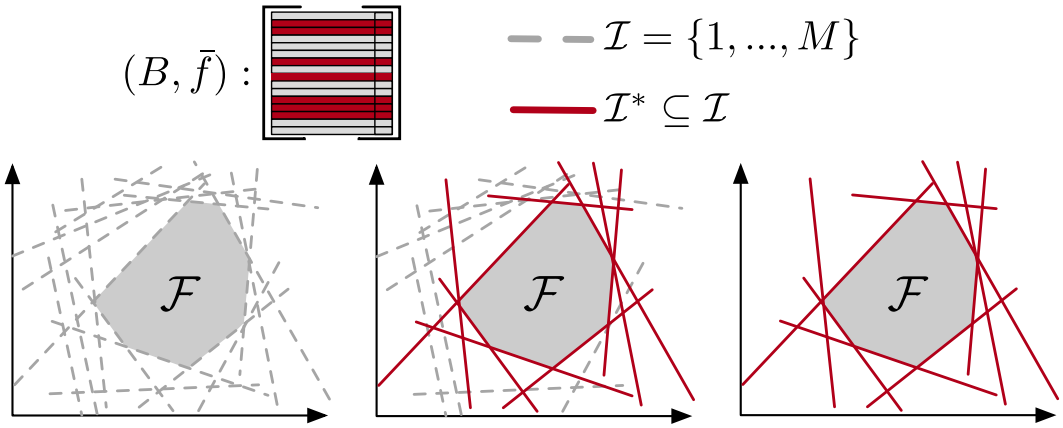

Figure 3.1: Schematic representation of the equivalent description of a feasible region $\mathcal{F}(B, \overline{f}, \mathcal{I})$ by $\mathcal{F}(B, \overline{f}, \mathcal{I}^*)$ where $\mathcal{I} = \{1, ..., M\}$ is the set of all indices of system $(B, \bar{f})$ and $\mathcal{I}^* \subseteq \mathcal{I}$ is the essential set of indices.

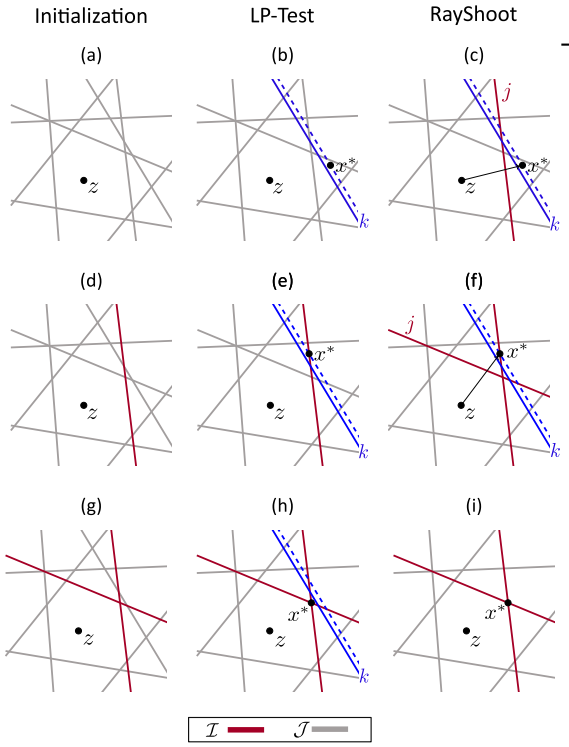

Algorithm 1: `RedundancyRemoval`$(B, \overline{f}, z)$

input : System of inequalities given by B and $\overline{f}$, Interior point z
output: Returns the set $\mathcal{I}$ of non-redundant inequality indices of the system $Bx \leq \overline{f}$

begin
  $\mathcal{I} \leftarrow \emptyset$; `// Set of essential indices`
  $\mathcal{J} \leftarrow \{1, ..., M\}$; `// Indices to check`
  while $|\mathcal{J}| > 0$ **do**
    select an index k from $\mathcal{J}$;
    $(p^*, x^*) \leftarrow$ **solve** LPTest$(B, \overline{f}, \mathcal{I} \cup \{k\}, k)$;
    if $\exists x^*$ ***and*** $p^* > \overline{f}_k$ **then**
      $\alpha \leftarrow true$;
      $j \leftarrow$ `RayShoot`$(B, \overline{f}, z, x^*)$;
      `// Returns an essential index`
    else
      $\alpha \leftarrow false$;
    end
    if α **then**
      $\mathcal{I} \leftarrow \mathcal{I} \cup \{j\}$; `// Update essential`
      $\mathcal{J} \leftarrow \mathcal{J} \setminus \{j\}$; `// Remove checked`
    else
      $\mathcal{J} \leftarrow \mathcal{J} \setminus \{k\}$; `// Remove checked`
    end
  end
  return $\mathcal{I}$
end

Figure 3.2: Graphical (left) and algorithmic (right) itemization of essential set discovery procedure, where each row in the graphic corresponds to one iteration step of the algorithm and each column corresponds to one specific task that is performed in each iteration (as given by the column headers). Gray lines represent the constraints with indices to be checked, red lines represent the found essential constraints, blue solid lines represent the constraint that is checked in the current iteration and blue dashed lines represent the corresponding relaxed constraint $(\overline{f}_k + 1)$, see (3.11). (a) Initial state with $\mathcal{J} = \{1, ..., M\}$, $\mathcal{I} = \emptyset$ and z some interior point; (b) Some index k is selected from $\mathcal{J}$ and LP-Test$(B, \overline{f}, \mathcal{I}, k)$ is performed; (c) Because $\mathcal{I}$ is empty in the initial iteration k is always non-redundant against $\mathcal{I}$ and the most restricting constraint j in the direction of $(x^* - z)$ is added to $\mathcal{I}$; (d) The next iteration starts with $\mathcal{I}$ now containing one essential index; (e) Because k was non-redundant in the last step, it remains selected and LP-Test$(B, \overline{f}, \mathcal{I}, k)$ is performed; (f) Now, k is again non-redundant against $\mathcal{I}$ and the most restricting constraint j in the direction of $(x^* - z)$ is added to $\mathcal{I}$; (g) The next iteration starts with $\mathcal{I}$ now containing two essential indices; (h) Because k was non-redundant in the last step, it remains selected and LP-Test$(B, \overline{f}, \mathcal{I}, k)$ is performed; (i) Index k is now redundant against set $\mathcal{I}$ and is therefore removed from set $\mathcal{J}$; The procedure repeats until all elements have been removed from $\mathcal{J}$.

We consider the set of feasible solutions (feasible region) $\mathcal{F}(B, \overline{f})$ to a linear program (LP) defined by system ($B \in \mathbb{R}^{M \times N}, \overline{f} \in \mathbb{R}^M$) with $M > N$ and set of indices $\mathcal{I}$ such that:

$$\mathcal{F}(B, \overline{f}, \mathcal{I}) = \{x \in \mathbb{R}^N : B_i x \leq \overline{f}_i, \forall i \in \mathcal{I}\}, \tag{3.10}$$

where B_i is the i-th row of matrix B and $\overline{f}_i$ is the i-th entry of vector $\overline{f}$. If follows from (3.10) that if $\mathcal{I} = \{1, ..., M\}$, then $\mathcal{F}(B, \overline{f}, \mathcal{I}) = \{x : Bx \leq \overline{f}\} = \mathcal{F}(B, \overline{f})$.

Definition 1 (Non-redundant/Redundant Index)**.** Index $k \in \mathcal{I}$ is called *non-redundant* against set of indices $\mathcal{I}$ if $\mathcal{F}(B, \overline{f}, \mathcal{I})$ changes when index k is removed from $\mathcal{I}$:

$$k \in \mathcal{I} \text{ is non-redundant iff } \mathcal{F}(B, \overline{f}, \mathcal{I} \setminus \{k\}) \neq \mathcal{F}(B, \overline{f}, \mathcal{I}).$$

In analogy, index $k \in \mathcal{I}$ is called *redundant* if $\mathcal{F}(B, \overline{f}, \mathcal{I})$ does not change when k is removed from $\mathcal{I}$:

$$k \in \mathcal{I} \text{ is redundant iff } \mathcal{F}(B, \overline{f}, \mathcal{I} \setminus \{k\}) = \mathcal{F}(B, \overline{f}, \mathcal{I}).$$

Definition 2 (Essential Set/Index)**.** A set of indices $\mathcal{I}^* \subseteq \{1, ..., M\}$ is called *essential* to the system $(B, \overline{f})$ if it contains all indices that are non-redundant against all indices $\{1, ..., M\}$ of this system. In other words, no $k \in \mathcal{I}^*$ can be removed from $\mathcal{I}^*$ without changing $\mathcal{F}(B, \overline{f}, \mathcal{I}^*)$ and $\mathcal{F}(B, \overline{f}, \mathcal{I}^*) = \{x : Bx \leq \overline{f}\}$. Accordingly, any index $k \in \mathcal{I}^*$ is called essential index.

Fig. 3.1 schematically illustrates a region $\mathcal{F}(B, \overline{f})$ defined by a redundant system $(B, \bar{f})$ and indicates the relation between essential and non-essential indices.

3.3.1 Essential set identification

To identify essential set $\mathcal{I}^*$, first we require a procedure that determines whether or not index k is redundant in $\mathcal{F}(B, \overline{f}, \mathcal{I})$. Following Fukuda 2016, Proposition 8.5, $k \in \mathcal{I}$ is non-redundant if and only if the optimal solution x^* and the corresponding optimal value

p^* of the LP:

$$\text{LP-Test}(B, \overline{f}, \mathcal{I}, k): \quad p^* = \max_x B_k x \tag{3.11a}$$

$$\text{s.t.} \quad B_i x \leq \overline{f}_i \quad \forall i \in \mathcal{I} \setminus \{k\} \tag{3.11b}$$

$$B_k x \leq \overline{f}_k + 1 \tag{3.11c}$$

is strictly greater than $\overline{f}_k$. Note that LP-Test will always find an optimal solution since set $\mathcal{F} \neq \emptyset$ because it always contains at least 0. Using the LP-Test as given in (3.11), it is possible to identify essential set $\mathcal{I}^*$ by running LP-Test$(B, \overline{f}, \mathcal{I}, k)$ with $\mathcal{I} = \{1, ..., M\}$ for all $k \in \mathcal{I}$. However, this requires solving a M-dimensional LP M times. This complexity can be significantly reduced by populating $\mathcal{I}$ iteratively with identified essential indices, instead of always checking against complete set $\mathcal{I} = \{1, ..., M\}$ (Szedlak 2017; Clarkson 1994).

The resulting iterative process `RedundancyRemoval` is illustrated in Fig. 3.2. The procedure takes system $(B, \bar{f})$ and an interior point $z \in \mathcal{F}^\circ(B, \overline{f})$ as input and returns set $\mathcal{I}^*$ of essential indices of system $(B, \bar{f})$. Here $\mathcal{F}(B, \overline{f})$ defines the feasible region of nodal injection vectors with respect to transmission limits and contingency scenarios. Therefore, $z = 0$ will always be a point in the interior of this region, because zero nodal injections and thus zero-flows are always a solution to the power flow equations. The procedure is initialized with empty set $\mathcal{I} = \emptyset$, which is iteratively filled with essential indices, and the full set $\mathcal{J} = \{1, ..., M\}$, which stores all indices that have to be checked. First, the procedure randomly selects an unchecked index k from $\mathcal{J}$ and solves the LP-Test$(B, \overline{f}, \mathcal{I} \cup \{k\}, k)$, which returns p^* and x^* as per (3.11). If the LP-Test returns an objective value $p^* > \bar{f}_k$, then $\mathcal{I}$ does not yet contain the index of a constraint that restricts $\mathcal{F}(B, \bar{f}, \mathcal{I})$ in the direction of $x^* - z$, see Fig. 3.2 b). However, because set $\mathcal{I}$ is initialized empty, indices can be non-redundant against $\mathcal{I}$ but not essential to $(B, \overline{f})$. In other words, there might exist a constraint with index j in the direction of $x^* - z$ that is more restrictive than the constraint with index k. As shown in Fig. 3.2 c), the auxiliary procedure `RayShoot` identifies this most restrictive constraint in the direction of $x^* - z$ by shooting a ray from z in the direction of $x^* - z$ and returning index j of the first hyperplane $\{x : B_j x = \overline{f}_j\}$ that it crosses. This index j is guaranteed to be an essential index of $(B, \bar{f})$ and is thus added to $\mathcal{I}$ and removed from $\mathcal{J}$. See Appendix A.1.3 for a detailed description of `RayShoot`. Note that if $j \neq k$, then k remains in $\mathcal{J}$ to be checked again, see Fig. 3.2 e). If LP-Test$(B, \overline{f}, \mathcal{I} \cup \{k\}, k)$ determines k to

be redundant against $\mathcal{I}$, see Fig. 3.2 h), then k is guaranteed to be not essential because $\mathcal{I}$ only contains essential indices. In this case, no new essential index has been found and k is removed from $\mathcal{J}$, see Fig. 3.2 i). The process is repeated until $\mathcal{J}$ is empty, thus guaranteeing a termination of the algorithm in finite time. The resulting set $\mathcal{I}$ contains all essential indices and therefore $\mathcal{I} = \mathcal{I}^*$ (Szedlak 2017, Theorem 2.2.1). This essential set $\mathcal{I}^*$ is a minimal representation of the contingency feasible region, see (3.7), and each essential index represents a specific critical line under a specific outage and therefore can be denoted as a minimal set of CBCOs.

While the complexity of `RedundancyRemoval` remains dominated by the LP-Test, it is now performed M times with *at most* $|\mathcal{I}^*|$ constraints. The worst-case performance of `RedundancyRemoval` occurs when all essential indices are found in the first $|\mathcal{I}^*|$ iterations. Then, LP-Test is performed $|\mathcal{I}^*|$ times with less than $|\mathcal{I}^*|$ constraints and $M - |\mathcal{I}^*|$ times with $|\mathcal{I}^*|$ constraints. The `RayShoot` procedure performs basic vector calculations in the $\mathbb{R}^{M\times N}$ space and is performed $|\mathcal{I}^*|$ times. Thus, its complexity is linear against MN and dominated by the complexity of LP-Test.

Remark 7. The capacity of a line is independent from the direction of the flow, which leads to identical constraints on the nodal injections for the upper and the lower bound but with reversed sign. Therefore, an essential set related to the upper bounds directly corresponds to an essential set for the lower bounds and it is sufficient to perform the `RedundancyRemoval` only on the positive PTDF matrices to speed-up the essential set identification.

3.3.2 Conditional redundancy

The essential set identification as presented in previous Section 3.3.1 only depends on redundancies that are inherent to system $(B, \bar{f})$, i.e. that are given by the power flow limits and contingency scenarios as in (3.7)–(3.9). Thus, resulting essential set $\mathcal{I}^*$ contains all non-redundant indices assuming that x is unbounded. While it is useful to find such a general essential set, practical application usually includes specific generation units, demand- and renewable time-series along with the grid infrastructure. This allows to determine upper and lower bounds for nodal injections x_t. Considering bounds on x_t in the proposed algorithm, can render certain essential indices unnecessary, because the specific allocation of nodal injections to overload certain CBCOs will never occur given the known technical limits. In other words, we can find a set $\mathcal{I}^*|_{(\underline{x},\overline{x})} \subseteq \mathcal{I}^*$ by bounding x_t as schematically illustrated in Fig. 3.3. Resulting set $\mathcal{I}^*|_{(\underline{x},\overline{x})}$ is then sufficient to define

$\mathcal{F}(B, \overline{f})$ *under the condition* that x is bounded by $(\underline{x}, \overline{x})$:

$$\begin{aligned} \mathcal{F}(B, \overline{f}, \mathcal{I}^*) &= \mathcal{F}(B, \overline{f}, \mathcal{I}^*|_{(\underline{x},\overline{x})}) \\ &= \{\underline{x} \leq x \leq \overline{x} : Bx \leq \overline{f}\}. \end{aligned} \tag{3.12}$$

Bounds $(\underline{x}, \overline{x})$ strictly relate to the parameters and available data of the modeled system. In typical applications, the modeled system remains static over $\mathcal{T}$, so that implicit bounds on nodal injections will always hold and a smaller essential set will provide a reduction of model complexity without compromising the validity of the resulting SCOPFs. First, we compute asymmetrical bounds by determining the maximum positive and negative nodal injections:

$$\check{x}_n = \min(d_{t,n},\ t \in \mathcal{T}) + \min(M_n \underline{g}_t, t \in \mathcal{T}) \tag{3.13}$$

$$\hat{x}_n = \max(M_n \overline{g}_t,\ t \in \mathcal{T}), \tag{3.14}$$

where $\check{x}_n$ and $\hat{x}_n$ are the maximum negative and maximum positive nodal injection at n given the available demand and generation parameters. Note that these bounds can be extended to accommodate renewable in-feed time series or storage capacities. However, as indicated in Remark 7, feasible region $\mathcal{F}(B, \overline{f})$ is symmetric. Thus, bounds on x have to be included symmetrically and we define:

$$-\underline{x}_n = \overline{x}_n = \max(|\check{x_n}|, |\hat{x_n}|). \tag{3.15}$$

Note that symmetric definition of the bound in (3.15) also assures that $z = 0$ remains an interior point of feasible region $\mathcal{F}(B, \overline{f}, \mathcal{I}^*|_{(\underline{x},\overline{x})})$. Using these bound to compute $\mathcal{I}^*|_{(\underline{x},\overline{x})}$ will further reduce the resulting problem size of the SCOPFs (3.9). Note that the identification of the conditional essential set uses the extreme (upper and lower) technical limits of all resources connected to a node. Therefore $\mathcal{I}^*|_{(\underline{x},\overline{x})}$ can also be applied to solve SCOPFs problems that impose additional constraints on the behavior of these resources, see Remark 6.

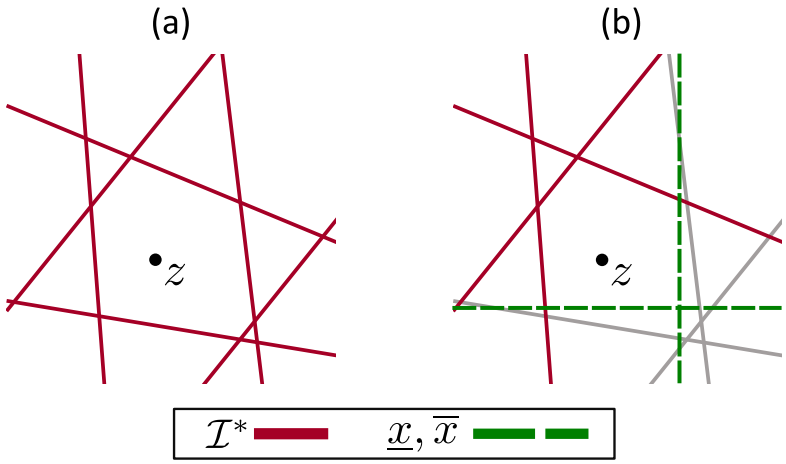

Figure 3.3: Illustration of two essential sets $\mathcal{I}^*$ with and without considerations for bounds on x: a) $\mathcal{F}(B, \overline{f}, \mathcal{I}^*) = \{x : Bx \leq \overline{f}\}$ b) $\mathcal{F}(B, \overline{f}, \mathcal{I}^*|_{(\underline{x},\overline{x})}) = \{\underline{x} \leq x \leq \overline{x} : Bx \leq \overline{f}\}$

3.4 Impact Screening

The run-time of the `RedundancyRemoval` is directly related to the initial number of constraints M since each index $k \in \{1, ..., M\}$ has to be checked. It is therefore desirable to reduce the number of constraints beforehand if possible. As described in Section 3.2.2, contingencies are considered by computing how line flows are distributed across all other lines in the case of an outage. Each line is only significantly affected by an outage of its physical neighbors in close proximity, while a large number of contingencies in greater electrical distance have hardly any effect on its post-contingency power flow.

Consider the outage of a line $o \in \mathcal{L}$. As per (3.3), LODF_{lo} determines how the pre-contingency power flow of line o is distributed among all other lines $l \neq o, l \in \mathcal{L}$. Because the power flow on any line is bounded by $\overline{f}$, the impact any line outage can have on any other line is bounded by the respective LODF multiplied with the maximum flow on this line:

$$|f^o_{t,l} - f^0_{t,l}| = |\,\text{LODF}_{lo}\, f^0_{t,o}| \leq |\,\text{LODF}_{lo}\, \overline{f}_o|. \tag{3.16}$$

By reserving a small capacity margin η on each line, every outage that impacts this line

by less than η can be disregarded. In other words, all rows PTDF_l^o can be omitted if

$$\frac{\text{LODF}_{lo}\,\overline{f}_o}{\overline{f}_l} < \eta, \tag{3.17}$$

effectively reducing the length of the input matrix B and therefore reducing the run-time of the `RedundancyRemoval`.

Depending on the implementation, chosen threshold η either reflects a safety margin by reducing the available line capacity $(1-\eta)\overline{f}_l$ or an allowable *worst-case* short-term overload by virtually increasing the line capacity $(1+\eta)\overline{f}_l$. Both approaches are typically used in practice to accommodate parameter uncertainty (Bienstock 2015). Note that if η is defined as a safety margin, the results of the SCOPFs may be altered because less line capacity is available.

3.5 Case Study

This section investigates the mechanics of the proposed constraint reduction process on two specific data sets. First, we solve the N-1 DC SCOPFs for the IEEE 118 bus system with 186 lines and line capacity information taken from Christie (2019). This system is a suitable example to illustrate proposed methodology and allows comparability to related methods due of its common application, e.g. in Ardakani and François Bouffard (2013) and Ardakani and Francois Bouffard (2015). Second we use a larger 453-node data set of the German transmission system (DE case) to showcase the performance for common real-world multi-period applications. The DE case comprises almost 2 million constraints related to its 995 lines. Table 3.1 summarizes both cases.

Table 3.1: Overview: Case Studies

	Nodes	Lines	Generators	N-1 Flow Constraints
IEEE 118	118	186	116	66,216
DE	453	995	4226	1,934,280

We show four stages of constraint reduction that have been used to solve the N-1 SCOPFs. Stage "Full" considers all combinations of branches and outages in the positive halfspace, i.e. no explicit constraint reduction has been applied beyond ignoring the symmetry of the flow limits as discussed in Remark 7. The "Pre" (preprocessed) stage includes the impact screening as described in Section 3.4. The stages "RR" and "CRR"

apply the `RedundancyRemoval` algorithm on the impact-screened N-1 PTDF without and with conditional redundancies, see Section 3.3.2. Note that those stages are presented here to itemize the effect of the different parts of the reduction algorithm. For actual application of the proposed method there is only one stage to use, i.e. "CRR". All results are compared in terms of the resulting number of constraints and the corresponding time to solve the optimal power flow model (3.6) using these constraints.

Remark 8. The implementation of the SCOPFs problem in this case study is based on the PTDF formulation in (3.6), where the used B^c contingency PTDFs have been reduced to represent the minimal set of constraints given by essential set $\mathcal{I}^*$. However, other implementations of the SCOPFs are possible, e.g using voltage angles or decomposition techniques, since the CBCOs given by essential set $\mathcal{I}^*$ exactly define the lines and contingencies that have to be included.

The computations have been performed on a standard PC workstation with an Intel 8th generation i5 processor and 16GB memory. The optimal power flow model and the reduction procedures have been implemented in the open source *Power Market Tool* (POMATO, Weinhold and Mieth (2020b)). The tool is written in Python for data pre- and postprocessing and uses the Julia/JuMP package (Dunning, Huchette, and Lubin 2017), in combination with the Gurobi solver (Gurobi Optimization LLC 2018), as its optimization kernel. To allow direct comparison, dual simplex was used and the presented times are the times reported by the solver, including presolve.

3.5.1 IEEE 118 bus case

Table 3.2 itemizes the number of constraints, the respective solve times and objective values for all constraint reduction stages in the IEEE 118 bus case. The OPF has been solved for a single time step. For the preprocessing phase, the impact screening margin set to $\eta = 5\,\%$ which reduces the set of constraints by $87\,\%$ to $4,152$ and thus reducing the solve time by $81\,\%$. The small objective value increase (approximately $3\,\%$) results from the implicit line capacity reduction of the impact screening margin, see Section 3.5.3 below.

Running `RedundancyRemoval` further reduces this set by 41% to $2,465$ and including conditional redundancy, as described in Section 3.3.2, yields a set of only 518 CBCOs, that guarantee a N-1 SCOPFs. Thus, instead of L relevant contingencies for L lines we observe an average of 2.78 critical outages per line. This represents a total removal of over $98\,\%$ of the constraints and results in a $97\,\%$ reduction of the time needed to

Table 3.2: IEEE 118 bus case constraint and solve time reduction

	Full	Pre	RR	CRR
# Constraints	33,108	4,152	2,465	518
Process Time [s]	1.22	0.215	396	64.9
Presolve [s]	3.84	0.45	0.27	0.07
Solve Time [s]	7.13	1.34	0.76	0.23
Objective	119,996	124,103	124,103	124,103
total constraint reduction*:		87%	93%	98%
additional constraint reduction*:		87%	41%	79%
total solve time reduction*:		81%	89%	97%

*Relative to "Full"

solve the problem. Furthermore, we observe that the objective value remains unchanged after the impact screening. This verifies, that the reduction due to Algorithm 1 indeed only removes redundant constraints. The process time of `RedundancyRemoval` for the 118 bus case is around 7 min without and below 1 min with conditional redundancy. This demonstrates, that the process time of the presented algorithm reduces the more redundant the system is, i.e. the fewer non-redundant constraints can be found. Note that the reported process times of the "Full" and "Pre" stages reflect the time needed to calculate the N-1 PTDF matrices only, while the process times of the "RR" and "CRR" stages also include the run time of the `RedundancyRemoval`. The process time is lower in the "Pre" stage, since the N-1 PTDF computation is integrated with the impact screening methodology and, thus, a smaller PTDF matrix is generated. When using the full N-1 PTDF as the input to the `RedundancyRemoval`, we find a potentially larger set of CBCOs in significant more process time (RR: 3265 constraints in 1216 s, CRR: 518 constraints in 171 s), both guaranteeing SCOPFs with the same objective value as the "Full" case as the full line capacity is available. This example shows that the technical limits imposed by the "CRR" stage are often more restrictive than the impact screening, leading to the same essential set with and without impact screening.

The reduction in solution time does not match the reduction in constraints. Since the SCOPFs for the IEEE 118 case study is solved, in contrast to common economic applications, for a single time step since the IEEE cases do not come with time series, the major advantage that each market clearing profits from the preprocessing, does not apply.

Table 3.3: DE case constraint and solve time reduction (single time step)

	Full	Pre	RR	CRR
# Constraints	967,140	14,523	10,695	2,629
Process Time [s]	134	2.62	136,495	11,719
Presolve [s]	NA	7.56	5.73	0.77
Solve Time [s]	NA	12.61	10.76	3.20
Objective	NA	726,505	726,505	726,505
total constraint reduction*:		98.5%	98.9%	99.7%
additional constraint reduction*:		98.5%	26%	75%
total solve time reduction*:			15%	68%

*Relative to "Pre"

3.5.2 DE case

The DE case solves single and multi-period nodal market clearing for the German power system including inter-temporal constraints for energy storages. The power plant data is based on Weibezahn et al. (2018) and the spacial distribution and grid topology is based on Kunz et al. (2017). The large set of power plants is due to a detailed regionalization of small scale, decentralized power plants. This case represents a real world application with a prohibitively large linear problem. Indeed, the the full set of constraints cannot be solved by the computer hardware used for this case study as the system runs out of memory before an optimal solution has been obtained. While approaching the problem with more powerful hardware might be able to overcome this, the application of the proposed redundancy removal procedures makes this problem solvable. Table 3.3 shows that the "CRR" method removes 99.7 % of all constraints within 195 min processing time. The resulting average number of critical outages per line is 2.64 which is surprisingly similar to the 118 bus case. Preprocessing alone reduces the number of constraints already by over 98 % with a impact screening margin of $\eta = 5\,\%$. An additional 26 %, 75 % are achieved by the `RedundancyRemoval` without and with conditional redundancy, respectively. Again, the processing time of the `RedundancyRemoval` itself is larger in the "RR" stage relative to "CRR" as the problem is less redundant. The resulting set of CBCOs is used to solve the SCOPFs for a single time step and two time series of 10 and 24 time steps. The 24 time steps are the hours of an arbitrarily chosen day in January 2017, with the 10 time steps being the first ten. In the 24 time step run, 26 different line and contingency constraints are active. Since the bounds for the conditional

Table 3.4: DE case solve time reduction (10 time steps)

	Full	Pre	RR	CRR
Presolve [s]	NA	93.4	84.41	13.5
Solve Time [s]	NA	283.19	250.29	44.82
Objective	NA	2,993,021	2,993,021	2,993,021
total solve time reduction*:			12%	84%

*Relative to "Pre"

Table 3.5: DE case solve time reduction (24 time steps)

	Full	Pre	RR	CRR
Presolve [s]	NA	507.7	220.53	22.87
Solve Time [s]	NA	1,707.56	714.37	89.53
Objective	NA	8,764,696	8,764,696	8,764,696
total solve time reduction*:			58%	95%

*Relative to "Pre"

redundancy have been determined for the whole year, the set of CBCOs will guarantee a contingency secure solution for all time steps, however with a potentially different set of active constraints. The solve times and objective values are itemized in Tables 3.4 and 3.5. As there is no data for the "Full" stage, the time reductions are reported relative to the "Pre" stage. While the problem was not solvable with the full set of constraints, after "CRR" reduction an optimal solution was found within 3.2 s for the single time step run, 13.5 s for the 10-time step run and 22.87 s for the 24-time step run.

Compared to the single and 10-time step run, the 24-time step run shows a higher total time reduction both absolute as well as relative to the constraint reduction. This highlights the positive effect of the larger time series, where the benefits of the constraint reduction apply in every time step. All stages in the two runs result in exactly the same objective value verifying the the removal of only redundant constraints.

3.5.3 Impact screening

As described in Section 3.4, the impact screening implicitly reduces the available line capacity in favor of disregarding outages which can not exceed this margin in case of an outage. While this significantly reduces the number of considered contingencies, the

available transfer capacity of the network is reduced. The reduced network capacity correlates with a higher objective value as cheaper generators are more restricted to supply electrically distant nodes. To itemize the effect of the choice of the margin η, the DE case 10-time step run was repeated with different settings for η, where no further reduction was applied. Fig. 3.4 shows the number of constraints resulting from the impact screening, and objective values in the optimal solution. Note that the $\eta = 5\,\%$ data-point in Fig. 3.4 matches the "Pre" stage from Table 3.4.

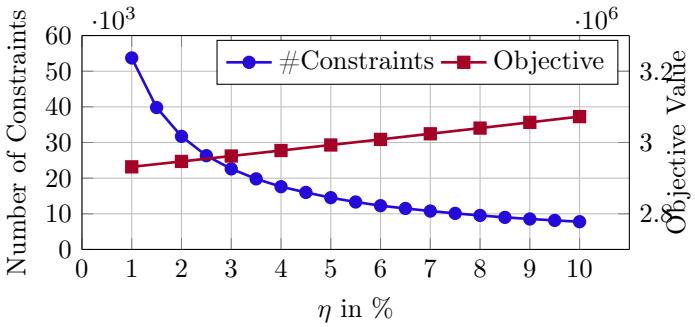

Figure 3.4: Effect of impact screening margin η on the resulting number of constraints for the DE 10-time step case.

The effect of η on the objective is closely linear and we observe that an increase in η of 1 % translates into a mild increase of the objective value of approximately 0.5 %. On the other hand, the resulting number of constraints is reduced drastically already by small values of η. Those results highlight how every outage in a meshed grid only has a certain reach and that the number of outages relevant for a specific branch is spatially restricted. Fig. 3.5 shows this effect by color-coding the relative outage sensitivity of all lines in the network towards the highlighted blue line. By showing all lines with an impact of less than 1 % in gray, we see that mostly neighboring and parallel lines in close proximity have a significant impact on the highlighted line.

3.6 Larger test cases and scalability

This section investigates the scalability of the method and discusses some considerations for practical implementation. Here we used the 1159 bus Central Western Europe (CWE) data-set from Schönheit, Weinhold, and Dierstein 2020 and the A&M synthetic 2000 bus network (ACTIVSg2000) from Birchfield et al. 2017. Our experiments showed that a direct implementation of the described algorithm is able to find a solution also

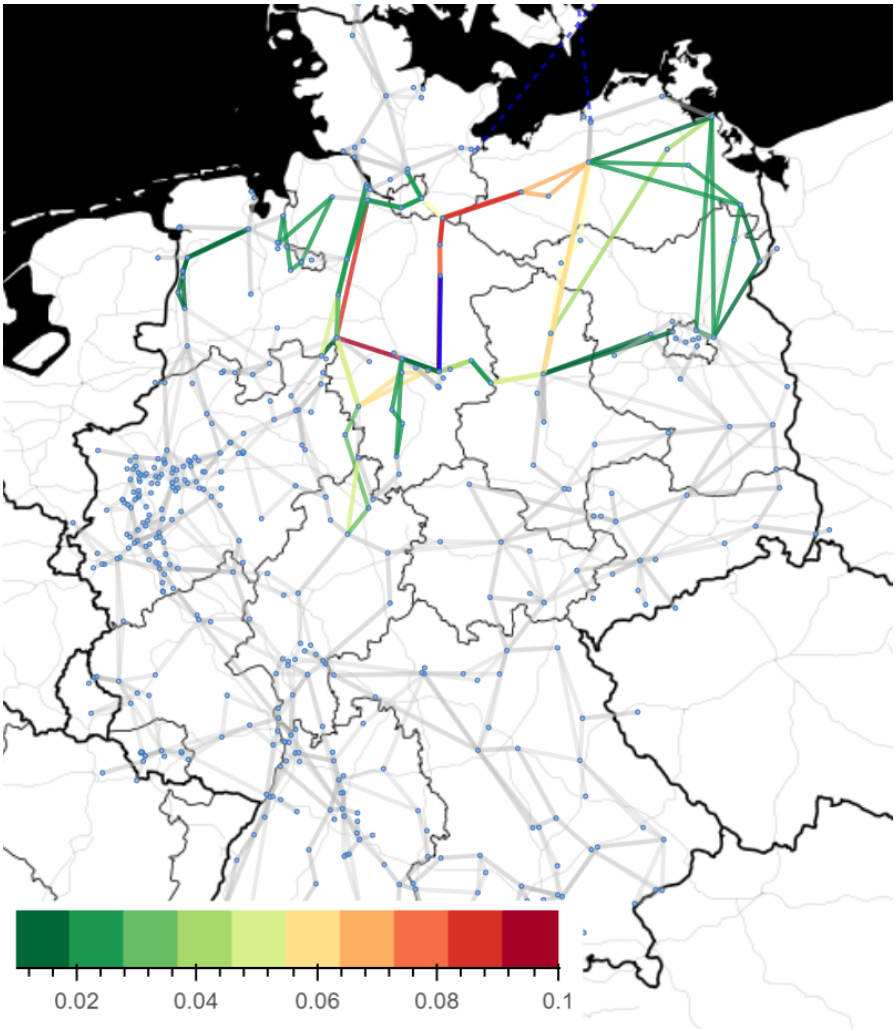

Figure 3.5: Impact of outages towards the highlighted (blue) line; Grey lines indicate a sensitivity of less than 1 %

.

for larger test cases, but exceeds desirable time frames. However, using a more effective execution of the proposed algorithm, process times are reduced to a reasonable level without changing the proposed method itself. Notably, the inherent sequential nature of `RedundancyRemoval` obstructs parallel computation, because every constraint is checked against both already identified essential indices and unchecked indices, see Fig. 3.2. However, it is possible to run the algorithm multiple times in parallel using segments of the full set of indices. Indices found redundant in a segment are also redundant against the whole set and can thus be removed. However, indices identified as non-redundant in a

Table 3.6: Overview: Larger Test Cases

	Nodes	Lines	Generators	N-1 Flow Constraints
CWE	1,159	2,438	4,797	11,278,188
A&M 2000	2,000	3,206	3,535	17,671,472

Table 3.7: Larger Test Cases Results (using "CRR")

	# Constraints	Process Time [s]	Solve Time [s]
CWE	5,349	3,906	13.96
A&M 2000	10,869	66,735	1,676

segment are not necessarily essential with respect to the whole set and therefore need to be either confirmed or discarded as an essential index by running a final instance of the algorithm with all remaining indices. Note that the segmentation does not alter the algorithm as described in Section 3.3, nor affects the final result of the `RedundancyRemoval`, but only reduces the process time.

For both of the larger cases, with parameters as reported in Table 3.6, we applied the "CRR" method with impact screening as described in Section 3.5. The resulting number of CBCOs, the process time of the algorithm and the solve time of the SCOPFs (in the implementation described in Remark 8) are itemized in Table 3.7. In both cases, the resulting CBCOs constitute a constraint reduction of over 99.9 % and enabled solving an SCOPFs of the CWE case in 13.96 s and the A&M 2000 bus case in 27 min. Notably, as the the 2000 bus network contains a larger number of medium voltage lines with lower thermal rating, fewer constraints can be considered redundant. This leads to an over proportional increase in process and solve time, considering that the 2000 bus network has only 30 % more lines than the CWE case. Further, comparing the process times of the DE case (11,719 s, see Table 3.3) with the larger CWE case (3,906 s, see Table 3.7) illustrates how significant performance improvements can be achieved with more effective execution of the algorithm as outlined at the beginning of this section.

3.7 Conclusion

This paper proposed a methodology to identify the minimal set of constraints that define the space of feasible nodal injections in an electricity transmission network with contingency scenarios. This set of critical branches under critical branch under critical outages

(CBCOs) can be used to significantly reduce the dimensionality, and thus computational complexity, of security-constrained optimal power flows (SCOPFs) problems.

First, we presented an algorithm that identifies the indices of the constraints that define the CBCOs, for a given system of linear inequalities. This procedure yields feasible process times by iteratively selecting only constraints that correspond to the innermost hyperplanes defining the solution space and, therefore, are non-redundant. Second, we proposed two methods to further reduce the run time of the algorithm and the resulting number of CBCOs by internalizing technical limits of the nodal injections and enforcing a minimal worst-case impact of contingencies to line flows.

The proposed algorithm has been applied to solve SCOPFs problems for the IEEE 118 bus system, the A&M synthetic 2000 bus system, as well as two real-world data sets of the German and European transmission system. The algorithm is shown to return all CBCOs within reasonable time (within minutes for smaller cases and hours for the larger cases) and for every case at least 95 % of the constraints are identified as redundant. Using the identified set of CBCOs to solve SCOPFs problems for these networks showed significant improvements in solve time. For example, a single DC SCOPFs for the IEEE 118 bus system has been solved in 0.23 s and the German data set has been solved for 24 time steps in less then 90 s. All code and input data have been published supplementary to this paper as open-source software.

Considerations for practical implementation and solving larger cases have been discussed. For the presented data-sets the resulting solve times are feasible for the intended application of enabling multi-period electricity market studies, e.g. in the context of flow-based market coupling. However, experiments with even larger indicate a need for further study of the design and implementation of the proposed techniques to achieve practical process times. We reserve these extensions for future work.

Part III

Applications

Chapter 4

The Impact of Different Generation Shift Key Strategies on the Flow-based Market Coupling Domain: A Model-based Analysis of Central Western Europe

"Assume that I have to pay so much for going from this node to that node, this is how much of that transmission service I demand."

(Ehrenmann and Smeers (2005))

The contents of this chapter have been published in Applied Energy 258 (Schönheit, Weinhold, and Dierstein 2020). Available Online: https://doi.org/10.1016/j.apenergy.2019.114067. Appendix B contain the original appendix to this publication. For this dissertation the original article has been adapted to ensure consistent notation and format.

4.1 Introduction and background

Market coupling between different zones or countries enables the trading of electricity across borders and represents the foundation of a liberalized single market for electric energy (Van den Bergh, Boury, and Delarue 2016). This is the stipulated goal of the EU for maintaining high levels of security of supply and attaining competitive energy prices (European Commission 2009b). For market coupling, cross-zonal capacities are provided by the transmission system operators (TSOs) (Amprion et al. 2011). Capacity calculations are realized on a *static* basis, through net transfer capacities (NTCs), or by means of flow-based market coupling (FBMC), a *dynamic* method that represents the grid, load flows and restrictions in a simplified form (Amprion et al. 2011; Energinet et al. 2014). In parallel to the existent NTC method, FBMC was tested from 2013 to 2014. It was subsequently launched in Central Western Europe (CWE) in 2015 because of increases in welfare and high levels of reliability, stability and robustness (Van den Bergh, Boury, and Delarue 2016); (see Aguado et al. (2012) for an earlier study on better price convergence due to FBMC). It is therefore the preferred method for calculating cross-zonal capacities, stipulated by Commission Regulation (EU) 2015/1222 (European Commission 2015). FBMC is planned to be launched in the Core Region, including CWE and Central Eastern Europe (CEE) (ACER 2016), by the end of 2020 (Amprion 2019), a goal the involved TSOs are working toward (50Hertz et al. 2017).

One major challenge of market coupling is the consideration of physical grid constraints when calculating and providing cross-border capacities to the market. FBMC approaches this challenge by converting available information during market coupling, i.e. the bids of involved power exchanges and resulting import/export positions for each country, into node- and line-specific information, namely expected changes in power outputs and line flows. For this, FBMC relies on generation shift keys (GSKs), a parameter that needs to be determined prior to MC, and the so-called "base cases" of the TSOs . While base cases try to accurately describe the market situation and corresponding network flows two days prior (Van den Bergh, Boury, and Delarue 2016), GSKs attempt to predict, which generating units participate in net position (balance of exports and imports) changes of the zone they are located in. Thus, GSKs provide the necessary translation between zonal and nodal information and render possible the prediction of how critical network elements are affected by market coupling (Energinet et al. 2014; Amprion et al. 2014). This prediction is crucial in order to screen what market situations are compatible with the available grid capacities. This preemptive consideration of physical constraints aims

to reduce necessary preventative and curative congestion management measures and their associated costs. GSKs and base case computation are major uncertain parameter in the flow-based methodology (Energinet et al. 2014; Marien et al. 2013; Schönheit and Sikora 2018) but despite their decisive role, research on their effect on domains and network elements is limited (Van den Bergh, Boury, and Delarue 2016).

This analysis sets out to analyze and quantify the effect of different GSK strategies on the flow-based market coupling domain in the CWE region, with a focus on Germany. In the context of FBMC, "strategy" refers to the selection of power plants, anticipated to participate in zonal balance changes, as well as mapping their behaviour, i.e. quantifying the extent of their predicted participation. The analysis proposes a new method to compute base cases, which incorporate actual, historical reference flows on relevant network elements and reference net positions. Based on the base case results, common GSK strategies are used to obtain and compare n-1 secure FBMC domains. Furthermore, line-specific changes are analyzed to quantify the effect of GSKs on individual network elements. This analysis focuses on answering the question whether or not the choice of GSK strategy substantially affects the availability of cross-border capacities and purposely refrains from evaluating the quality of GSK strategies. The novelty of this paper is fourfold: (1) The development and application of a new method for the estimation of base cases, relying on matching historical power flows on critical network elements, (2) the analysis of common GSK strategies for the entire CWE region, applying the strategies universally to systematically parse the effect of GSKs on flow-based market coupling domains, (3) the computation of n-1 secure market coupling domains and (4) the analysis of the impact of GSKs on an aggregated trading domain level as well as on a network element-specific level.

The remainder of the paper is structured as follows. In Section 4.2, the main elements of the flow-based market coupling framework are explained. Section 4.3 describes the existing literature regarding GSKs and base case computations. The developed methodology, the analyzed timeframe and underlying data for this analysis are described in Section 4.4. The results and implications are presented and discussed in Section 4.5. Finally, Section 4.6 concludes this analysis, summarizes key insights and identifies required future research.

4.2 Theoretical framework: Flow-based market coupling parameters

In the following, the fundamental concept and main parameters of flow-based market coupling are described, including a mathematical formulation in Section 4.2.2. This serves to explain the relations between the parameters and helps to identify the most important determining factors in flow-based market coupling: GSKs and base cases.

4.2.1 Fundamental concept of flow-based market coupling

The trading of electricity between market zones is enabled through market coupling. Cross-border exchanges are subject to capacity limits, which are provided by the TSOs and are computed through NTC/ATC or flow-based constraints (Amprion et al. 2011; Energinet et al. 2014). Available transfer capacities (ATCs) are a result of subtracting long-term nominations from NTCs and statically determine the maximum flow between bidding zones (Amprion et al. 2011; Weber, Graeber, and Semmig 2010). While ATCs are provided *prior* to market coupling, the flow-based methodology determines cross-border capacities *during* market coupling. This is made possible because the flow-based market coupling algorithm incorporates the grid and its most critical restrictions through power flow calculations, which are derived from available market information, i.e. bids of national power exchanges and consequent desired exchanges between countries (Amprion et al. 2011). For the domain computation, the algorithm takes into account the net positions of *all* participating zones, which often enables market clearing points outside of the NTC/ATC domain (Amprion et al. 2011; Energinet et al. 2014; Consentec 2012).

The power flow calculations employ a linearized power flow model commonly used in techno-economic applications, known as linear power flow (DCPF). Due to its linearity it allows to incorporate thermal capacities of transmission lines into dispatch decisions with sufficient accuracy (Bienstock 2015). In its essential form, DCPF represents a linear sensitivity between nodal injections and line flows. This relation is, in matrix form, known as power transmission distribution factors (PTDFs) (Christie, Wollenberg, and Wangensteen 2000). This concept can be extended to a linear sensitivity between an outage of a line and the line flows on all other lines, denoted as a matrix of load outage distribution factors (LODFs) (Christie, Wollenberg, and Wangensteen 2000; Jiachun et al. 2009) to account for outages or contingencies.

While load flows rely on nodal information, during market coupling only zonal infor-

mation is available. The balance of each zone can be expressed as the net position, the aggregated imports subtracted from the aggregated exports. The *realized* net positions during day-ahead market coupling deviate from the *anticipated* reference net position from the base case, originating from the so-called "2-Days Ahead Congestion Forecast" files (2-days ahead congestion forecast (D2CF)) created by the responsible TSOs . These represent the best possible forecast of the hourly grid load two days in advance. In addition to detailed power plant utilization and demand, switching state, network topology and trading purposes are also taken into account[1] (Amprion et al. 2014). In the D2CF, this results in key market coupling parameters, such as the net position of the market zone, the capacity utilization of individual power plants and the load flows on individual lines, so-called reference flows. The main purpose of the FBMC algorithm is to predict how the discussed net position changes affect load flows and to what extent deviations from the reference flows are permissible with the goal of providing the associated magnitude of permitted cross-border exchanges to the market.

In order to determine an hourly estimate of the grid load situations for individual lines, it is necessary to forecast nodal generation and demand. This is based on data from a reference day selected by the responsible TSO , which is supplemented by recent events, e.g. expected renewable feed-in. Since the TSOs are exclusively responsible for the transmission grid, the load on the transmission grid resulting from the lower grid levels can only be estimated to a limited extent on the basis of historical data. In particular, the expansion of renewable energies, predominantly connected at medium-voltage level, is causing great uncertainty. Therefore, TSOs ' internal expert knowledge is also used to make predictions as precise as possible. The relationship between the different sources used to estimate the actual market result differs both between the individual TSOs and within each TSO depending on the grid situation (Boury 2015; Tennet 2015).

The D2CFs of all affected TSOs are combined to map all market zones involved in market coupling. This combination is referred to as the base case. The base case represents the basis of any kind of currently performed market coupling applications and is used in both the NTC and FBMC procedures. Based on the load flows determined in the base case, the line capacities available for further trading are determined. In the NTC method, the NTC values result indirectly from this. In the FBMC method, cross-border capacities are calculated directly, further described in Section 4.2.2. Compared to

[1]The base case calculation is based on the Common Grid Model. This is a network model method standardized on the basis of capacity allocation and congestion management (CACM) for all TSOs . The results of the individual D2CF must be submitted by 6 p.m. two days before the examination day (Boury 2015).

the NTC method, the FBMC method provides dependencies between the base case and the GSK values dependent upon the selected GSK strategy. In addition, the changes in the net position of a market zone in the FBMC are decisive factors for determining the trading domain. The more precise the forecast of the base case is, the lower are possible errors in the determination of the domain and the more electricity can be traded without a congestion effect between two market areas with corresponding positive effects on the overall welfare (Logarithmo and E-Bridge 2017).

4.2.2 Main parameters of flow-based market coupling

During market coupling, market results and the associated net positions can deviate from the predictions made in the base case. Equation 4.1 shows that $\mathbf{x}$ is the difference between the day-ahead net positions of all involved zones $\mathbf{n^{DA}}$ and their D-2 predicted counterparts $\mathbf{n^{D2}}$ from the base case (50Hertz et al. 2017). $\mathbf{x}$, $\mathbf{n^{DA}}$ and $\mathbf{n^{D2}}$ are z-by-1 vector.

$$\mathbf{x} = \mathbf{n^{DA}} - \mathbf{n^{D2}} \tag{4.1}$$

The incorporation of grid constraints within FBMC is realized through translating nodal into zonal line sensitivities. This is done by means of the already mentioned GSKs, which anticipate how a net position change ΔNP_z, a single element of $\mathbf{x}$, is distributed across the generating units in the respective zone. In effect, GSKs weight nodes according to the anticipated participation of units (connected to a node) in net position changes. The choice of power plants, i.e. *which* units are considered in the GSK, as well as the quantification of their predicted participation, i.e. *how much* weight is ascribed to the units, is subsumed in a GSK "strategy", further discussed in Section 4.3 and 4.4.5. The GSK, as defined in Equation 4.2 (Amprion et al. 2014), expresses the relation between power output changes ΔP_u and zonal net position changes ΔNP_z, according to the weight w_u ascribed to every unit.

$$GSK_u = w_u = \Delta P_u / \Delta NP_z \tag{4.2}$$

For instance, a GSK strategy can weight units according to their capacities in relation to the overall installed capacity in the respective zone, namely $w_u = P_{\max,u}/\Sigma_u P_{\max,u}$. With two units in one zone that have capacities of 750 MW and 250 MW, respectively, the weights are $w_1 = 0.75$ and $w_2 = 0.25$. Consequently, 75% of the net position change

is expected to come from unit 1 and 25% from unit 2, according to Equation 4.2.

Individual unit-specific GSK values GSK_u are consolidated by node and summarized as $GSK_{n,z}$. This value expresses what fraction of net position changes in zone z are expected to come from node n. All $GSK_{n,z}$ values are summarized as $\mathbf{G}$, the GSK matrix containing all GSK values, which is of dimension n-by-z.

The calculation of GSKs, as a predictive element of FBMC, enables the transformation of a nodal PTDF matrix $\mathbf{P^N}$, which contains node-injection-to-line sensitivities (Van den Bergh, Delarue, and D'haeseleer 2014), into a zonal PTDF matrix $\mathbf{P^Z}$ (50Hertz et al. 2017; Gebrekiros et al. 2015), which describes how net position changes affect the lines (Weber, Graeber, and Semmig 2010), see Equation 4.3 (50Hertz et al. 2017).

$$\mathbf{P^Z} = \mathbf{P^N} \cdot \mathbf{G} \tag{4.3}$$

While in DC power flow calculations, $\mathbf{P^N}$ contains all lines or network elements and has the dimension l-by-n, the FBMC algorithm only incorporates nominated critical network element (CNE). Consequently, $\mathbf{P^N}$ is a c-by-n matrix and $\mathbf{P^Z}$ is a c-by-z matrix. As described below in more detail, CNEs become critical network elements and contingencies (CNECs), when outages (n-1 cases) are considered.

The creation of GSKs and the subsequent calculation of $\mathbf{P^Z}$ enables the FBMC algorithm to calculate flow changes on network elements based on zonal changes. This translation renders possible the challenge of considering physical constraints during market coupling based on market (zonal) information, as described Section 4.1 and 4.2.1.

It is important to note that the net position changes of *all* zones, $\mathbf{x}$, are used to compute $\mathbf{f^C}$ (c-by-1 vector), the expected flow changes for all CNEs, as depicted in Equation 4.4. This is because the flows on CNEs are also affected by net balance changes of other zones (50Hertz et al. 2017; Matthes, Spieker, and Rehtanz 2017).

$$\mathbf{f^C} = \mathbf{P^N} \cdot \mathbf{G} \cdot \mathbf{x} = \mathbf{P^Z} \cdot \mathbf{x} \tag{4.4}$$

Equation 4.4 combines all the available information to compute flow changes on CNEs in a predictive manner: (1) The known line sensitivities based on nodal injections ($\mathbf{P^N}$), (2) the *predictive* translation of net position (zonal balance) changes into node injections ($\mathbf{G}$) and (3) the net position deviations observed during market coupling ($\mathbf{x}$) that determine the extent of expected flow changes. Importantly, also $\mathbf{x}$ represents a prediction because the reference net positions from the base cases are predictions themselves, making the net position deviations predictions as well, i.e. only $\mathbf{n^{DA}}$ is known but the entire

base case, and thus also $\mathbf{n^{D2}}$, is subject to uncertainty.

To constrain the FBMC domain and respect the limits of the considered network elements, CNE-specific positive and negative remaining available margins (RAMs) are computed and serve as upper and lower limits for the flow changes, as shown in Equation 4.5. The vectors $\mathbf{r}^-$ and $\mathbf{r}^+$ contain the negative and positive RAMs, RAM_c^- and RAM_c^+, for all CNEs and are computed according to Equation 4.6 and 4.7. $\mathbf{f^M}$ and $\mathbf{f^R}$ contain the maximum flows $F_{\mathrm{max},c}$, according to the thermal capacities, and reference flows $F_{\mathrm{ref},c}$ of all CNEs, respectively. The CNE-specific (expected) reference flows $F_{\mathrm{ref},c}$ are computed in the base case and deducted from the maximum flows $F_{\mathrm{max},c}$. Lastly, a CNE-specific final adjustment value (FAV_c) and reliability margin (FRM_c) are subtracted from the physical limit, or added in the case of the negative RAM.[2] Their values are contained in the vectors $\mathbf{a}$ and $\mathbf{m}$ (50Hertz et al. 2017). All discussed elements of Equation 4.5-4.7 are c-by-1 vectors.

$$\mathbf{r}^- \leq \mathbf{f^C} \leq \mathbf{r}^+ \tag{4.5}$$

$$\mathbf{r}^+ = \mathbf{f^M} - \mathbf{m} - \mathbf{a} - \mathbf{f^R} \tag{4.6}$$

$$\mathbf{r}^- = -\mathbf{f^M} + \mathbf{m} + \mathbf{a} - \mathbf{f^R} \tag{4.7}$$

It is crucial to mention that different definitions exist for reference flows. While some reference flows already include the flows caused by (anticipated) trade within the FBMC area, in the form of reference net positions, reference flows can also correspond to the flows that occur at net positions of zero (see 50Hertz et al. (2017) and Matthes et al. (2019) for further information). This analysis uses the former definition. Thus, the FBMC domains depicted in Section 4.5.1 will display the reference net positions as the coordinate origin.

The above-discussed relations are visualized in Figure 4.1. Note that the two-dimensionality of the figure only depicts the expected flow change on CNE c that is based on the net position change of *one* zone z. The slope of the blue line is equivalent to $PTDF_{z,c}$, the element of $\mathbf{P^Z}$ corresponding to c and z. The total expected line change depends on the net position change of zone z in this simplified depiction but in reality it depends on net position changes of all zones (refer back to Equation 4.4). RAM_c^+ and RAM_c^- limit the flow change and thus the permitted magnitude of net position changes. When the flow

[2]The final adjustment value (FAV) is sometimes omitted, cf. (Amprion 2019).

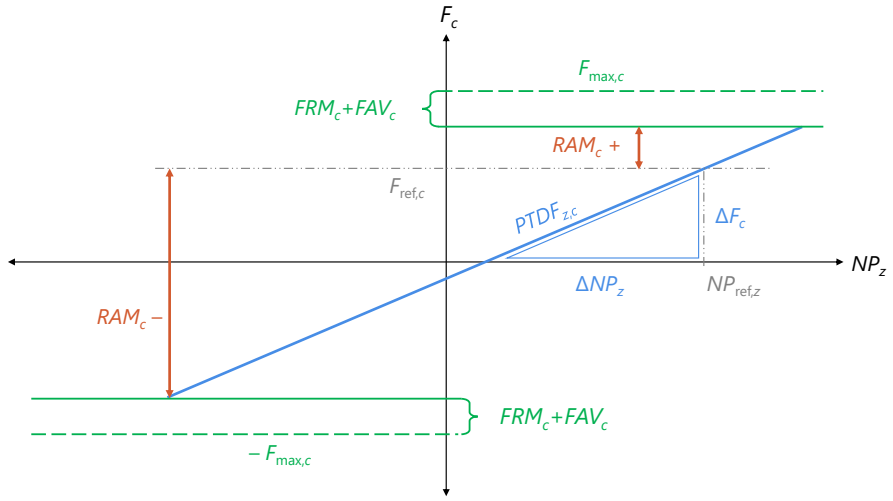

Figure 4.1: Depicted is the relation between the main flow-based market coupling parameters. The x-axis describes the net position of a zone z and the y-axis the power flow on a CNE c. The positive and negative RAMs limit deviations from the expected reference flow and the corresponding net position deviation. Source: Own figure based on (Amprion et al. 2011) and (Energinet et al. 2014)

change is equal to the positive or negative RAM, the CNE limits the FBMC domain.

These relations highlight the strong influence of GSKs on zonal PTDFs and, in turn, on computing, how much of the RAMs are "used" by net position changes during market coupling. It is therefore one of the main uncertain parameter of FBMC.

An additional uncertainty, heavily influencing zonal PTDF matrices, are line outages, which can result in varying line sensitivities depending on the n-1 case.[3] Equation 4.8 describes how the flow changes are calculated, taking into account the effect of line outages.

$$\mathbf{f}_{co}^{\mathbf{C}} = (\mathbf{P}_{c}^{\mathbf{N}} + \mathbf{L}_{c,co} \cdot \mathbf{P}_{co}^{\mathbf{N}}) \cdot \mathbf{G} \cdot \mathbf{x} \tag{4.8}$$

$\mathbf{L}_{c,co}$ is the LODF matrix of contingency (or critical outage) co ($co \in l$), with dimension c-by-l, and describes how the flow of an outage line is distributed across the remaining CNEs, which are now critical network elements under a contingency (CNECs. $\mathbf{L}_{c,co}$ is multiplied with $\mathbf{P}_{co}^{\mathbf{N}}$, the nodal PTDF matrix of the outage line of dimension l-by-n with a single row entry. The product describes the *additional* flows on all CNECs caused by

[3]Note that this description assumes static nodal PTDF matrices, which implies the lack of grid topology changes.

the outage and is added to $\mathbf{P}_c^{\mathbf{N}}$, the nodal PTDF matrix of all CNECs.[4] As a result, $\mathbf{f}_{co}^{\mathbf{C}}$ is computed, the flow changes on CNECs under the specific outage *co*. The restrictions in Equation 4.5 have to be respected for $\mathbf{f}_{co}^{\mathbf{C}}$ for all outages.

In summary, the combination of GSK and considered n-1 cases determine the expected flow changes on CNECs and thus, which elements constrain the domain.[5] The net position changes, in turn, determine the limiting CNEC(s) of the domain. Deviations in zonal balances are highly dependent on the reference net positions computed in the base case, highlighting the importance of accurate D2CF computations. Thus, GSKs and base case computations constitute the main deliberate factors within the flow-based market coupling framework, whose design and computation are subject to great uncertainty. This is further discussed in Section 4.4, which presents the methodological approach for addressing these aspects.

4.3 Review of empirical findings

In addition to the theoretical advantages of FBMC, the literature highlights the challenges of implementation. As CREG (2017) shows, challenges are especially the discretionary actions of TSOs in combination with a missing adaptation of the current bidding zone configuration causing large variations in the resulting constraints of FBMC and thus in the domains. The study pays particular attention to the lack of conformity of the discretionary actions with applicable rules and regulations and the lack of transparency or uniform regulation for all TSOs . The authors recommend a revision of the CNEs selection process, the introduction of a minimum RAM and a revision of the current bidding zones. Since GSKs, base case construction and CNE computation also belong to the discretionary actions of the TSOs , it is mandatory to ensure increased transparency by harmonizing the approaches and analyzing the FBMC results.

However, despite the importance of Generation Shift Keys, base case construction and n-1 computations for the accuracy of FBMC results, the effect of these main uncertain components on the resulting domain, cross-border capacities and individual network elements has not been subject to extensive research. Also, some studies conducted by TSOs is not publicly accessible, which further limits the available body of research.

[4] If $co \in c$, the entries in the respective row of $\mathbf{P}_c^{\mathbf{N}}$ are replaced with zeroes. If $co \notin c$, $\mathbf{P}_c^{\mathbf{N}}$ remains unchanged.

[5] Note that an additional determinant of restrictions is the selection of CNEs that are considered in the PTDFs. Usually, this is based on a threshold value for zone-to-zone PTDF values, e.g. 5% or 8% cf. 50Hertz et al. (2017) and Amprion (2019). Zone-to-zone PTDFs are further discussed in Section 4.5.2.

General guidelines for GSKs are provided by Van den Bergh and Delarue 2016, who recommend the splitting of injection shift key (ISK) into GSKs and demand shift key (DSK). Furthermore, the authors advise against time-averaging of ISKs to avoid a loss of accuracy. They also recommend the disaggregation of zones for higher accuracy, which is not an option within the CWE (and CORE) FBMC framework due to predefined zones. Therefore, only an increase of the time resolution is a feasible method.

In existing literature, similar GSK strategies are deployed. These often include strategies that weight power plants according to fixed power plant characteristics, such as the installed capacity or maximum power output $P_{\max}$. Also, strategies assigning weights by predicted power output levels (P) or remaining power output margins ($P_{\max} - P$) are tested. Often, the flat strategy, with a uniform distribution across nodes, is tested as a benchmark because it is seen as more robust when net position deviations are large (Energinet et al. 2014).

In Dierstein 2017 the author compares the influence of three different GSK strategies in the CWE region with regard to the evaluation criteria welfare, trade volume and congestions. The study is based on the assumption that the German-Austrian bidding zone is divided into two market areas with minimized congestions. The author also considers the differences between the harmonized application of a GSK strategy in all bidding zones and an individual application. Differences can be identified with regarding the evaluation criteria for the individual GSK strategies, a clear preference, however, cannot be derived. Thereby, the increased need for research in this area is explicitly emphasized.

Testing eight different GSK strategies for Denmark, Finland, Norway and Sweden, including P, $P_{\max}$, $P_{\max} - P$ and the flat strategy, Jegleim 2015 and Svarstad 2016 find that $P_{\max}$ is the best global strategy, with small differences in accuracy across strategies. The flat strategy is characterized by an average performance. Interestingly, the GSK strategies have a substantial effect, when evaluated for individual CNEs . For the construction of base cases, Jegleim 2015 uses day-ahead data and estimated flows. Therefore, net position deviations are measured between the current day and the day-ahead "base case". The optimal GSK strategy is determined by the smallest deviations from the estimated flows, which is done by applying GSK strategies on three levels of detail (global, area-based and individual CNEs).

The effect of six different GSK strategies on market coupling outcomes and ensuing unit commitment is evaluated by Finck, Ardone, and Fichtner 2018. Hourly base cases are computed for Germany, the Czech Republic and Poland by obtaining dispatch results

with NTC values as cross-border capacities. Subsequently, RAMs for all cross-border and internal lines are determined based on the PTDFs, which are calculated with the different tested GSKs. When comparing fuel-specific generation aggregated by zone, differences between GSK strategies are minute. However, GSK strategies substantially affect the scheduling of individual units, especially in smaller zones. The authors stress that this can affect the economic feasibility of generating units.

Other studies decouple GSK computations from fixed power plant characteristics. The utilization of power plants according to a merit order is tested by Consentec 2012. The study finds that participation and behavior of units in the GSK are not (purely) based on profitability considerations because a merit order-based GSK leads to high estimation errors in the analysis. The method proposed by Schönheit and Sikora 2018 detaches the computation of GSKs from generating unit capacities, merit-order assumptions and predictions of output magnitude from the base case. The estimations of GSKs still relies the on/off-status of generating units from the base case but not on the power output levels. The method derives GSKs based on regression models, using historical power plant output and fundamental data, such as load and renewable energy generation.

Empirical findings on GSK strategies and base case computation are far from exhaustive. On an aggregated level, existing literature suggests that GSK strategies often have a small effect. However, on the level of individual CNEs or power plants, effects can be large. Various methods for the calculation of base cases are deployed, which often disregard the accuracy of (historical) reference flows. The combination of a transparent and near-reality base case determination, which is mostly represented by simplifications, the n-1 secure calculation of CNEs and the associated analysis of different GSK strategies is lacking. Furthermore, most in-depth studies examining the impact of GSK strategies on the resulting market domains in the CWE region have not been able to assign these effects to specific transmission lines. Also neglected is the focus on Germany as one of the key market areas in the CWE region. This is also made clear by references to changes in market domains solely due to the nomination of CNEs by Amprion and the currently favorable role of Germany in the FBMC (CREG 2017). Finally, there is a lack of transparency in addition to the overall low availability of research. Models or data sets are only partially available to the public. The novelty and contribution of this analysis, as enumerated in Section 4.1, is addressing these shortcomings in a targeted manner, described in the following.

4.4 Methodological approach

To achieve a meaningful representation of the flow-based market coupling domains and quantify the impact of GSK strategies, a number of input factors and their relations have to be considered. This section aims to structure and explain the input and output parameters and the various methods and assumptions that are part of the methodology. Based on the explanations in Section 4.2, Figure 4.2 depicts three main determining factors for the construction of flow-based market coupling domains: (1) Base cases, as the underlying and combining element of this methodology, and the grid representation based on (2) GSKs and (3) the consideration of n-1 cases in the form of LODFs. The colors highlight the dynamic nature of the elements, which involves hourly re-calculations because of dependencies and definitions of contingency cases as well as deliberate choices in the case of GSKs and base cases.

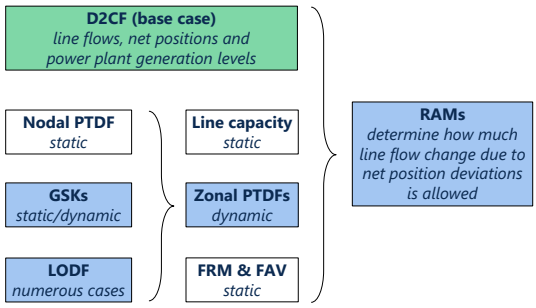

Figure 4.2: The major determinants of the flow-based market coupling domains and their relations. Source: Own figure.

Following the definitions from Section 4.2, the grid is represented by zonal PTDF, derived from nodal PTDFs, which are static under the assumption of static topology and line characteristics (Finck, Ardone, and Fichtner 2018). The variable determinants of zonal PTDFs are GSKs and LODFs. While LODFs are a decisive factor in the computation of zonal PTDFs due to many existing combinations, the effect of outages on line sensitivities is static. GSKs, however, need to be *determined deliberately* and their construction is therefore the most important choice influencing the computation of zonal PTDFs. In combination with exogenous line capacities and FRM and FAV values[6], zonal

[6]Line characteristics and reliability margins are not necessarily static but are exogenous in this analysis, as they are obtained from the Joint Allocation Office (JAO) database (see Section 4.4.6). Reliability margins are adjustable by the TSOs and therefore affect RAMs as well. Line capacities can be dynamic, e.g. in relation to the time of the year to reflect the temperature dependency of thermal capacities (Amprion 2019).

PTDFs determine the RAMs.

The RAMs are contingent upon the line flows computed in the base case and determine, what magnitude of net position changes are permitted. Only critical network elements (CNEs) under specific contingencies (CNECs) are considered and the RAM depends on the respective CNE's restrictions under a specific contingency case (see Section 4.2). Therefore, the resulting FBMC domain depends on the reference flows as well as reference net positions of the base case.

The base case represents a forecast of the grid load, as described in Section 4.2. There are several methods for determining the base case, as explained in Section 4.2 and exemplified in Section 4.3. The base case computation in this analysis is done for a selected week and relies on the matching of critical network elements. This entails the matching of CNE names to the line names in the database used in this application as well as matching CNE reference flows, obtained from the JAO database (see Section 4.4.6). These inputs are used in an economic dispatch model to obtain the base case.

The different parts of this methodology are depicted in Figure 4.3 and also structure the remainder of this Section. The construction of the base case is divided into endogenously modeled aspects (economic dispatch and domain generation) and inputs (CNECs, D2CF data and GSK strategies). These inputs are described in detail in Sections 4.4.3, 4.4.5 and 4.4.6.[7]

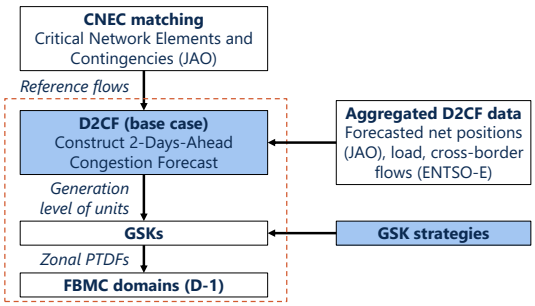

Figure 4.3: Overview of the applied methodology and data sources for the construction of base cases and computation of flow-based market coupling domains. Source: Own figure.

The base case computation in this analysis is done for a selected week, which is described in Section 4.4.2. The economic dispatch model is defined in Section 4.4.4. All

[7]The data compilation for critical network elements, GSK computations, statistical evaluations and visualizations are conducted using R (R Core Team 2018), specifically relying on packages **ggplot2** (Wickham 2009), **plyr** (Wickham 2011) and **data.table** (Dowle and Srinivasan 2017).

components combined allow to represent the flow-based market coupling domains within a fundamental model framework and are the setup for the numerical analysis of the impact of different GSK strategies in Section 4.5.

4.4.1 Selected analysis scope

The analysis concentrates on the status quo in the CWE region as the only region with an established FBMC and deliberately neglects the forecasting of future developments. For example, effects of an extension of the FBMC to include the CEE region or a stronger penetration of the energy system with renewable energies are therefore purposely excluded in order to focus on the fundamental effects of different GSK strategies. Due to the organizational, structural and spatial characteristics of the German market zone, the analysis focuses on Germany, as this is where the greatest effects can be expected (Amprion 2019). In comparison to the other CWE countries, Germany has a densely meshed network and deals with the complexity of organizing large, partly geographically concentrated renewable feed-in in coordination with four TSOs in one of the largest bidding zones in Europe with strong intra-zonal transmission capacity utilization. Germany is also connected to other, non-flow-based market zones via ATCs, some of which are large economies like Poland. The combination of peculiarities and relevant influencing parameters makes the German bidding zone especially interesting for an investigation of possible effects of GSK strategies on the market coupling domain (CREG 2017).

4.4.2 Selected analyzed week

For this analysis, one week is chosen, for which hourly base cases are constructed. Figure 4.4 displays the analyzed week, which ranges from Tuesday, February 13, 2018 to Monday, February 19, 2018.

The week has many net position situations typical for Germany, namely an export situation up to 5000 MW. On day 2 and 3, there is a peak in net position and day 6 is characterized by an import situation for almost every hour. The green, solid lines represent the median, 5th and 95th percentile of the net position values of this week. The red, solid lines represent the same distribution moments for the entire dataset available at the time of download, which is January to July 2018. The average and extreme values of the chosen week align closely with the overall dataset, which is why the analyzed week can be seen as a representative week.

Complementary, Figure 4.5 depicts the hourly demand as well as generation from

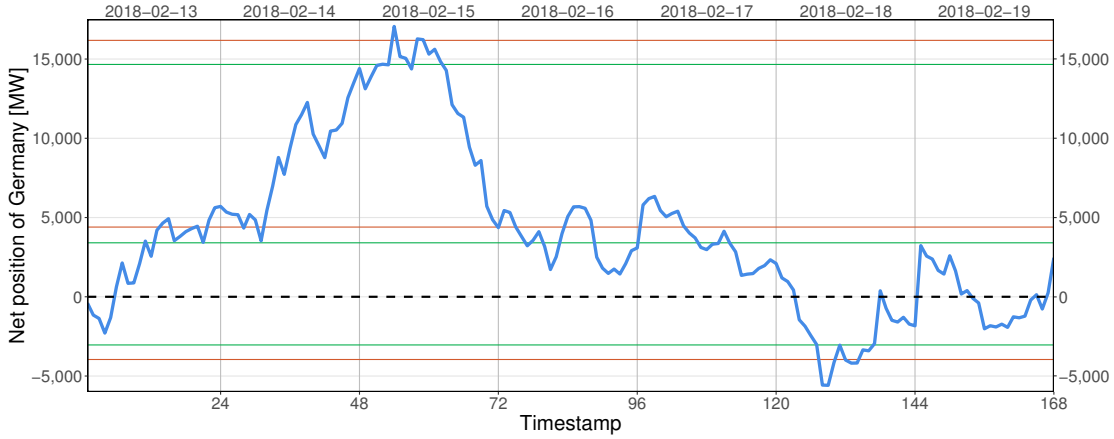

Figure 4.4: Germany's net position (D-2 forecast) for all 168 timesteps of the analyzed week, February 13-19, 2018, for which the hourly base cases are created. Median, 5th and 95th percentile of the net position values are represented by solid vertical lines (green for this week, red for available dataset). Source: Own figure.

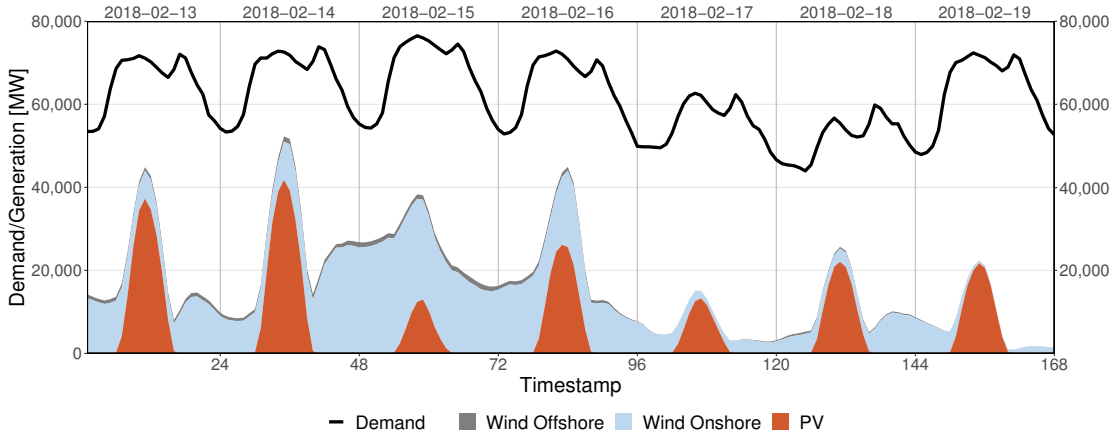

Figure 4.5: Germany's demand and renewable energy generation for all 168 timesteps of the analyzed week, February 13-19, 2018. Source: Own figure.

photovoltaik (PV), onshore and offshore wind for Germany. The space between the black demand line and the stacked renewable generation is the residual load. The selected week is not only characterized by many different export-import situations but also by different amounts of renewable feed-in. To a certain extent, the net position of Germany correlates positively with the onshore wind energy generation, especially evident at the end of day 2 and on day 3 (high amount of wind energy and high net position) and day 6 and 7 (low

amount of wind and low net position, with mostly import situations). Day 1 and 2 are characterized by high PV feed-in, which likely contributes to the high net positions.

Selecting one week for this analysis bears the risk of capturing a non-representative effect of GSKs. Unfortunately, the analysis of an entire year is beyond the scope of this work due to the very time-intensive process of matching critical network elements, described in the following section. To abate this issue, we selected a representative week, characterized by a large variation in net positions and availability of renewable energy sources to capture many different market and grid situations.

4.4.3 Matching of critical network elements

Table 4.1 shows two exemplary entries in a daily CNEC file from the JAO database. For each CNE, every relevant outage (contingency) is listed, along with the respective maximum power flow, reference power flow, the reliability margins (FRM and FAV) and the resulting positive RAM (cf. Equation 4.6). With the available information, the negative RAMs can be computed according to Equation 4.7.

Table 4.1: Exemplary daily information on critical network elements (and contingencies) from Joint Allocation Office Utility Tool. Zone refers to Bidding Area

CNE	Outage/Contingency	Zone	RAM	$F_{\max}$	F_{ref}	FRM	FAV
L 400kV N0 1 AVELIN-GAVRELLE	N-State	BE	1619	2301	376	306	0
L 400kV N0 1 AVELIN-GAVRELLE	L 400kV N0 1 MERY-SUR-SEINE-VESLE	BE	1548	2301	447	306	0

Source: Own table based on data from Joint Allocation Office (2019).

Figure 4.6 summarizes the process and exclusion rules of obtaining the relevant information from the daily CNEC files. For the 168 analyzed hours, almost 850 000 entries are available. From these, all entries with no outages are obtained, represented by the entries “N-State” or “Basecase”. The CNEs with non-anonymized names are matched to the database used in this application, which is possible for roughly 75% of CNEs . Redundant entries are removed from the reduced dataset. If a positive and negative reference flow are available, both entries are removed from the dataset since no definite flow direction can be concluded. Of the remaining entries, some combinations of CNE and timestamp have numerous entries either with different values for the reference flow or different maximum flow. The entry with the larger $F_{\max}$ or F_{ref} is kept. The maximum F_{ref} is chosen to avoid the underestimation of reference flows.

In total 10 606 entries remain. This is an average of roughly 63 entries for each of

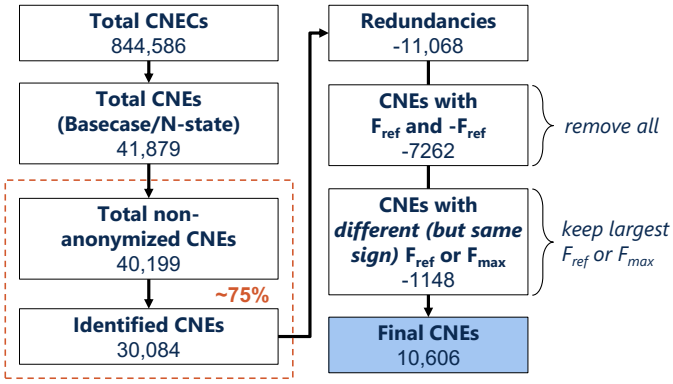

Figure 4.6: Flow chart for matching of critical network elements with exclusion rules in cases of inconsistencies and redundancies. Source: Own figure.

the 168 timesteps. For every CNE entry, the timestamp and reference flow are used for the construction of the base case, which is described in the following. Note that not only names are matched but also the direction of flow that (for some CNEs) is defined differently in the JAO database and the grid data used in this application. The cross-border lines not identified through this process are added as further CNEs .[8]

4.4.4 Model-based computation of dispatch

To achieve a full representation of the base case, a dispatch model, commonly used to model electricity markets, is calibrated for the specified time period to match the historical values for reference flows on CNEs and forecast (D-2) net positions. The dispatch model follows a common formulation, minimizing system costs defined by cost of generation (i.e. Leuthold, Weigt, and von Hirschhausen (2012)) while employing technical constraints regarding storage behavior, availability and curtailment of RES and transport constraints. Formulation 4.9 outlines a brief model description. A full mathematical formulation can be found in Appendix B.2.

To make the result of this dispatch problem resemble the historical base case, additional constraints are added to meet reference flows on identified CNEs and meet the net position for each market area within the CWE region. Neighboring market areas are represented via historical physical cross border flows from non-CWE countries.

[8]The assumption is that the reference flows take into account long-term nominations, which are not publicly available as separately disclosed values for individual lines. This conclusion is based on the available data and explanations. If this is not the case, we neglect long-term nominations.

Objective function	
Minimization of total marginal cost	(4.9a)
Subject to	
Power plant capacity constraints	(4.9b)
Energy storage constraints	(4.9c)
Renewable energy generation	(4.9d)
Nodal demands	(4.9e)
Reference net positions for CWE zones	(4.9f)
Net exports for non-FB borders	(4.9g)
Reference flows of CNEs	(4.9h)
Line capacity constraints	(4.9i)

Power flow constraints apply to all lines denoted as CNEs, which includes not only the lines that have reference flows but also cross border lines, some of which are not identified through the matching of CNEs (see Section 4.4.3). If reference flows on CNEs are not available over the full time frame or the CNEs are manually added, power flow constraints apply. The power flow constraints also account for critical outage (CO) to incorporate the n-1 character of the underlying load flows in the base case, which are also part of the matched reference flows. The COs are defined as outages that cause a change in line flow on the critical branch (CB) of more than 5% of $F_{\max,c}$. Additionally, only 75% of line capacities are available in the base case calculation for CNEs without reference flow.[9]

Solving this optimization problem over the described time horizon of one week yields the full power plant schedules for all modeled regions. The resulting nodal net injections allow to compute line flows in the whole network as well as RAMs for all network elements under all possible contingencies. Some GSK strategies also rely on the power output calculations of the base cases as detailed in the following section.

[9]The 25% is chosen to cover for FRM and FAV security margins, which are already part of the matched reference flows.

Table 4.2: Explanation and mathematical formulation of tested GSK strategies

GSK strategy	Description	w_u for unit u weighted according to	Considers D2CF
$P_{\max}$	Maximum power output or capacity	$P_{\max,u}/\Sigma_u P_{\max,u}$	No
P	Scheduled power output	$P_u/\Sigma_u P_u$	Yes
$P_{\max} - P$	Available power output ("margin")	$(P_{\max,u} - P_u)/\Sigma_u(P_{\max,u} - P_u)$	Only for P_u
Flat	Uniform distribution of weights	$1/card(n)$	No

Source: Own table.

4.4.5 Tested Generation Shift Key strategies

Table 4.2 describes the GSK strategies tested in this analysis. They are strategies frequently used or tested in academia and by TSOs (see Section 4.3). The goal is to quantify how strategies affect the flow-based market coupling domain on an aggregated level and the zonal PTDF values of individual CNEs . An evaluation of the quality of strategies, e.g. quantifying the redispatch measures caused by the accuracy of GSKs, is beyond the scope of this analysis.

The tested GSK strategies weight generating units according to their capacity, scheduled output or the available power output margin. The weights of all units are summed up depending on the nodes they are connected to (U_n, see Appendix B.2). These strategies are tested against a "naive" strategy, the so-called "flat" strategy, which uniformly distributed net position changes across all nodes (see Section 4.3). Note that weighting only considers units u located in the same zone (U_z, see Appendix B.2) as the unit, for which the weighting is done, as exemplified in Section 4.2.

While weighting is the first choice of constructing a GSK, with the goal of mapping unit behavior correctly, the second choice entails selecting *which* units participate in the GSK. This often consists of a general choice dependent on power plant characteristics. Regarding the "static" characteristics of power plants, such as fuel and technology, GSKs generally encompass market-driven generating units with flexible output (Van den Bergh, Boury, and Delarue 2016; Amprion et al. 2014), i.e. mostly dispatchable conventional power plants with sufficient flexibility. In this analysis, all conventional power plants with the exception of nuclear power plants are considered for the GSKs, in addition to biomass and waste-fueled power plants. Supply-dependent renewable energy sources, PV and wind energy, do not participate in the GSKs. Pumped-storage power plants are considered, while all other forms of hydro power plants are not included. Note that the power plants do not have to fulfill any other criteria, such as a minimum capacity.

Additionally, daily information can be taken into account for the construction of the

GSK, namely which units are expected to be operating. This is depicted in the last column of Table 4.2. The flat strategy does not consider information from the daily D2CF and is therefore the same for every timestamp. For the strategy weighting according to capacities, all considered units are taken into the GSK, regardless of D2CF information. The strategy therefore becomes a capacity-weighted flat strategy. The strategy weighting according to scheduled outputs *only* considers units that are expected to run based on the D-2 forecast.[10] The strategy weighting according to the available margin considers D2CF information only for P_u. A unit, which is not expected to run, is weighted according to its full capacity.

In this analysis, hourly GSKs are deployed to adequately map unit behavior. Time averaging of GSKs, e.g. creating GSKs for peak and off-peak times, can lead to loss of accuracy in the power flow computations, especially when the considered variability in GSKs is high (Van den Bergh and Delarue 2016). Also Dierstein 2017; Schönheit and Sikora 2018 advise against time averaging and suggest to use hourly GSK values, the latter based on a statistical analysis of hourly marginal effects of net position changes on power outputs. For the flat strategy and the capacity-weighted strategy time averaging would not pose an issue, as they are constant across time steps. The other two strategies consider D2CF information and lead to weights with considerable time variability, which is why this analysis refrains from time averaging.

It is important to note that the same GSK strategy is applied universally for all considered CWE control zones in this analysis. While this is not a *realistic* representation of the operative status quo it helps to *identify the influence* of GSK strategies on the FBMC domain and individual network element. Essentially, all aspects are held constant with GSK strategies as the only changing parameter. The purpose of using "pure" GSK strategies is to facilitate the comparison between them. In reality, different countries, and even control zones within countries, deploy different GSK strategies (Van den Bergh, Boury, and Delarue 2016; 50Hertz et al. 2017). Establishing a GSK strategy is a prerogative of each TSO and is likely shaped by aspects such as grid topology, power plant portfolio, control zone-specific expertise and operative feasibility.

Lastly, as indicated in Section 4.1, this analysis explicitly refrains from evaluating the "goodness" of GSK strategies. A compulsory element of such an evaluation is the quantification of day-ahead market costs *and* accruing congestion management costs, especially

[10] Note that the capacity strategy $P_{\max,u}$ could also only take into account operating units. In the deployed linear dispatch model, however, P_u is often equal to $P_{\max,u}$ since no positive spinning-up reserves are imposed. Thus, the first two strategies would result in very similar, and at times equal weighting of nodes.

redispatch and curtailment. For instance, counter trading costs caused by different GSK strategies is quantified by Dierstein (2017). This means that simply reporting the lowest day-ahead dispatch costs as a criterion for "good" GSK strategies can be misleading as the strategy resulting in the largest domains would be preferred. However, domains that are "too large" can spawn extensive and costly curative measures by TSOs , such as curtailment and redispatch. A full evaluation of system costs associated with GSK strategies is necessary for evaluating the goodness of GSK strategies, which is beyond the scope of this work. Rather, the analysis at hand focuses on methods for modeling FBMC and evaluating if GSK strategies substantially affect FBMC domains and critical network elements.

4.4.6 Underlying data

The analysis relies on several data sources. One main data source is the JAO Utility Tool, which allows for downloading flow-based pre-coupling and post-coupling operational data, cf. Joint Allocation Office (2019). From this, daily data files regarding the critical network elements can be retrieved as well as daily aggregated data, such as the D-2 net positions. The usage of JAO data is further described in Section 4.4.2 and 4.4.3.

Load time series can be obtained from JAO's aggregated D2CF data as well. The values, however, are not equal to the total load, as the *vertical* load is reported. Thus, the aggregated load from the ENTSO-E Transparency Platform serves as a proxy in the methodology described in Section 4.4.4, to adequately represent the total demanded energy and compute a representative dispatch. Lastly, cross-border flows of non-CWE borders are also ENTSO-E values. Here, only *actual* flows are available. Hence, the model suffers from differences between anticipated cross-border flows of the "true" D2CFs, not publicly available, and actual flows.

In addition to data regarding FBMC, other datasets are used to compute a base case. The power plant data is based on Weibezahn et al. (2018) and Schlecht (2018), generation cost assumption on Schröder et al. (2013) and Egerer et al. (2014) and grid topology as well as the spacial distribution of demand are based on the methodology proposed in Kunz et al. (2017), however generalized for all regions within the CWE. Note that the grid data set used in this study is openly available and is based around information gathered from open-source geographical data sets as described in Kunz et al. (2017). There are differences in topology and technical parameters compared to the visually

available ENTSO-E grid map[11] and the TYNDP 2018 grid dataset, which is available by request, but not republishable.[12] The model used is POMATO (Weinhold 2020b) which combines grid and market perspectives into a comprehensive framework and is available under Lesser GNU Public Licence.

4.5 Results and implications

The effect of GSK strategies are discussed on two levels of detail. On an aggregated level, Section 4.5.1 shows the resulting FBMC domains, exemplary for one timestep and selected borders and their bilateral exchanges. In Section 4.5.2, the effects on two exemplary individual CNECs are visualized. The impact on all relevant CNECs is quantified and evaluated. Note that the chosen timesteps for visualization are *not* representative of the analyzed week. The visualizations merely serve to facilitate the understanding of the complex and many-sided aspects of FBMC results.

4.5.1 Effect on flow-based market coupling domain

The visualization of resulting domains gives an impression of the effect different GSK strategies have on flow-based market coupling. For this, an exemplary timestep, t134 (February 18, 2018 between 13:00 and 14:00), is selected. This hour is chosen because it exhibits visually easily detectable differences in FBMC domains. Figure 4.7 depicts the generation by fuel and aggregated load for all five zones during the selected hour. The timestep is characterized by an export situation for France and import for Germany and the Netherlands. Belgium is close to a balance of zero.

Figure 4.8 displays the domains for the borders Germany-France and Germany-Netherlands for the selected timestep t134. As discussed in Section 4.2, specifically in Figure 4.1, each constraint represents a specific CNEC, its RAM as derived in the base case, and a sensitivity to changes in net position through the zonal PTDFs. The innermost CNECs define the domain and thus the available cross-border capacities to the market. The GSK strategy affects the sensitivity of a CNEC toward deviations in the net position and therefore changes the composition of a domain for an identical base case.

Four different domains are displayed in Figure 4.8, corresponding to the selected GSK strategies. The ranges of the axes are harmonized to ensure comparability. As described in Section 4.4, not only CNECs can constrain the domain, but all CWE cross-border

[11] See: https://www.entsoe.eu/data/map/
[12] See: https://docstore.entsoe.eu/stum/

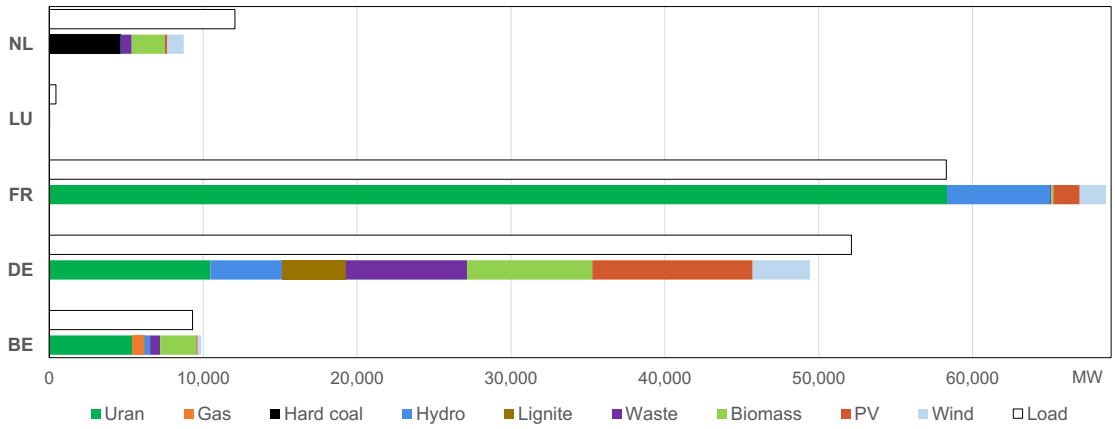

Figure 4.7: Generation by fuel and demand per zone for timestep t134. Source: Own figure.

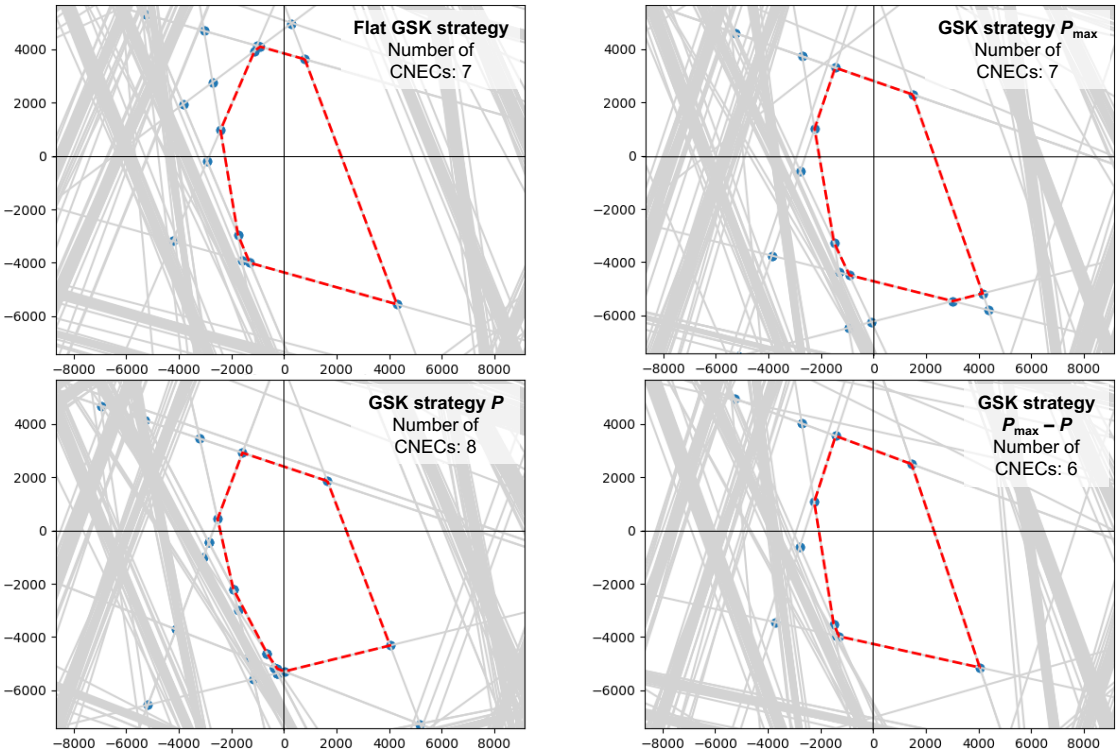

Figure 4.8: Two-dimensional domains (in MW) for the borders DE-FR (x-axis) and DE-NL (y-axis) for timestamp t134 depending on the chosen GSK strategy. Positive values express an increasing bilateral net position change, with more export from Germany to the respective importing country. Source: Own figure.

lines are included as well. The coordinate origin of all displayed domains refers to the reference net positions (cf. explanations in Section 4.2.2). Consequently, deviations from the origins represent net position *changes*, not total net positions.

Several aspects can be observed in Figure 4.8. First, the left sides of the domains are more restricted than the right sides. This means a further decrease of the bilateral net position DE-FR is more limited since the net position of France is already positive and large. Second, the domains are constrained by few CNECs, ranging from six to eight for this particular timestep. This aspect is true for most hours of the analyzed week. Third, there are differences in shape and size between the GSK-dependent domains.

On the upper end of the domain, representing an increasing bilateral net position change between DE-NL, the flat strategy allows for a change in exchange of roughly (0, 4000). This exchange is more limited under the three other strategies, especially when deploying the GSK strategy P, where the maximum is less than (0, 3000). The lower spectrum of the domain is most limited under the flat strategy and the strategy $P_{\max} - P$, at a point of (0, -4000). Here, strategy P allows for the greatest deviation in exchange, roughly (0, -5500). Also, the lower-right corner is substantially more "stretched" in the case of the flat strategy, reaching a point of almost (4000, -6000). Strategy P limits this combination of exchanges to roughly (4000, -5000).

While in this hour, the flat strategy and strategy P exhibit the greatest differences, this cannot be generalized. The strategies lead to varying results throughout the analyzed week, with different combinations of strategies showing similarities and a lack of an identifiable "outlier" strategy. The effect of GSK strategies is likely to be affected by the given market situation, such as aggregated loads, reference net position and renewable energy production. Also the composition of conventional power generation will affect how GSK strategies influence the FBMC domains.

The JAO domain for this timestep is displayed in Figure B.1 in Appendix B.1. Note that the JAO domain differs in size and shape from any obtained domains discussed above. This is due to deploying *pure* GSK strategies in this analysis, i.e. the same strategy is used for the entire CWE region, as described in Section 4.4.5. Therefore, the results do not match or represent the actual FBMC domains.

As described above, the choice of strategy can lead to substantial differences in permitted bilateral net position changes or combinations of bilateral net position changes. However, insights derived from a visualized analysis are limited and quantifying the effect of GSK strategies on the domain is a challenge. For this reason, a more detailed analysis of CNEC-specific effects is described in the following section.

4.5.2 Effect on critical network elements

While the exemplary results in Figure 4.8 give insights into the shape and size of the domains depending on the GSK strategy, it does not convey what CNECs actually compose the domain. The general question is, whether or not the same set of CNECs compose the domain for different GSK strategies and if so, how sensitive these specific CNECs are to net position changes.

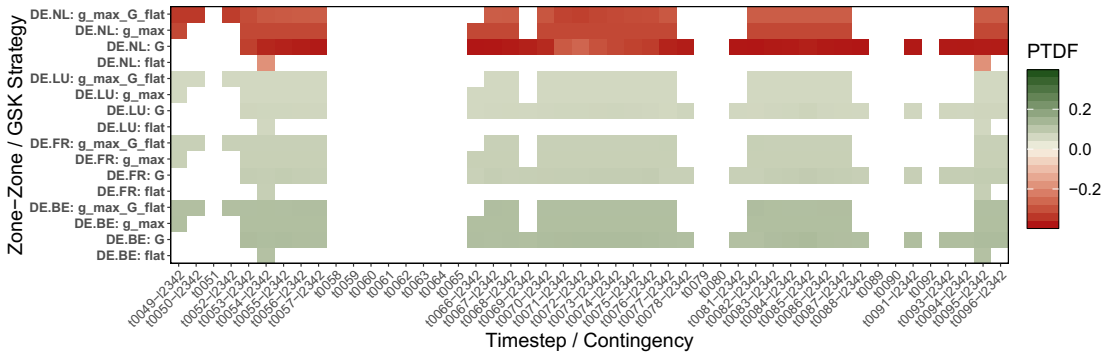

Figure 4.9: Zone-to-zone PTDF values for line l1695 ("Geertruidenberg-Krimpen a/d IJssel W" in NL) for each DE-to-zone combination during every timestep of day 3 and 4, depending on the analyzed GSK strategies. Source: Own figure.

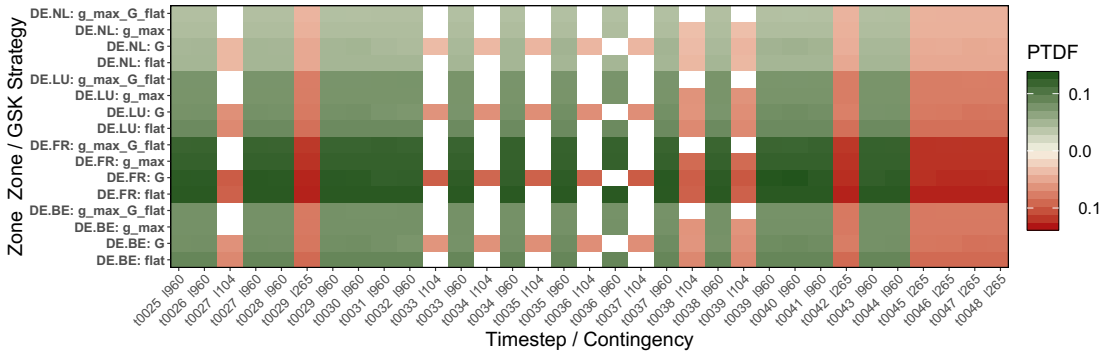

Figure 4.10: Zone-to-zone PTDF values for line l961 ("Vogelgrun - Eichstetten" cross-border line FR-DE) for each DE-to-zone combination during every timestep of day 2, depending on the analyzed GSK strategies. Source: Own figure.

The effects of different GSK strategies and n-1 cases for two exemplary CNECs are displayed in Figure 4.9 and 4.10. On the x-axis, the timesteps are shown in addition to the outage (contingency), under which the respective CNEC becomes a constraint of the FBMC domain. The y-axis displays the various zone-to-zone combinations including

Germany, under all tested GSK strategies. For all combinations of timestep/contingency and zone-to-zone/GSK strategy, the colors display the size of the respective zone-to-zone PTDF value. Zone-to-zone PTDFs are constructed by subtracting the zonal PTDF of zone B from the zonal PTDF of zone A. The interpretation of zone-to-zone PTDF values (in this example of the A-B zonal PTDF matrix) is the sensitivities of CNECs to bilateral net position changes, where the net position increase of zone A is countered by a net position decrease of zone B (50Hertz et al. 2017). In contrast to zone-to-slack PTDFs, one main advantage of zone-to-zone PTDF is their independence of the slack node location (50Hertz et al. 2017; Van den Bergh, Delarue, and D'haeseleer 2014). White indicates that for the combination in question the CNEC does *not* constrain the market coupling domain. Note that if this is the case for all combinations of zone-to-zone and GSK strategy for a specific timestep, no outage is indicated on the x-axis.

Figure 4.9 depicts the zone-to-zone PTDF values for CNEC l1695 for day 3 and 4 of the analyzed week. This line is located in the Netherlands. It constrains the domain often but not during all timesteps. Furthermore, it appears as a constraint always under the same contingency, namely l2342 ("Geertruidenberg-Krimpen a/d IJssel Z"). The zone-to-zone PTDF values are largest for the DE-NL combination, which is a sensible result due to its location. For the remaining zone-to-zone combinations, the PTDF values are comparatively smaller but still of substantial size, with the largest values for DE-BE. This exemplifies that CNECs are also affected by net position changes of zones, in which they are not located. Further, zonal PTDFs also exist for zone-to-zone combinations of zones, which are *not directly* connected by an inter-connector, such as Germany and Belgium. Within a coupled market, bilateral net position changes can still occur when the ensuing exchange of energy is realized through lines of neighbouring zone. In this case, the line in NL is affected by changes in the DE-BE exchange and can thus be the limiting constraint of the FBMC domain, even if only changes in the bilateral DE-BE exchange occur.

For CNEC l1695, zonal PTDFs values change across time and GSK strategies for the DE-NL combination. This is a first indication that GSK strategies can substantially alter zone-to-line sensitivities. For the remaining zone-to-zone combinations, the PTDF values are relatively similar.

In Figure 4.10, the zone-to-zone PTDF values for CNEC l961 are shown. This is an inter-connector between France and Germany, which constrains the domain for *every* timestep on day 2 at least under one GSK strategy. A noticeable difference to l1695 is that for many timesteps the CNEC appears *twice* as a domain constraint. This is

due to different contingencies, l960 ("Muhlbach-Muhlbach")[13] and/or l104 ("Asphard-Kuhmoos") for the majority of timesteps, in addition to l265 ("Eichstetten-Muhlbach ROT") for a few timesteps.

The zonal PTDF values are largest for the DE-FR combination, which is a logical result. For all zone-to-zone combinations, values change across timesteps and GSK strategies. The greatest effect, however, stems from the contingencies. For timesteps, during which the CNEC accounts for two domain constraints, zonal PTDF values vary most substantially. Concretely, the values change signs with alternating outages.

Both lines, CNEC l961 and l1695, exemplify that GSK strategies can substantially affect zonal PTDF values. Also, the GSK strategy often determines whether or not a CNEC constrains the domain. The visualization gives a good impression of how PTDF values change across timesteps, GSK strategies and contingencies. The magnitude of numerical differences, however, is hard to observe for some timesteps.

To quantify the difference of PTDF values across GSK strategies, all PTDF values of a CNEC within a zone-to-zone combination are grouped according to the GSK strategies. The "GSK groups" contain the PTDF values for all timesteps and contingencies, irrespective of whether the CNEC is part of the domain or not. Subsequently, for each CNEC a one-way analysis of variance (ANOVA) test is conducted to test if there is a substantial difference between the expected PTDF values of the GSK groups.

Table 4.3 displays the resulting p-values of the ANOVA tests for all combinations of CNEC and zone-to-zone. All CNECs that are part of the domain during at least one hour of the analyzed week are displayed. For all combinations, the p-value is well below any significance level, e.g. 0.01 or 0.001. This indicates that there are significant differences of the mean PTDF values between the GSK groups. As the ANOVA-test evaluates the ratio of between-group and within-group variance, it is sensible to quantify the differences in group means. Therefore, the maximum difference between group means for all combinations is computed and displayed on the right-hand side of Table 4.3.[14]

While all the mean differences are significant, not all of them are of large magnitude.

[13] l960 represents a shorter line which is essentially an extension of l265, however with different orientation.

[14] Note that pairs of parallel lines exist, namely l970-2083, l1688-l2355, l1691-l2338 and l1704-l2351. Due to the same start and end nodes, in addition to the same line characteristics (e.g. reactance), they are characterized by the same resulting nodal PTDF values, zonal PTDF values and difference in average PTDF values between the GSK groups. However, other parallel lines are missing (e.g. l2342, cf. discussion on Figure 4.9 above). This can be attributed to the ConvexHull algorithm employed to determine the domain as well as preprocessing beforehand to limit the amount of data, where lines with very similar parameters can be eliminated.

Table 4.3: ANOVA test and maximum difference for means of zone-to-zone Power Transfer Distribution Factor values from different Generation Shift Key strategies

Critical Network Element		p-values of ANOVA test on mean PTDF values of "GSK group"				Maximum difference between mean PTDF values of "GSK group"			
ID	JAO name or (*) *cross-border line from database used in this application*	DE-BE	DE-FR	DE-LU	DE-NL	DE-BE	DE-FR	DE-LU	DE-NL
l27	Gronau - Hengelo HENGL SW					0.009	0.006	0.006	0.015
l71	(*) *Oberzier - Maasbracht DE-NL*					0.018	0.012	0.013	0.040
l77	(*) *St.Avoid - Ensdorf FR-DE*					0.001	0.018	0.002	0.004
l341	Großkrotzenburg-Urberach					0.015	0.017	0.016	0.023
l360	Diele-Meeden SCHWARZ					0.009	0.009	0.009	0.030
l787	(*) *Sotel - Aubange LU-BE*					0.016	0.004	0.012	0.008
l789	(*) *Aubange - Moulaine BE-FR*					0.026	0.006	0.008	0.005
l811	L 400kV N0 1 DOEL-MERCATOR					0.018	0.001	0.002	0.009
l961	(*) *Vogelgrun - Eichstetten FR-DE*					0.008	0.007	0.007	0.006
l970	(*) *Avelin - Ruien FR-NL*					0.018	0.002	0.004	0.008
l1688	Ens-Lelystad W		0.000			0.005	0.002	0.003	**0.090**
l1691	Diemen-Lelystad W					0.005	0.002	0.003	**0.101**
l1695	Geertruidenb.-Krimpen a/d IJssel W					0.005	0.002	0.003	**0.104**
l1700	Eindhoven-Maasbracht W					0.016	0.003	0.004	0.037
l1704	L 400kV N0 1 ZANDVLIET-DOEL					0.019	0.002	0.003	0.017
l1821	Diele-Meeden WEISS					0.009	0.009	0.009	0.030
l1852	Conneforde-Diele WEISS					0.019	0.019	0.019	0.014
l2083	(*) *Avelin - Ruien FR-NL*					0.018	0.002	0.004	0.008
l2335	Ens-Lelystad Z					0.005	0.002	0.003	**0.090**
l2338	Diemen-Lelystad Z					0.005	0.002	0.003	**0.101**
l2351	L 400kV N0 2 ZANDVLIET-DOEL					0.019	0.002	0.003	0.017

Note that CWE cross-border lines are added if not already included as identified CNECs from the JAO database. Their names are marked by (*).

This is due to the small variance of many PTDF values within a group, which also makes small differences in group means significant. The underlined values are greater or equal to 0.01 and the bold-faced values exceed 0.05. The zone-to-zone PTDFs of Germany and the Netherlands show the greatest amount of large mean differences. This is the only bilateral combination with values exceeding 0.05. Germany-Belgium shows mean differences greater than 0.01 for about half of the CNEs . DE-FR and DE-LU mostly have small mean differences.

Note that even a difference in expected values of 0.01 can have large effects. First, it is an average value, which means that differences for individual hours are greater. Second, it translates into an additional percentage point of net position change expected to accrue on this CNE. The magnitude of this effect depends on the extent of net position changes.

This analysis indicates that the tested GSK strategies can lead to substantially different zonal PTDF values and consequently different compositions, sizes and shapes of FBMC domains. While this is not true for every CNEC and every zone-to-zone combination, some network elements are heavily affected by the GSK strategy choice.

This systematic evaluation and the CNE-specific quantification of the effect of GSK strategies can help TSOs to identify, which network elements are affected most. While the CNE selection process is an important element of flow-based market coupling, an evaluation along the lines of the presented analysis can facilitate to assess and anticipate the magnitude of network element-specific effects resulting from parameter choices, such as GSK strategies.

4.6 Conclusion and summary

Flow-based market coupling enables the creation of market coupling domains, taking into account a simplified form of the grid and its restrictions. It relies on the nomination of critical network elements, the construction of base cases, the estimation of Generation Shift Keys and the consideration of outages to ensure n-1 security. While all factors are sources of uncertainty for the accuracy of flow-based market coupling, GSKs and base case computation represent the two main deliberate aspects.

Therefore, this analysis proposes a new approach for the construction of base cases, relying on the matching of historical flows on critical network elements. A base case dispatch is created for one representative week, ensuring that aggregated D-2 properties and the reference flows on most critical network elements match the historical ones. This novel method has the advantage of achieving a close approximation of the domain

origins, composed of reference net positions and reference flows, from which domains are created. Upon the constructed base case for one analyzed week, several common GSK strategies are deployed universally across all zones to systematically isolate their effects. The impact of GSK strategies is evaluated not only on an aggregated level and but also on a detailed critical network element-specific level, setting this analysis apart from previous research.

The results indicate that GSK strategies can have a profound effect on the shape and size of flow-based market coupling domains. While this is true for many hours of the analyzed week, the effect is neither universally large nor can one outlier GSK strategy be identified. This leads to the conclusion that the effect of GSK strategies heavily depends on the given market situation, such as load, export balance, penetration of renewable energies and conventional power generation. Other insights include that domains tend to be constrained by a small amount of CNEs, often fewer than ten.

The critical network element-specific evaluation reveals that GSK strategies have a statistically significant effect on how CNECs are expected to be affected during market coupling, expressed by zone-to-zone PTDF values. While the effect is significant for all relevant CNECs, the magnitudes of differences between GSK strategies vary across CNECs. A large fraction of CNECs show maximum absolute differences between PTDF value means of "GSK groups" less than 0.01 and many CNECs show differences between 0.01 and 0.05. For a few CNECs, the differences exceed 0.05, for some even 0.1. This corroborates the conclusion that choosing a GSK strategy does not have a universal effect but is relevant for certain grid element, as exemplary shown. It largely depends on the location of CNECs and the weighting of nearby nodes.

In light of the extending geographical scope of flow-based market coupling, this analysis highlights the importance of developing accurate and transparent flow-based market coupling parameters, especially GSKs, and a detailed model-based representation of the base case to capture and quantify the effects of GSK strategies.

A systematic evaluation of how exogenous factors influence the impact of GSKs is subject of further research. This especially pertains to the effect of renewable energy penetration on GSK strategies, requiring dynamic GSK computation based on predicted exogenous factors, as well as the effect of renewable energy generation on the impact of GSK strategies. Some GSK strategies may prove to be more accurate and/or robust with changing renewable feed-in situations, which is an issue of growing importance. Ideally, the analysis should be done based on an entire year, which will be facilitated when CNECs are determined endogenously. Also, the goodness of GSK strategies has to be evaluated,

which entails computing day-ahead dispatch costs, based on GSK-dependent cross-border capacities as well as the quantification of ensuing congestion management costs to correct for possible estimation errors stemming from base cases and GSKs. The overall welfare needs to be quantified to balance the trade-off between large trading domains with better price convergence and the reduction of congestion management costs. Further research should also address the issue of time averaging of GSKs and its effect on the accuracy of calculations. The juxtaposition of simpler GSK strategies and time averaging of GSK strategies, as two method of simplification, poses an interesting research question. Lastly, the effect of country-specific or transmission system operator-specific GSKs has to be evaluated. While this analysis focuses on "pure" strategies to isolate their effects on the flow-based market coupling domain, a more realistic representation of "mixed" strategies should be the basis of future research.

Chapter 5

Uncertainty-Aware Capacity Allocation in Flow-Based Market Coupling

"Finally, renewable generation depends on the availability of energy sources such as wind and sun that are not only uncontrollable but also unpredictable."

(Kirschen and Strbac (2004))

This chapter is the submitted to *Applied Energy*. The preprint is available online: https://arxiv.org/abs/2109.04968. Appendix C contains the nomenclature to this publication.

5.1 Introduction

The development of the European internal energy market (IEM) for electricity aims to establish a free pan-European trading platform, under a policy triangle of security of supply, affordability and sustainability (European Commission 1997). The achievement of coupling the vast majority of Europe's electricity consumption in a single market is the result of over 20 years of continuous policy iteration for more effective market designs and procedures (Glachant 2010). The core of market coupling is defined by capacity allocation and congestion management (CACM) routines, i.e., methods to determine exchange capacities between market areas such that trade is as unconstrained as possible, while ensuring secure system operation.

While development of efficient methods for CACM where motivated in the early stages of the IEM by the scarcity of transmission capacity inherited from pre-liberalized market structures (Meeus and Belmans 2008), current developments are driven by the system's transformation towards a sustainable energy system (Directorate General for Energy 2019). Methods to derive available exchange capacities that are currently employed are the net transfer capacity (NTC) – and available transfer capacity (ATC) methods and flow-based market coupling (FBMC), which is the designated IEM target model. FBMC differs from NTC and ATC in how transmission capacity is allocated to markets. While NTC and ATC derive bounds for bilateral transactions, FBMC derives bounds on the net-position of all involved bidding zones, thereby capturing all transactions simultaneously. Hence, FBMC promises more efficient capacity allocation and better transparency. However, FBMC was inaugurated in 2015 as part of EC Directive 15/1222 (European Commission 2015), but was envisioned by the responsible market parties early in the development of the IEM (ETSO 2001a). Therefore, while FBMC improves (Rte et al. 2015), it was not envisioned to realise policy targets of high shares of renewable energy sources (RES).

As part of the Clean Energy Package (Directorate General for Energy 2019) and the accompanying update to the regulation on CACM, European Commission (2019a) explicitly addresses specifics in the capacity allocation process. Among others, the regulation requires the transmission system operators (TSOs) to allocate a minimum of physical line capacity to the market. This kind of engagement with specifics of the process illustrates the regulatory willingness to closer engage with market design to bring the process in line with sustainability targets. Therefore, FBMC, as an important part of the IEM, should become an active element of the transformation process.

5.2 Related Literature

Initial publications on FBMC stem from conceptional documentations of the involved TSOs and power exchanges (PXs) (ETSO 2001a; ETSO and EuroPEX 2004). As part of a "dry-run", meaning theoretical operation, in 2008 (Amprion et al. 2011) and a parallel run in 2013 (Rte et al. 2015) the process was evaluated and its efficiency verified. Additionally, FBMC is described in a continuously updated Documentation by the involved TSOs that is currently available as version 5 (50Hertz et al. 2020). Complementary descriptions and research of the involved parameters was published in different articles from TSO workgroups (Schavemaker et al. 2008; Aguado et al. 2012; Marien et al. 2013).

Over the past years, several academic publications provided various modeling approaches to the different components of FBMC. Byers and Hug (2020) provided insights into hte fundamental modeling process and numerically highlights the importance of its parametrization, Schönheit, Weinhold, and Dierstein (2020) and Finck, Ardone, and Fichtner (2018) evaluated the impact of different generation shift keys, a core parameter that describes how generators will participate in cross-border exchange, Schönheit et al. (2021a) described the relation of bidding zone configuration on the selection of network elements that are part of the capacity calculation.

These publications generally limit the scope to specifics of the process and evaluate the relation between parameter choices. However, the process's ability to accommodate policy decisions and impact of integration of large shares of RES is mostly absent. In Schönheit et al. (2021b) the authors describe the TSOs degree of freedom to influence the parametrization and its impact on results. The analysis also includes a scenario with moderate increase in RES capacities. Similarly Matthes et al. (2019) analysis FBMC in for the target year 2025 that results in higher shares of RES, but the implications on FBMC are not discussed.

In this paper we contribute to the body of literature on FBMC in three ways:

- We show how the concept of FBMC allows the inclusion of policy relevant considerations.
- We evaluate the capacity allocation methods of NTC/ATC and FBMC in regards to higher shares of RES.
- To alleviate the shortcoming of perfect foresight in models with high RES shares and no explicit representation of a real-time market, we propose a chance constrained formulation to robustify against network overloads caused by real-time deviations.

5.3 FBMC Concept and Simulation

FBMC is a three-stage process designed to allocate commercial exchange capacity between adjacent electricity markets (i.e., cross-border exchange). It is coordinated by the local TSOs and PXs and aims to accommodate inter-zonal electricity trading with respect to available transmission system capacity and physical power flows. Fig. 5.1 provides an overview of the three FBMC stages and shows their timing, involved stakeholders, parameters and results. For any given day D, the FBMC process starts two days in advance at $D-2$, with the calculation of the so called *basecase*. The basecase is informed by TSO-generated forecasts on the expected point-of-dispatch and provides "*a best estimate of the state of the [...] system for day D*" (50Hertz et al. 2020, p. 26). Based on these forecasts, on additional predefined policies and on regulatory constrains (see discussion below), the TSOs calculate the so called *flow-based parameters* that are used to constrain the commercial exchange in the following *market clearing* stage. Generation and load bids collected from all bidding areas that are part of the Central Western Europe (CWE) region are cleared in the day-ahead (DA) and intraday markets at $D-1$ and $D-0$, respectively. Lastly, during the *re-dispatch* stage, the TSOs may require changes to the generators' final point-of-dispatch to resolve any network congestion or other threats to system security due to real-time conditions (e.g., load and RES injections).

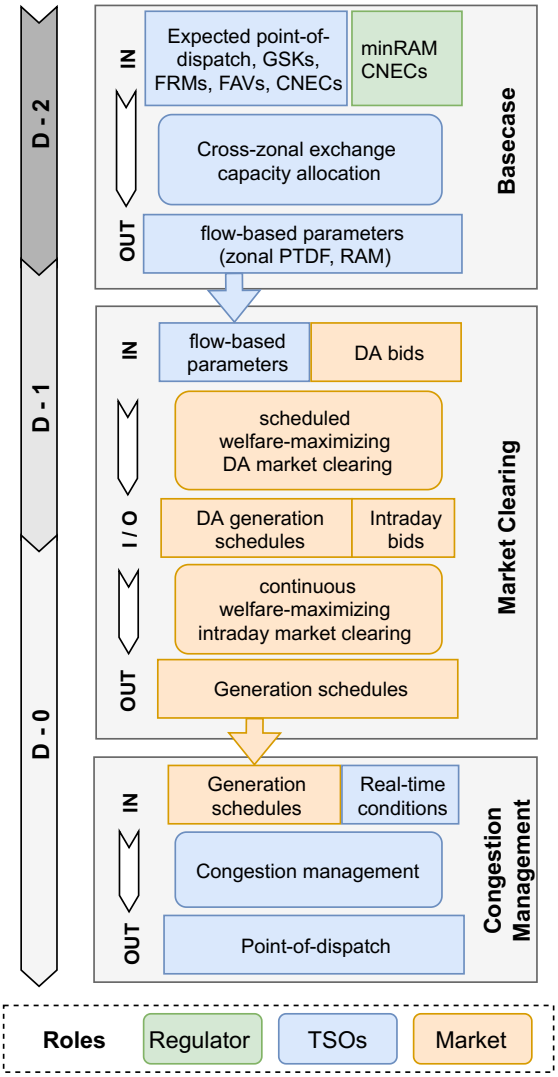

Figure 5.1: FBMC process overview.

5.3.1 Preliminaries

The FBMC process and the definition of the flow-based parameters relies on a model of the physical transmission system, which we formalize as follows. Consider an interconnected transmission network with n nodes and l lines. Further, let each node i be defined by its net power injection I_i collected in column vector $I = [i_i]_{i=1}^n \in \mathbb{R}^n$. If $I_i > 0$, then node i is a net generator, if $I_i < 0$, then node i is a net load. For each vector x there exists exactly one corresponding vector $f = [f_j]_{j=1}^l \in \mathbb{R}^l$ that collects the flows along each line j and is defined by the physics of power flow in a network. The maximum allowable flow (capacity) of each line j is given by $\overline{f}_j$ collected in vector $[\overline{f}_j]_{j=1}^l$. Power flow physics in high-voltage transmission networks allow a linear approximation of the relationship between f and I using a *power transfer distribution factor* matrix PTDF $\in \mathbb{R}^{l \times n}$ such that

$$f = \text{PTDF} \cdot I. \tag{5.1}$$

See, e.g., Weinhold and Mieth (2020a) for a more detailed derivation. Further, assume that the nodes of the network are grouped in z compact *market zones* such that each zone k collects nodes $\mathcal{N}_k$ and $\bigcup_{k=1}^z \mathcal{N}_k = \{1, ..., n\}$ and $\bigcap_{k=1}^z \mathcal{N}_k = \emptyset$. The set of all zones is denoted as $\mathcal{Z}$ and the sum of the injections of all nodes in one zone is called the *net-position* np_k of zone k collected in vector $np \in \mathbb{R}^z = [np_k]_{k=1}^z$. If $np_k > 0$, then zone k is a net exporter and if $np_k < 0$, then zone k is a net importer.

5.3.2 Flow-based formalism

The effectiveness of FBMC to enable least-cost, yet physically feasible day-ahead market outcomes across interconnected market zones hinges on the precise definition of the flow-based parameters, which specify (i) how cross-border power exchange affects power flow on transmission lines and (ii) how much capacity on each line is available to accommodate flow caused by cross-border exchange. Each specification (i) and (ii) is given by the following respective parameter:

(i) **Zonal PTDF**; Zonal PTDF$^z \in \mathbb{R}^{l' \times z}$ maps net-position vector np to the flow on a *selection* of $l' \leq l$ lines in the network, the so called *critical network elements* (CNE).

(ii) **Remaining available margin (RAM)**; For each critical network element (CNE), vector RAM $\in \mathbb{R}^{l'}$ defines the absolute capacity that is available for cross-border trading in the day-ahead market.

Although these parameters are generated, exchanged and published following specific rules requested by regulation and laid out in the documentation of the FBMC process in 50Hertz et al. (2020), they depend on the exact choice of the underlying forecast and meta-parameters that are either chosen at the discretion of the TSOs or given by policy requirements.

First, the exact definition of PTDF^z depends on the chosen CNEs, additional contingency scenarios and so called *generation shift key (GSK)*.

- **CNE/CNEC:** "*A CNE is considered to be significantly impacted by CWE cross-border trade, if its maximum CWE zone-to-zone PTDF is larger than a threshold value that is currently set at 5%.*"

  (p. 19f)

  Network elements are considered CNE only if TSOs determine that their flow is significantly driven by cross-zonal exchange. This selection prevents heavily loaded lines that are largely insensitive to changes in the zones' net-positions to limit inter-zonal exchange capacity allocation. Further, for each network element the TSOs identify a set of contingencies (C), i.e., unplanned outages of network elements, that highly impact the flow on said CNE. The resulting set of critical network elements and contingencies (CNECs), the full PTDF matrix and additional linear outage factors, which capture flow shifts during the selected contingencies, form the basis for PTDF^z computation.

- **GSKs:** "*A GSK aims to deliver the best forecast of the impact on Critical Network Elements of a net-position change [and] is calculated according to the reported available market driven power plant potential of each TSO divided by the sum of market driven power plant potential in the bidding zone.* ". (p. 38ff)

  Since line flows f depend on the injection at every node, the computation of PTDF^z requires an estimation of how changes in net-position np are distributed to changes in net injections I. Assuming that the difference between forecasted net-position in the basecase and the realized net-position in the market phase is small, the set of generators that will serve this difference by "shifting" their production levels can be anticipated. The resulting nodal contribution to net-position changes is formally captured in vector $\text{GSK} \in \mathbb{R}^{n \times z}$ that maps a change Δnp in net-positions to a change in nodal injections ΔI such that

$$\Delta I = \text{GSK}\, \Delta np, \tag{5.2}$$

which further provides a clearer definition of PTDF^z as

$$\text{PTDF}^z = \text{PTDF} \cdot \text{GSK}\,. \tag{5.3}$$

Note that this approach implicitly attributes all possible changes to net-position *np* to changes of dispatchable generators and is ignorant to *np* changes caused by forecast errors of load and RES.

Second, the final RAM value can be corrected by additional *flow reliability margins* (FRMs) and *final adjustment values* (FAVs).

- **FRM:** "*[F]or each Critical Network Element, a Flow Reliability Margin (FRM) has to be defined, that quantifies at least how [...] uncertainty impacts the flow on the Critical Network Element.*"

  (p. 47)

  flow reliability margins (FRMs) are static RAM reductions that are informed by past observations on how the flow on each CNE changed between the basecase forecast and the point-of-dispatch realization. Therefore, FRM captures forecast uncertainty of load and RES injections.

- **FAV:** "*With the Final Adjustment Value (FAV), operational skills and experience that cannot be introduced into the Flow Based-system can find a way into the Flow Based-approach by increasing or decreasing the remaining available margin (RAM) on a CNE for very specific reasons [...] to eliminate the risk of overload on the particular CNE.*"

  (p. 25)

  FAVs decrease or increase RAM based on the operational experience of the TSOs. It may reflect remedial actions at the point of dispatch or other complex system security considerations.

Finally, the available commercial exchange capacity between market zones is defined by constraining the zonal net-positions *relative to the basecase*. For the basecase, the TSOs forecast the expected flow f^{bc} on all CNEs and the expected net-positions np^{bc}. The net-positions that can be realized during the market stage (np^{da}) can only differ from np^{bc} if CNE limits $\overline{f}$ (corrected by FRMs and final adjustment values (FAVs)) are maintained:

$$\text{PTDF}^z(np^{da} - np^{bc}) \leq \overline{f} - (\text{FRM} + \text{FAV}) - f^{bc}. \tag{5.4a}$$

Note that the explicit introduction of np^{bc} in (5.4a) is necessary to ensure the validity of the GSKs and, thus, PTDF^z. See also Schönheit, Weinhold, and Dierstein (2020) for a broader discussion. Eq. (5.4a) can be rewritten as follows:

$$\text{PTDF}^z \cdot np^{da} \leq \overline{f} - (\text{FRM} + \text{FAV}) - f^{bc} + \text{PTDF}^z \cdot np^{bc} \tag{5.4b}$$

$$\Leftrightarrow \quad \text{PTDF}^z \cdot np^{da} \leq \overline{f} - (\text{FRM} + \text{FAV}) - f^{ref} \tag{5.4c}$$

$$\Leftrightarrow \quad \boxed{\text{PTDF}^z \cdot np^{da} \leq \text{RAM}\,.} \tag{5.4d}$$

In Eq. (5.4c), $f^{ref} = f^{bc} - \text{PTDF}^z \cdot np^{bc}$ denotes the *reference flow* that captures a residual between the parameter choices made in PTDF^z and the forecasted f^{bc}. While f^{ref} can be assumed small, it is not necessarily zero. Eq. (5.4d) yields the desired limit on market-based net-positions np^{da} subject to the flow-based parameters PTDF^z and RAM (50Hertz et al. 2020, p. 60). The space of all possible net-positions that fulfill (5.4d) is called *flow-based domain*.

Irregardless of the formal RAM definition, regulations, e.g., the European Commission (2019a, Art. 16), prescribe specific conditions that define a minimal percentage of CNE capacity that must be made available for cross-border exchange and that ensures the feasibility of long-term traded capacities.

- **minRAM:** "*CNECs with a RAM of less than the minRAM factor multiplied by Fmax at zero-balance are assigned an AMR value (adjustment for minRAM) in order to increase the RAM.*"

  (50Hertz et al. 2020, p. 64)

  The minRAM criterion defines a lower bound for the RAM based on the CNEs capacity and is applied after FRMs and FAVs:

  $$\text{RAM} = \max(\text{minRAM} \cdot \overline{f}, \overline{f} - (FRM + FAV) - f^{ref}). \tag{5.5}$$

- **Long-term allocations:** "*the long-term-allocated capacities of the yearly and monthly auctions have to be included in the initial Flow Based-domain*" (p. 66)
  This requirement ensures that trades on energy futures and bilateral delivery contracts outside of the day-ahead or intraday market clearing stage have to be feasible within the flow-based domain.

FRMs, FAVs, minimum remaining available margin (minRAM) and long-term allocations either enlarge the flow-based domain to enable higher price convergence (minRAM),

shrink the flow-based domain to accommodate security margins (FRM), or go both ways (FAV).

5.3.3 Flow based discussion

It is clear, that the resulting flow-based parameters do not only reflect formal definitions, but also methods to account for uncertainty or imperfections, e.g., arising from zonal aggregation and required forecasts. Further, their specific configuration depends on policy considerations on the desired level of restrictions on commercial cross-border exchange. Regulation states a clear goal of achieving higher price convergence (European Commission 2019b). As a result, solely cross zonal tie lines are encouraged to be nominated as CNEs (ACER and CEER 2018, p.8) and the a minRAM of 70% will be required by 2025. This indicates that large trading domains are desirable and that potentially higher cost for congestion management (e.g., real-time redispatch) fall into the responsibility of local TSOs.

In previous academic studies, derivation and application of the flow-based parameters is mostly understood as a strictly formal process. Studies generally focus on the formal dimension in their numerical experiments by describing the relation of a specific parametrization policy to a chosen metric, e.g., system cost or welfare, with the goal to provide a better understanding of parameter choices. Current literature on flow-based parameter policies in relation to system cost exist for GSKs (Voswinkel et al. 2019), minRAMs (Schönheit, Dierstein, and Möst 2021), commercial exchange and uncertainty in the basecase parametrization (Byers and Hug 2020) and selection of CNECs (Schönheit et al. 2021b). All contribute to better understanding the relation between the parameters, however comparability remains difficult since it requires similar definitions on how flow-based domains should be used. Most studies do not explicitly discuss which overall target the capacity allocation strives for.

Since the current regulation explicitly requires a parametrization to provide higher capacities to the markets with the goal to ensure the integration of higher shares of RES (European Commission 2019a) it is important to make these considerations part of the modeling and academic process. Without such considerations the effectiveness of FBMC to accommodate higher shares of RES cannot be definitively answered. With this paper we aim to contribute to this discussion by providing a transparent parametrization of the FBMC process and the underlying market simulations an by numerically show the effects of higher shares of RES. We explicitly discuss different consideration regarding

the permissiveness of day-ahead trading domains by minRAM and CNEC selection and the effect on total system cost and congestion management. In addition we provide a sensible way to include risk-aware security margins FRMs in the modeling process. The permissive capacity allocation in systems with high shares of intermittent generation raises the question of operability. Thus we include process-considerations regarding expected deviations from scheduled generation to make the system more robust.

5.4 Model Formulation

5.4.1 Market Simulation

In addition to computing flow-based parameters, modeling and studying the three-step FBMC process as shown in Fig. 5.1 requires a simulation of basecase, market clearing and congestion management processes. We model all of these steps as a multi-period economic dispatch (ED) problem, where each step is constrained by a specific set of network or transport constraints. The ED is given as:

$$\min \quad \sum_{t\in\mathcal{T}} c(G_t) + p(e^T C_t) \tag{5.6a}$$

$$\text{s.t.} \quad 0 \leq G_t \leq \overline{g} \qquad \forall t \in \mathcal{T} \tag{5.6b}$$

$$0 \leq C_t \leq r_t \qquad \forall t \in \mathcal{T} \tag{5.6c}$$

$$\mathrm{m}^n G_t + \mathrm{m}^n (r_t - C_t) - d_t = I_t \qquad \forall t \in \mathcal{T} \tag{5.6d}$$

$$\mathrm{m}^z G_t + \mathrm{m}^z (r_t - C_t) - m^z d_t = NP_t \qquad \forall t \in \mathcal{T} \tag{5.6e}$$

$$NP_{t,z} = \sum_{z'\in\mathcal{Z}} \mathrm{EX}_{t,z,z'} - \mathrm{EX}_{t,z',z} \qquad \forall t \in \mathcal{T}, \forall z \in \mathcal{Z} \tag{5.6f}$$

$$e^T I_t = 0 \qquad \forall t \in \mathcal{T} \tag{5.6g}$$

where t indicates the market clearing time steps (e.g., hour or 15 minutes) and $\mathcal{T}$ is the set of times steps. Objective function (5.6a) minimizes system cost given by the cost of generation $c(G_t)$ and the cost of curtailing RES pC_t, where $c(\cdot)$ is a generator cost function model, G_t is the vector of generator production levels, C_t is the vector of RES curtailment, p is a scalar curtailment penalty and e is the vector of ones in appropriate dimensions. Constraint (5.6b) enforces limits $\overline{g}$ on generator outputs G_t and constraint (5.6c) limits curtailment C_t to available capacity r_t. Finally, Eqs. (5.6d) and (5.6e) balance power on a nodal and zonal resolution. Nodal energy balance (5.6d) defines

nodal power injections I_t in terms of nodal load and generation by mapping generator and RES injections to each node via map m^n. Similarly, the zonal energy balance defines the zonal net-position NP_t as the difference between zonal load and generation mapping resources and loads into each zone via map m^z. Eq. (5.6f) defines auxiliary variable $\mathrm{EX}_{t,z,z'} \geq 0$, which denotes the bilateral exchange from zone z to zone z'.[1] Eq. (5.6g) enforces system balance. Note that all decision variable of the model are written in capital letters, while are parameters are given as lower case symbols.

Nodal power injections or zonal net-positions of ED (5.6) can be subject to limitations given by the transmission system capacity and chosen power flow model. Hence, FBMC-based market clearing can be modeled by using ED (5.6) and additionally enforcing

$$NP_t \in \mathcal{F}^z \coloneqq \{x : \mathrm{PTDF}_t^z \, x \leq RAM_t\} \qquad \forall t \in \mathcal{T}, \tag{5.7}$$

where $\mathcal{F}^z$ is the flow based domain as derived in Section 5.3 above. Not that the zonal PTDF may be different for each time step, indicated by index t. Alternatively, nodal market clearing, i.e., an economic dispatch that is is constrained by all network transmission lines, can be modeled by constraining (5.6) with

$$I_t \in \mathcal{F}^n \coloneqq \{x : \mathrm{PTDF}^n \, x \leq \overline{f}\} \qquad \forall t \in \mathcal{T}. \tag{5.8}$$

Nodal market clearing limits the cross-zonal exchange only implicitly by taking into account the transmission capacity of the whole network. On the other hand, we can constrain cross-zonal exchange $\mathrm{EX}_{t,z,z'}$ directly using static bilateral NTCs:

$$EX_t \in \mathcal{F}^{ntc} \coloneqq \{x : 0 \leq x \leq ntc\} \qquad \forall t \in \mathcal{T}. \tag{5.9}$$

Notably, the approach in (5.9) does not include a physical power flow model.

All FBMC steps can be modeled through (5.6) in combination with either (5.7), (5.8) or (5.9) as summarized in the FBMC column of Table 5.1. Notably, the basecase is a nodal market clearing, following the intuition that the basecase should resemble D-0 as well as possible. The day-ahead market is cleared zonally with flow-based parameters PTDF_t^z and RAM derived from the basecase results as per (5.4). D-0 congestion management again relies on a nodal network representation (5.8) and requires additional constraints

[1] Note, when constraints apply to net-positions only, the EX remains unconstrained. Therefore, a small penalty factor for EX is included in the objective function to discourage excessive exchange but does not distort model results with less than 0.5% of the objective value.

that impose cost for deviating from the market clearing results:

$$C(G^{red}) = c^{red} \sum_{t \in \mathcal{T}} |G_t^{red}| \tag{5.10a}$$

$$G_t - g_t^{da} = G_t^{red} \qquad \forall t \in \mathcal{T} \tag{5.10b}$$

$$C_t \geq c^{da} \qquad \forall t \in \mathcal{T}, \tag{5.10c}$$

where g_t^{da} and c_t^{da} are the decisions on G_t and C_t from the previous market clearing stage. Note that we do not explicitly model an intraday market stage and, for now, assume that load and RES injections do not change between the market stage and the real-time point of dispatch.

For reference, zonal market clearing using static bilateral NTCs and a nodal market clearing are modeled and their resulting formulations are itemized in Table 5.1 as well. The NTC market clearing is modeled in two steps, because it does not require a basecase computation. The necessary congestion management step is the same as for FBMC. The nodal market is a one-shot optimization of (5.6) subject to nodal power flow constraints (5.8). Notably, the nodal market does not require a congestion management stage, because generation and network are co-optimized.

5.4.2 Probabilistic FRMs via Chance Constraints

The formulations of the previous section model FBMC under perfect foresight of load and RES injections. The intention to provide efficient commercial exchange capacities to the market in combination with high shares of intermittent renewable generation poses the question of operability and how the forecasting characteristics of the basecase can

Table 5.1: Model configuration for FBMC, Nodal and NTC market clearing.

	FBMC	**NTC**	**Nodal**
D-2: Basecase	(5.6a) s.t. (5.6b)–(5.6g), (5.8)	–	–
D-1: Market Clearing	(5.6a) s.t. (5.6b)–(5.6g), (5.7)	(5.6a) s.t. (5.6b)–(5.6g), (5.9)	(5.6a) s.t. (5.6b)–(5.6g), (5.8)
D-0: Congestion Management	(5.6a)+(5.10a) s.t. (5.6b)–(5.6g), (5.8), (5.10b), (5.10c)		

be used to robustify results against RES uncertainty. As outlined in Section 5.3 above, the FBMC concept recognizes the existence of forecast uncertainties in the basecase by introducing FRMs, which are tuned based on historical data and TSO-defined *risk levels* (50Hertz et al. 2020, Fig. 4-2). Specifically, TSOs use historical data to estimate the $(1-\epsilon)$-percentile of the absolute deviation between forecasted basecase flows f^{bc}, corrected by changes in the market schedule, and the realized real-time flows. By setting FRMs to at least the value of this $(1-\epsilon)$-percentile, TSOs ensure that lines are not overloaded due RES or load forecast errors with a probability of $(1-\epsilon)$. Thus, ϵ defines the risk level and is usually chosen small (e.g., $1-5\%$).

To date, studies on FBMC have not considered FRMs in terms of an uncertainty model and risk-threshold, but rather employ fixed security margins that are applied uniformly to all CNEs, see e.g., Schönheit, Dierstein, and Möst (2021), Schönheit et al. (2020b), and Wyrwoll et al. (2019). While such simplifications may be motivated by a lack of historical data to simulate the FRM computation process prescribed by regulation, ignoring the specific impact of real-time control actions caused by intermittent renewable injections may obstruct a clear assessment of the effectiveness of FBMC in high RES systems. As an alternative, we propose to model risk-aware FRMs that explicitly internalize an RES uncertainty model and the impact of real-time generator control actions on each CNE. To this end, instead of creating an empirical uncertainty model of the flow forecast error on each CNE, we rely on a parameterized RES forecast error distribution and control participation factors. This approach leverages results on chance-constrained optimal power flow proposed by Bienstock, Chertkov, and Harnett (2014).

We model the uncertain injection from RES generators as $r_t(\omega) = r_t + \omega_t$, where ω_t is a zero-mean random vector that captures the forecast error of renewable generation r_t. We assume that the distribution can be modeled as a normal distribution such that $\omega_t \sim N(0, \Sigma_t)$, where Σ_t denotes the covariance matrix of ω_t. Following the empirical results of Dvorkin et al. (2016b), we will rely on the assumption that ω_t is normally distributed for the remainder of this paper, but note that the proposed approach can be modified to accommodate different distributional assumptions, see e.g., Roald et al. (2015) and Dvorkin (2020). Next, we realize that, because the basecase and day-ahead markets are cleared based on forecast r_t, error ω_t creates a system imbalance and assume that the systems reaction to this imbalance can be anticipated. Similar to how GSKs capture the estimated distribution of Δnp to all generators, we introduce vector of control participation factors α_t that maps the reaction of generators to imbalance ω_t

as:

$$G_t(\omega_t) = G_t - \alpha_t(e^T\omega_t). \tag{5.11}$$

Since ω_t and, thus, $G_t(\omega_t)$ are random variables, we first formulate the zonal ED as a probabilistic problem

$$\begin{aligned}
\min \quad & \mathbb{E}[C(G(\omega))] && && \text{(5.12a)}\\
s.t. \quad & \\
& \mathbb{P}[0 \le G_{g,t}(\omega) \le \overline{g_g}] \ge 1-\epsilon && \forall t \in \mathcal{T},\ \forall g \in \mathcal{G} && \text{(5.12b)}\\
& \mathbb{P}[\mathrm{PTDF}^z_{j,t} \cdot NP_t(w) \le \overline{f}_j - f^{ref}_{j,t}] \ge 1-\epsilon && \forall t \in \mathcal{T},\ \forall j \in \mathrm{CNEC} && \text{(5.12c)}\\
& \mathrm{m}^z_g G_t(\omega) + \mathrm{m}^z_r r_t(\omega) - C_t - d_t = \mathrm{NP}_t(w) && \forall t \in \mathcal{T},\ \forall \omega \in \Omega. && \text{(5.12d)}
\end{aligned}$$

Objective (5.12a) minimizes the expected system cost. Constraints (5.12b) and (5.12c), ensure that the probability a generator can not fulfill its required response $\alpha_t(e^T\omega_t)$ or of a CNEC being overloaded at least $(1-\epsilon)$. These so called *chance constraints* resemble the value-at-risk, a risk metric commonly used in the finance industry (Bienstock, Chertkov, and Harnett 2014). Lastly, Eq. (5.12d) ensures that the system is balanced for all possible outcomes of $\omega \in \Omega$.

Problem (5.12) can not be solved directly, but allows a computationally tractable deterministic reformulation. First, recall that ω_t is zero mean, i.e., $\mathbb{E}[\omega_t] = 0$. For a linear cost function model $c(G)$ we therefore get $\mathbb{E}[c(G(\omega_t))] = c(G(\omega_t))$. See, e.g., Mieth (2021) for the derivations for quadratic cost functions. Next, chance-constraints (5.12b) and (5.12c) can be reformulated by realizing that for any random vector $x \sim N(\mu, \Sigma)$ it holds that (Bienstock, Chertkov, and Harnett 2014):

$$\mathbb{P}[x \le \overline{x}] \ge (1-\epsilon) \quad \Leftrightarrow \quad \mu + \Phi^{-1}(1-\epsilon)\sigma(x) \le \overline{x}, \tag{5.13}$$

where Φ is the cumulative distribution function of the standard normal distribution and $\sigma(x)$ is the standard deviation of x. Using (5.13) to reformulate (5.12b) and (5.12c) we

get:

$$\mathbb{E}[G_{g,t}(\omega_t)] = \mathbb{E}[G_{g,t} - \alpha_{g,t}(e^T\omega_t)] = G_{g,t} \tag{5.14}$$

$$\sigma(G_{g,t}(\omega_t)) = \sqrt{\mathrm{Var}[\alpha_{g,t}(e^T\omega_t)]} = \sqrt{\alpha_{g,t}^2(e^T\Sigma_t e)} = \alpha_{g,t}S_t \tag{5.15}$$

$$\begin{aligned}\mathbb{E}[\mathrm{PTDF}^z_{j,t}\cdot NP_t(w)] &= \mathbb{E}[\mathrm{PTDF}^z_{j,t}(m^z_g G_t(\omega) + m^z_r r_t(\omega) - m^z_d d_t)] \\ &= \mathrm{PTDF}^z_{j,t}(m^z_g G_t + m^z_r r_t - m^z_d d_t)\end{aligned} \tag{5.16}$$

$$\begin{aligned}\sigma[\mathrm{PTDF}^z_{j,t}\cdot NP_t(w)] &= \sqrt{\mathrm{Var}[\mathrm{PTDF}^z_{j,t}(m^z_g G_t(\omega_t) + m^z_r r_t(\omega_t) - m^z_d d_t)]} \\ &= \sqrt{[\mathrm{PTDF}_{j,t}(m^z_r - m^z_g\alpha e^t)]\Sigma_t[\mathrm{PTDF}_{j,t}(m^z_r - m^z_g\alpha e^t)]^T} \\ &= \|\mathrm{PTDF}^z(m^z_r - m^z_g\alpha e^T)\Sigma_t^{1/2}\|_2,\end{aligned} \tag{5.17}$$

where we define $S_t^2 = e^T\Sigma_t e$ and $\|\cdot\|_2$ denotes the 2-norm. For more a more detailed explanation we refer to Bienstock, Chertkov, and Harnett (2014) or Mieth (2021). Lastly, (5.12d) holds for all ω_t, if the system is balanced in expectation and the sum of all control actions is exactly equal to the system imbalance, i.e.,:

$$e^T\alpha_t(e^T\omega) = e^T\omega_t \quad \Leftrightarrow \quad e^T\alpha_t = 1. \tag{5.18}$$

Thus, the deterministic reformulation of (5.12) is given as:

$$\min \quad C(G(\omega)) \tag{5.19a}$$

$$s.t. \quad G_t + z_\epsilon\alpha s \le \overline{g} \qquad \forall t \in \mathcal{T} \tag{5.19b}$$

$$-G_t + z_\epsilon\alpha s \ge 0 \qquad \forall t \in \mathcal{T} \tag{5.19c}$$

$$\mathrm{PTDF}^z_{j,t}\,\mathrm{NP}_t \le \overline{f}_j - f^{ref}_{j,t} - z_\epsilon T_{j,t} \qquad \forall t \in \mathcal{T},\ \forall j \in \mathrm{CNEC} \tag{5.19d}$$

$$\|\mathrm{PTDF}^z_{j,t}(m^z_r - m^z_g\alpha e^T)\Sigma^{1/2}\|_2 \le T_{j,t} \qquad \forall t \in \mathcal{T},\ \forall j \in \mathrm{CNEC} \tag{5.19e}$$

$$\mathrm{m}^z_g G_t + \mathrm{m}^z_r\hat{r}_t - \mathrm{m}^z_d d_t = \mathrm{NP}_t \qquad \forall t \in \mathcal{T} \tag{5.19f}$$

$$e^T\alpha_t = 1 \qquad \forall t \in \mathcal{T} \tag{5.19g}$$

where we use $z_\epsilon = \Phi^{-1}(1-\epsilon)$ for a more concise notation and introduce auxiliary variable $T_{j,t}$ to denote the standard deviation of the flow across CNEC j. Constraint (5.19e) is a second-order conic constraint, which is convex and can be solved efficiently by modern off-the-shelf solvers. The variable α can be chosen as parameter, similarly to the GSK, or optimized as a decision variable in (5.19). In this paper we use the latter approach, thus allowing for an optimized generator response. Additionally, the risk-level is defined

with $\epsilon = 5\%$ and Σ is calculated with an assumed standard deviation of $10\% \cdot \hat{r}$, that is consistent with other publications (Mieth 2021; Dvorkin et al. 2016b, p.29).

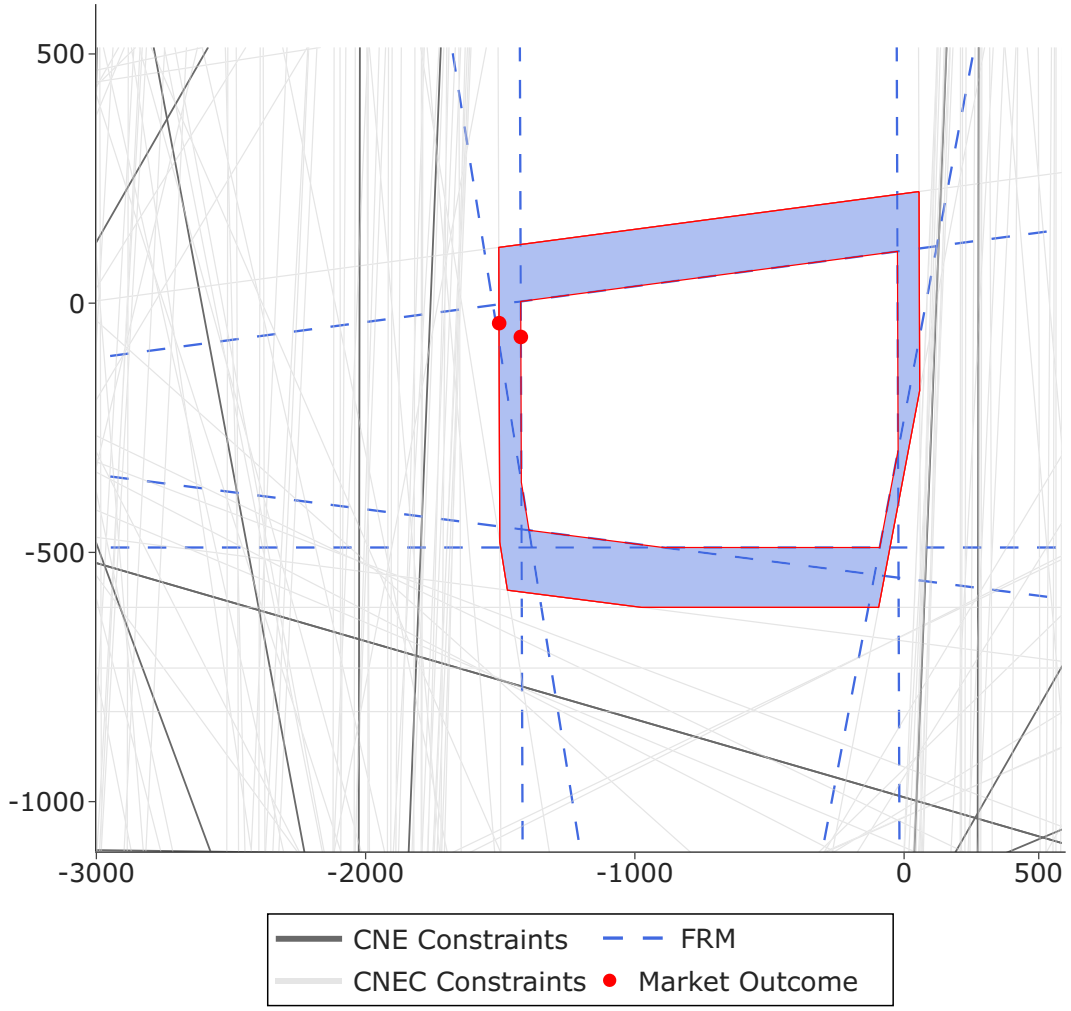

Figure 5.2: Flow-based domain with FRMs for exchange *Zone 1* - *Zone 2* (x-axis) and *Zone 2* - *Zone 3* (y-axis).

We interpret term $z_\epsilon T_{j,t}$ in Eq. (5.19d) as the endogenous FRM that reduces capacity for each CNEC based on the RES uncertainty model. Fig. 5.2 shows the resulting impact on the flow-based domain for a single time step for exchange from *Zone 1* to *Zone 2* on the x-axis and *Zone 2* to *Zone 3* on the y-axis. See Fig. 5.3 in Section 5.5 below for an illustration of the zones. Each line in the figure corresponds to a row of the zonal power transmission distribution factor (PTDF) matrix and colored light grey for CNECs and dark grey for CNE. The The FRMs (dashed blue) reduce the flow-based domain by the

blue area. Subsequently, the market outcome (red dot) will also move inward, leading to lower commercial exchange. However, Fig. 5.2 shows, that the necessary margin to achieve $(1 - \epsilon)$ security differs among CNEs, which indicates that a fixed FRM proxy margin would over- or underestimate the RAM on some CNE.

5.5 Case Study

5.5.1 Data Set

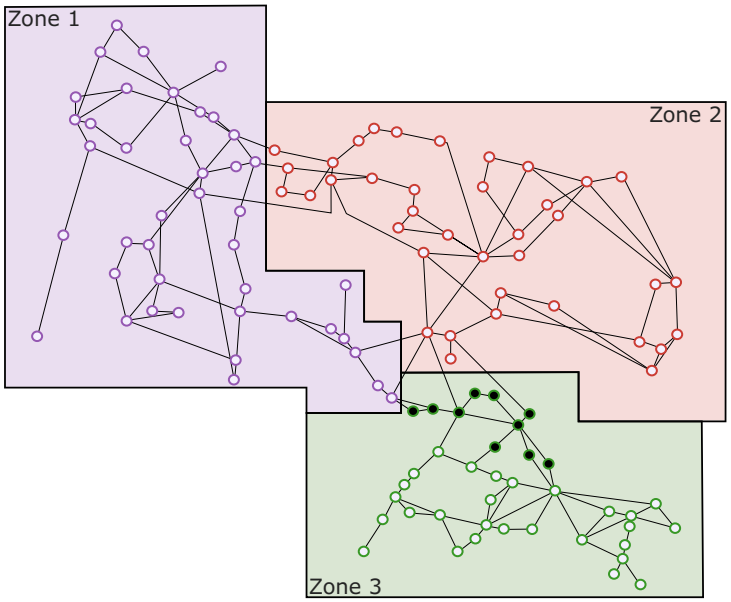

Figure 5.3: Topology of the IEEE 118 bus case, zones indicated by color. Changes in topology from the original data are indicated with filled nodes.

The numerical experiments build on the Pena, Martinez-Anido, and Hodge (2017) version of the IEEE-118 bus case, which augments the well known case study by additional generation technologies, zonal configuration and hourly load and RES injection timeseries for a full year. In Pena, Martinez-Anido, and Hodge (2017) the authors kept the original topology from the original IEEE-118 bus network, but line capacities are generously (4x-5x) scaled with installed capacity.

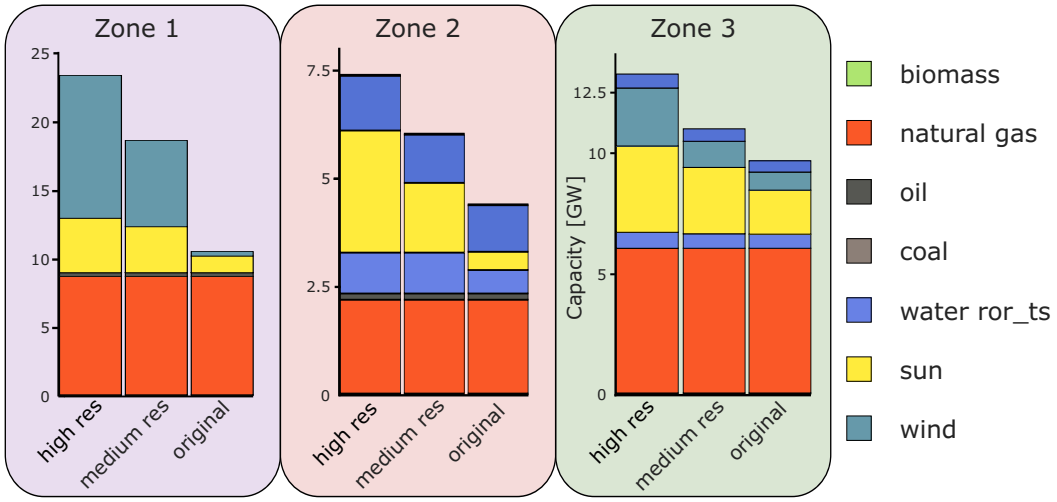

Figure 5.4: Installed capacities three scenarios *original*, *medium res* and *high res*.

The original data in Pena, Martinez-Anido, and Hodge (2017) is complemented in this study with two scenarios that further increase the share of RES generation in the total generation over the model horizon from 26% in the original data to 50% (*medium res*) and 70% (*high res*). The resulting installed capacities are itemized in Fig. 5.4 for the three scenarios *original*, *medium res* and *high res*. To better reflect the scarcity of transmission capacity, all line capacities are scaled down by 30%. Additionally, the zonal configuration was slightly adjusted so all zones have shared borders. This is indicated in Fig. 5.3 by nodes that are filled solid black, which where allocated to "Zone 2" (red) and are now allocated to "Zone 3" (green).

We analyze the effectiveness of FBMC by comparing system cost, which are composed of generation cost at the market clearing stage and additional congestion management (redispatch) in D-0. See also (5.10). We set the cost for redispatch to 30$ per MWh and curtailment cost to 5$ per MWh. Note that congestion management does not just revert a zonal solution to an optimal nodal solution, but tries to achieve a network-feasible solution with minimal deviations from the zonal solution.

5.5.2 Zonal benchmarks

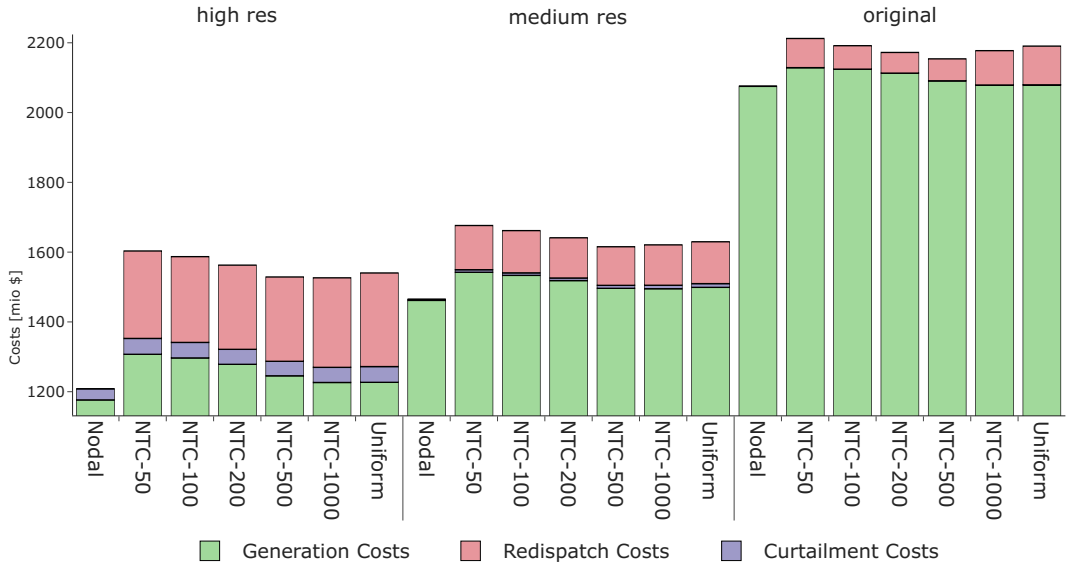

Figure 5.5: Cost composition of zonal NTCs market clearing and the nodal reference.

Fig. 5.5 shows the benchmark reference results for the three scenarios for nodal market clearing and zonal market clearing subject to NTCs. See also Table 5.1. System cost are evaluated after congestion management and include cost for curtailment and redispatch. The Nodal solution on the left represents the economic optimum that does not require redispatch. Zonal market clearing is shown with increasing NTCs from left to right. The "Uniform pricing" case describes market clearing without any commercial exchange constraints.

The results show the expected pattern:

- Generation cost decrease with higher shares of cheap generation from RES.
- The nodal dispatch is the least cost solution, with no redispatch required. Additionally, due to cost for congestion management, zonal solutions often show increased generation cost.
- For zonal market clearing, more exchange capacities lead to lower generation cost. However, cost for congestion management can outweigh these savings.

Notably, an NTCs of 500 MW leads to the lowest cost dispatch for zonal market clearing. In the following, this results will be used as a benchmark for the FBMC results.

5.5.3 Flow-based parametrization

As described in Section 5.3.1, the flow-based parameters are used to solve the day-ahead stage in FBMC. They are composed of the zonal PTDF and RAM values and calculated from basecase generation schedules g^{bc}, power flows f^{bc} and net-positions np^{bc}. For our numerical experiments we aim to stay as close as possible to the reference given by the documented process by 50Hertz et al. (2020). We model the basecase as nodal pricing with full network representation (nodal). The zonal PTDF is composed of all cross-border lines and internal lines with a zone-to-zone PTDF value larger than 5%. Contingencies are included based on a 20% line-to-line sensitivity in case of an outage using so called load-outage distribution factors as per Jiachun et al. (2009), i.e. lines are considered contingencies that distribute 20% of line loading to the CNE. For all scenarios we use a so called *Pro-Rata* approach to calculate GSKs, i.e., changes in net-position are distributed based on the online dispatchable generation capacity at each time step (50Hertz et al. 2020; Dierstein 2017). Consistent with current practises (Amprion 2019), a 20% minRAM is employed. This also ensures feasibility of (5.4c) as the feasible region (5.7) is cases where a suboptimal GSK leads to negative RAM values. The resulting FBMC configurations is denoted as *FBMC* in the following results section. To illustrate the the impact of less restrictive flow-based parameterization a second parametrization is evaluated that only considers cross-border lines as CNEs and enforces a minRAM of 70%, denoted as $FBMC^{+}$.

All scenarios and market configurations where solved using the open Power Market Tool (POMATO) (Weinhold and Mieth 2020b) written in Python and Julia. The calculation where done on standard PC hardware with a Ryzen 7 and 32GB of memory using the Gurobi solver (Gurobi Optimization LLC 2018) for the deterministic configurations and the Mosek solver (MOSEK ApS 2021) for configurations using chance constraints.

5.5.4 Deterministic FBMC

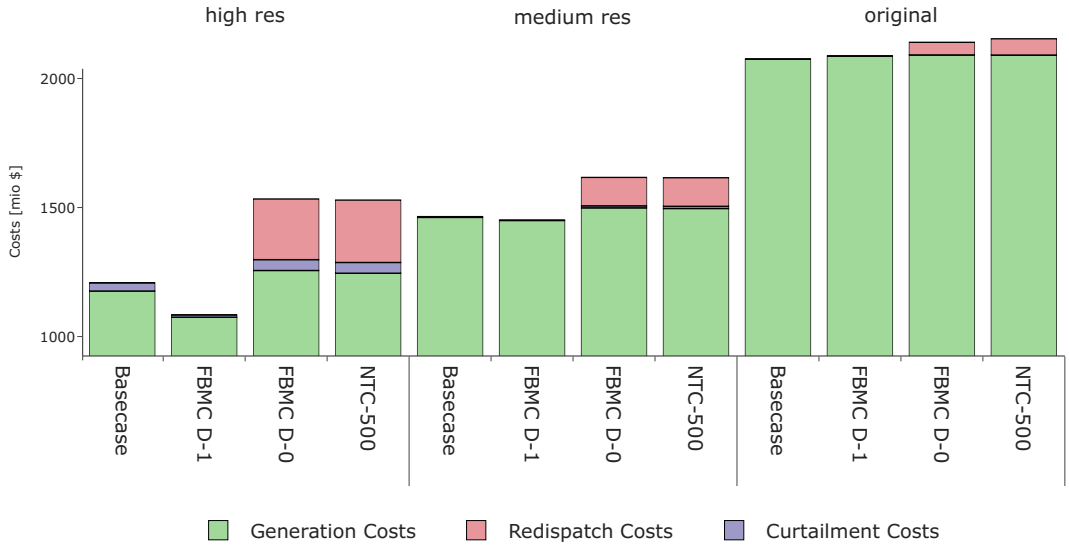

Figure 5.6: Cost composition of FBMC and NTC market clearing. For each scenario: Basecase, D-1 zonal market clearing and D-0 redispatch and NTC reference.

Fig. 5.6 shows the FBMC results for the three scenarios. The total system cost in *D-0* are also depicted in Table 5.2. The three market steps are depicted as *Basecase* (D-2), *FBMC D-1* for the day-ahead stage and *FBMC D-0* for congestion management. *NTC-500* is included as the least cost zonal reference. For each scenario the basecase represents the expected market outcome, from which the flow-based parameters are derived and used to clear the market stage. The composition of this market result shows different characteristics for the three scenarios. For the *original* data, the cost are higher compared to the nodal *Basecase*. The flow-based parameters overly constrains zonal exchange and therefore lead to sub-optimal market result, whereas for the *high res* scenario shows lower cost in the market result. The additional cost for congestion management depend on the systems ability to accommodate the market result. Here the *FBMC* and *NTC* solutions are very close, with *FBMC* generally resulting in higher generation cost, but lower cost for congestion management. Similarly to the reference results from Section 5.5, the NTC and FBMC solutions illustrate the trade-off between capacity allocation and congestion management, where FBMC is more restrictive and generally leads to less congestion management at higher cost in generation.

The results from the more permissive $FBMC^{+}$ configuration, which enforces a 70% minRAM and only considers cross-border CNEs, further illustrates this point. Table 5.2

Table 5.2: System cost including generation and congestion management (CM) for each scenario.

		FBMC	FBMC$^+$	NTC-500	Nodal
original	Generation	2091.45	2083.82	2091.01	2075.16
	Curtailment	0.03	0.08	0.01	0
	Redispatch	48.76	89.28	62.89	0
	total CM	48.79	89.36	62.9	0
	total	2140.24	2173.18	2153.92	2075.16
medium res	Generation	1498.85	1499.01	1496.28	1461.68
	Curtailment	7.8	9.97	8.55	3.06
	Redispatch	110	115.91	110.61	0
	total CM	117.8	125.88	119.17	3.06
	total	1616.66	1624.89	1615.44	1464.74
high res	Generation	1256.1	1239.05	1245.6	1176.48
	Curtailment	42.1	42.73	41.57	31.81
	Redispatch	234.89	243.57	241.63	0
	total CM	276.99	286.29	283.2	31.81
	total	1533.09	1525.35	1528.8	1208.29

shows the cost decomposition and Table 5.3 show the respective redispatch (R), curtailment (C) and combined congestion management (sum) volumes for each scenario and include the *FBMC*$^+$ configuration. Here, the *FBMC*$^+$ proves less restrictive than the NTC and FBMC configurations. With the original data, the relaxed flow-based parameters *FBMC*$^+$ lead to overall higher cost, due to increased congestion management. For higher shares of intermittent renewable generation, larger exchange capacities become more efficient and, while still with the higher congestion management volumes, provide the lowest cost for zonal market clearing.

Table 5.3: Quantities of redispatch (R) and curtailment (C) in TWh for each scenario.

	original			medium res			high res		
	C	R	C+R	C	R	C+R	C	R	C+R
FBMC	0.01	1.63	1.64	1.56	3.67	5.23	8.42	7.83	16.25
FBMC$^+$	0.02	2.98	3	1.99	3.86	5.85	8.55	8.12	16.67
NTC-500	0	2.1	2.1	1.71	3.69	5.4	8.31	8.05	16.36
Nodal	0	0	0	0.61	0	0.61	6.36	0	6.36

5.5.5 Probabilistic FRMs

The *high res* scenario reaches a share of intermittent renewable generation of 60 %. The dispatch of these share proves challenging when accounting for expected deviation between the day-ahead market stage and real-time. In Section 5.4.2 we propose a chance-constrained formulation for FRMs, that reduce the flow-based domain based on an assumed distribution of forecast errors ω_t. The results in the previous section illustrate the trade-off between permissive capacity allocation and increased congestion management, which can be desirable depending of the associated cost. However, the cost for congestion management will change, and presumably increase, if the real-time availability is subject to forecast errors. For the numerical experiment we take a closer look at the $FBMC^+$ scenario, as it provides the larges trading capacities and would be subject the largest impact of forecast errors.

Including FRMs, denoted as $FBMC^+$ *CC* will, in a deterministic case, lead to lower capacities allocated to the market and extension to higher cost in congestion management compared to the $FBMC^+$ scenario without FRMs. To evaluate the impact of forecast errors that occur in real time, congestion management is run multiple times for both $FBMC^+$ *CC* and $FBMC^+$ subject to randomized real-time deviations ω that follow a normal distribution with a relative standard deviation of 10% from expected infeed. The generator response α, that is an endogenous result from the chance constraint formulation, is used for both scenarios to calculate the generator response real-time deviations. The numeric results are obtained from 20 full-year runs, with hourly independent real-time deviations.

Table 5.4 shows that, indeed, the resulting expected cost for congestion management are indeed lower in the $FBMC^+$ *CC*, illustrating its higher robustness against real-time deviations. Here, we see the same values as in Table 5.2 with no deviations at real-time $\omega = 0$ with $FBMC^+$ *CC* resulting in higher cost for congestion management. With real-time deviations $\omega > 0$ cost for congestion management are overall lower in the $FBMC^+$ *CC* due to reduced exchange margins in response of expected deviations and the set generator's response.

The result is visualized in Fig. 5.7 that visualizes the range of hourly cost for congestion management in for randomized different real-time deviations. The blue band shows the range of cost for $FBMC^+$ and the red band show cost for $FBMC^+$ *CC* that includes the FRMs. The solid lines are the hourly cost without real-time deviations. The figure visualizes that, while often aligned, the $FBMC^+$ *CC* case provides a tighter band that

Table 5.4: Cost for redispatch (R) and curtailment (C) in relation to forecast error ω.

	$\omega = 0$			$\omega > 0$		
	C	R	C+R	C	R	C+R
FBMC$^+$	42.73	243.57	286.29	41.42	248.41	289.83
FBMC$^+$ CC	44.43	246.6	291.03	42.09	245.16	287.25

on average provides lower cost.

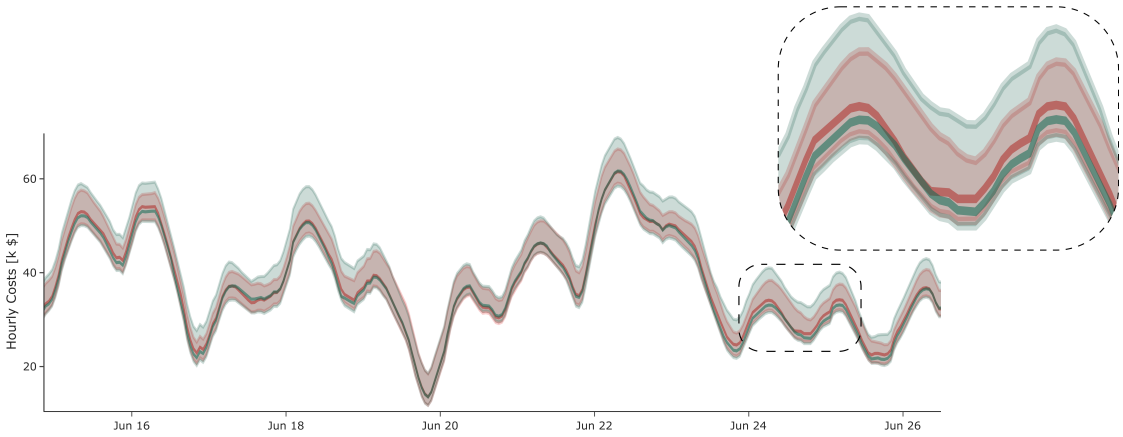

Figure 5.7: Range of hourly cost for congestion management for randomised real-time deviations ω for FBMC$^+$ (blue) and FBMC$^+$ CC (red)

5.5.6 Conclusion

In this paper we illustrate considerations necessary to model FBMC, in particular parameter choices that are policy relevant and consider high shares of intermittent renewable generation. The numerical experiments, conducted with the open power system model POMATO, highlight the effectiveness of FBMC in comparison to zonal market configurations using NTCs and quantifies the trade-off between permissive capacity allocation and increased congestion management.

Results on the extended IEEE 118 bus network of Pena, Martinez-Anido, and Hodge (2017) show, that for high shares of intermittent generation more permissive commercial exchange capacities provide the most effective configurations. Here, the additional cost for congestion management do not overcompensate lower cost in the market clearing stage. For smaller RES shares, more restrictive domains prove efficient.

With high shares of intermittent generation, the system becomes more susceptible to

real-time deviation or forecast errors. We propose a chance constraint formulation that builds on the forecasting characteristics of the D-2 basecase and results in risk aware security FRMs in the day-ahead market clearing stage. Initially, the reduced commercial exchange capacity provides higher system cost but proves more robust against real-time deviations than the deterministic counter part. The proposed formulation is a suitable extension to modeling FBMC.

Chapter 6

Evaluating Policy Implications on the Restrictiveness of Flow-based Market Coupling with High Shares of Intermittent Generation: A Case Study for Central Western Europe

> "The power system was fine until the economists took it away from the engineers."
>
> *(Unknown Engineer)*

This chapter is submitted to *Energy Policy*. The preprint is available online: https://arxiv.org/abs/2109.04940. Appendix D contains the original appendix to this publication.

6.1 Introduction

Europe's commitment to become climate neutral by 2050 (Directorate General for Energy 2019) draws a clear path towards a fully decarbonized electricity sector. This transformation is characterized by a large increase of intermittent renewable generation as well as decommissioning of conventional and nuclear generation capacities. The current understanding of the European internal energy market (IEM) for electricity aims to efficiently achieve climate targets while providing generators and consumers with non-discriminatory market access and ensuring affordable and secure provision of electricity (European Commission 2019a, Art. 1). Its central mechanism of capacity allocation and congestion management aims to efficiently use transmission infrastructure, ensures operational security and transparency (European Commission 2015). Capacity allocation summarizes methods and regulations that dimension electricity trading volumes that market participants can use based on the physical transmission capacity and operational considerations. Congestion management describes actions and protocols taken by the responsible transmission system operator (TSO) if network congestion occurs (European Commission 1997).

Previously, capacity allocation was implemented using static, bilateral net transfer capacities (NTCs) which are based on non-public network models and assessments of historic network loads (ETSO 2001c). NTCs do not account for restricting transmission assets within market zones, resulting in potentially too conservative capacity allocation and increased congestion management (Amprion et al. 2011). From 2015 flow-based market coupling (FBMC) replaced NTC as the preferred method for capacity allocation and is used in the Central Western European (CWE) region[1]. Its main advantages are increased transparency from a clear methodology that describes capacity allocation and, more importantly, the fact that capacity is allocated towards the net-position of each bidding-zone based on individual network elements rather than bilaterally. Thus FBMC ultimately better aligns with the goal to utilize the network infrastructure more efficiently and accommodate the transformation towards a decarbonized electricity system.

Since its inauguration, FBMC has proven to be the more efficient capacity allocation compared to NTCs while providing at least the same level of security (Rte et al. 2015). However, the regulation seeks to achieve high levels of price convergence between market areas leading to overall lower prices, unrestricted access to the internal European electricity market and thereby successful integration of renewable generation (ACER

[1]The CWE region consists of Belgium, France, Germany, Luxembourg and the Netherlands.

and CEER 2020). As a result, Regulation (European Commission 2019a) makes clear that capacity allocation has priority over congestion management and that TSOs should not restrict commercial exchange to solve internal congestion, as previously observed by ACER (2016), and explicitly requires that at least 70% of physical capacity is allocated to the market. This directly alters the method to derive trading volumes and makes clear that the formal process of deriving trading volumes using the flow-based methodology, which originally made the appearance to be a purely formal process, leaves room to implement policy decisions. While the canon of academic literature explains and depicts the formal side of the process and explores the effects of different parametrizations very well, policy decisions that define which outcome aligns with political targets are rarely discussed or numerically modeled.

Capacity allocation within FBMC is defined by the two objectives of market integration, meaning the provision of commercial exchange capacity, and secure operation whose outcome results in very different trading volumes. This paper aims to highlight this presumed trade-off and investigate how the policy decision to prioritize capacity allocation over congestion management affects the efficiency of FBMC and its ability to accommodate the transformation in the European electricity system.

6.2 Background on FBMC and Literature Review

FBMC is a multistage process coordinated by the TSOs which aims to allocate commercial exchange capacities to the markets. Specifically, this three step process, as depicted in Figure 6.1, consists of a D-2 capacity forecast, also called basecase, which represents the best estimate of the system state at delivery (50Hertz et al. 2020). The basecase is a result from forecasts on load and renewable energy sources (RES) feed-in and already allocated capacities e.g. long term nominations in conjunction with network models. Based on this forecast so called flow-based parameters are calculated and used to constrain the commercial exchange in the day-ahead market coupling stage. In the European IEM the central market clearing algorithm Pan-European Hybrid Electricity Market Integration Algorithm (EUPHEMIA) matches demand and supply bids subject to the flow-based parameters and maximizing welfare. Lastly, D-0 stage consists of intraday adjustments and congestion management, meaning the physical delivery.

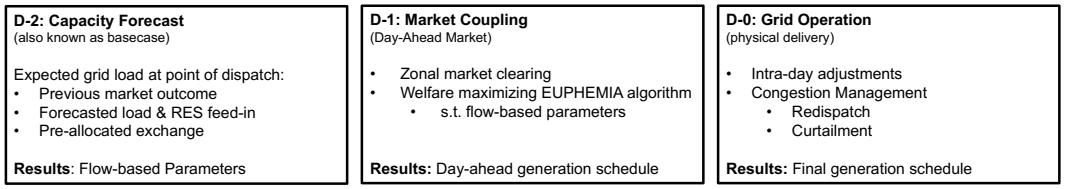

Figure 6.1: Flow-based market coupling process. Based on Amprion (2019)

Of particular interest are the so called flow-based parameters, which constitute the capacity allocation in FBMC and are generated, exchanged and published following specific rules requested by regulation (European Commission 2015). Details on how the parameters are obtained is laid out in the documentation of the flow-based process (50Hertz et al. 2020). Their composition is defined by the remaining available commercial exchange capacity, denoted as remaining available margin (RAM), in the expected market outcome (basecase) which are allocated towards the markets, i.e. to changes in net-position np between the forecasted basecase (bc) and day-ahead market coupling stage (da). Net-position changes are mapped to power flows in line elements by a so-called zonal power transmission distribution factor (PTDF) matrix and bounded by line capacities $\overline{f}$

Equations (6.1) formalise this intuition, i.e. remaining capacities on network elements are available changes in net-positions between day-ahead and basecase. Reformulation yields Equation (6.1c) that defines the flow-based parameters in terms of net-positions in the day-ahead market stage, the zonal PTDF matrix and RAMs and align with the formulation in p.55.

$$\mathrm{PTDF}^z(np^{da} - np^{bc}) \leq \overline{f} - f^{bc} \tag{6.1a}$$

$$\mathrm{PTDF}^z\, np^{da} \leq \overline{f} - f^{bc} + \mathrm{PTDF}^z\, np^{bc} \tag{6.1b}$$

$$\mathrm{PTDF}^z\, np^{da} \leq \overline{f} - f^{ref} = RAM \tag{6.1c}$$

A PTDF matrix expresses the physical relation between nodal power injections and power flows in the transmission network in a linear manner (Weinhold and Mieth 2020a). The PTDF is composed of a selection of network elements and contingencies and is thereby part of the parametrization. Commonly, critical network elements (CNEs) are selected based on their importance to commercial exchange. For each CNE a set of contingencies (C) can be considered if its outage significant impacts the respective CNE. The resulting set of critical network elements and contingencies (CNECs) comprises the

PTDF matrix. Given that the net-position delta between basecase and day-ahead is small, the set of generators that will serve this delta by "shifting" their output can be anticipated. The resulting participation factor is called generation shift key (GSK) and is used as a mapping to transform the nodal PTDF^n to zonal $\text{PTDF}^z = \text{PTDF}^n \cdot GSK$.

The resulting flow-based parameters define a feasible region for net-positions within the day-ahead market stage.

$$\mathcal{F}^z(\text{PTDF}^z, RAM) = \{x : \text{PTDF}^z\, x \leq RAM\} \qquad \forall t \in \mathcal{T} \tag{6.2}$$

The resulting feasible region (6.2) has to be at least non-empty, which is not necessarily given, and either requires specific parametrization of the basecase, e.g. enforcing margins on CNE or processing of the PTDF and RAM. This can be done by selecting specific networks elements that compose the PTDF, enforce minimum RAM values.

Therefore, the resulting flow-based parameters do not only reflect formal context but also methods to account for uncertainty or imperfections, e.g. from the zonal projections which allow or explicitly are used for the consideration of policy decisions towards the restrictiveness of commercial exchange. Generally, differences in parametrization can be explained by three reasons:

1. To ensure secure operation and reduce congestion management. This could be done through the addition of security margins on RAM or by selecting a larger set of CNECs, including internal network elements.

2. To enlarge the trading domain and provide increased capacity to the market. This is more in line with regulation, and aims to achieve a higher level of price convergence. This is done through minimum values for RAM, formally knows as the minimum remaining available margin (minRAM) criterion.

3. To be more accurate, for example reducing inaccuracies of the zonal projection via GSKs, by more precisely derived security margins based on historic data.

Academic publications on modeling FBMC and its parametrizations are still scarce. Early publications such as Van den Bergh, Boury, and Delarue (2016) and Boury (2015) formally describe the process and are extended recently by Schönheit et al. (2021b), Felten et al. (2021), and Byers and Hug (2020) that discuss input parameters and their effects, illustrated by stylized examples. Generally, most academic publications adhere

to a similar methodology that is depicted in Figure 6.1 and utilize an economic dispatch problem for each of the three steps.

Applications based around the status-quo in the CWE region exist and usually compare a result metric based on scenarios or different parametrizations. Matthes et al. (2019) explores how minRAMs affect exchange and the number of contingencies, Marjanovic et al. (2018) analyses prices and redispatch quantity for the planned expansion of the flow-based region from CWE to the CORE region[2], Wyrwoll et al. (2018) quantifies the effect of security margins on net-positions and generation schedules and Schönheit, Weinhold, and Dierstein (2020) the impact of GSKs on CNECs.

All papers provide valuable contributions to the field in illustrating the impact of parametrization, but focus on the formal composition of the parameters and do not attribute the dimension of the parametrization that allows to decide on the effect of the parametrization, namely the trade-off between capacity allocation and congestion management. A notable exception is Schönheit, Weinhold, and Dierstein (2020) that not only provides transparency by an open modelling approach but explicitly provides insight in the effect of a policy decision influencing an otherwise formal method. The authors also point out differences in how minRAMs can be included in the modelling process.

Extending on exiting research, this paper contributes to academic studies on FBMC in different ways:

1. It numerically shows the impact of prioritizing capacity allocation over congestion management in FBMC.

2. The case-study covers full CWE for the target year, explicitly covering the medium term influx of intermittent generation and its effect on the efficiency of FBMC.

3. All data and methods are provided open (under open licence) and accessible (tested and documented) as part of the Power Market Tool (POMATO) described in Weinhold and Mieth (2020b) and dedicated data processing in *PomatoData* (Weinhold 2021).

[2]The CORE region extends CWE by Austria, the Czech Republic, Hungary, Poland, Romania, Slovakia and Slovenia.

6.3 Model and Case Study

The numerical experiments are conducted using the electricity market model POMATO proposed in Weinhold and Mieth (2020b) which was created to model zonal electricity markets and explicitly synthesize the FBMC process. The used formulation follows the description in Chapter 5 and aligns with the process shown in Figure 6.1. Therefore, the model description in this section is limited to a brief description, the full formal description can be found in D.2.

Equations (6.3) represent a high level description of the economic dispatch problem that that is used in this study:

$$\min \ \text{OBJ} = \sum \text{COST GEN} + \text{COST CURT} + \text{COST CM} \tag{6.3a}$$

s.t.

$$\text{Cost Definition} \tag{6.3b}$$

$$\text{Generation Constraints} \tag{6.3c}$$

$$\text{Storage Constraints} \tag{6.3d}$$

$$\text{Energy Balances} \tag{6.3e}$$

$$\text{Network Constraints.} \tag{6.3f}$$

Each step, the *D-2 capacity forecast (basecase)*, *D-1 day-ahead market clearing* and *D-0 congestion management* utilize the same economic dispatch problem (6.3) that finds the most cost effective allocation of generation capacities, defined by generation cost COST GEN and cost for curtailment of intermittent generation COST CURT, to satisfy demand subject to generation capacity (6.3c) and storage (6.3d) constraints. Electricity is balanced for each network node in nodal net-injections and each market area in zonal net-positions (6.3e), which can be constrained by transport constraints (6.3f) that depend on the step in the flow-based process.

Specifically, the basecase is calculated with linear power flow constraints on nodal net-injections to ensure feasibility on all lines in the network. The day-ahead stage is modeled with transport constraints on net-positions as described in Section 6.2 and Equation (6.2) for the zones participating in FBMC, other zones are constraint with bilateral NTCs. Transmission on high-voltage direct-current (HVDC) lines is always

included as a decision variable, as HVDC lines are considered active network elements.

Congestion management, similarly to the basecase, solves a nodal market however with additional cost for congestion management COST CM, i.e. redispatch – deviations from generation schedules of the day-ahead market stage and only conventional, non-storage plants within the flow-based region are considered for redispatch. Curtailment from the market stage persists in congestion management, but can be further increased to maintain feasible power flows as part of the congestion management.

The resulting total cost reflect cost for generation as well as cost to ensure feasibility in the network. While cost based redispatch is desired, the *D-0 congestion management* should prioritize network feasibility. Therefore the cost parameters for curtailment and redispatch are imposed, that are additive to the generation cost. Both are chosen based on average cost for Germany (Bundesnetzagentur and Bundeskartellamt 2019), with around 25€ per MWh redispatch and 100€ per MWh curtailment.

6.3.1 Input Data

The model application covers the CWE region, as depicted in Figure 6.2, for the years 2020 and 2030. Zones part of the CWE are modeled with transmission network and neighboring countries are modeled as single nodes.

Figure 6.2: The geographical scope of the model application and mean solar (left) and wind (right) availability and the transmission network (middle).

The required data is extensive and collected as well as processed using different contributions by the open-data community and the ENTSO-E Transparency Platform. It uses the *Open Data Portal* of Forschungsstelle für Energie (FfE) (Ebner et al. 2019) for geo-information and regionalized RES potentials. Geo-information is collected based on the standardised Nomenclature of Territorial Units for Statistics (NUTS) data of the European Union, that divides countries in standardised regions and sub-regions and allows for

geo-referenced data collection. NUTS-level 0 defines countries and higher values indicate higher resolution. The *atlite* package for availability timeseries on NUTS-3 level (Hofmann et al. 2021) and hydro storage inflows (Liu et al. 2019) using the *HydroBASINS* database (Lehner and Grill 2013). Dispatchable generation capacities come from the *JRC Hydro-power plants database* (Felice, Peronato, and Kavvadias 2021) for hydro generation capacities and the *Open Power System Data Project* (Weibezahn et al. 2018) for conventional and nuclear power plants.

The underlying network data originates from the updated fork of the *GridKit* ENTSO-E gridmap extract (Wiegmans 2016) part of well as few specific expansions that were not included in the data, like the already online "Redwitz-Altenfeld" and "Vieselbach-Lauchstädt" connections. The process of estimating specific line parameters is part of the model documentation[3].

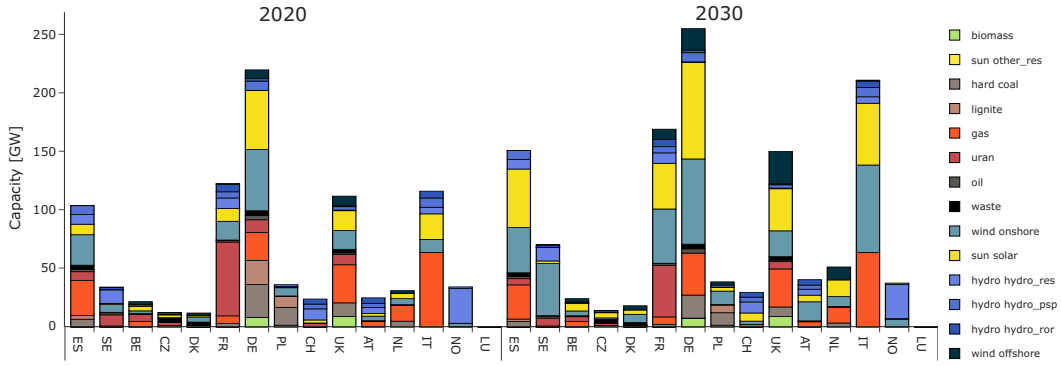

Figure 6.3: Installed capacities per country and year.

Nodal demand is derived from zonal load published on the *ENTSO-E Transparency Platform*[4] using sector specific standard load profiles and NUTS-3 data on energy consumption, and gross value added (Kunz et al. 2017). Additional data from *ENTSO-E Transparency Platform* that is used are scheduled commercial exchanges to derive NTCs for non-CWE bidding zones and weekly storage levels. The first are used to derive NTCs for zones neighboring the flow-based region and the latter for rolling horizon model execution that limits the model's foresight.

Installed capacities of wind and solar in 2030 are obtained from pathway optimization of the European energy system using *AnyMOD* (Göke 2021). In contrast to the values part of publications Göke et al. (2021) and Hainsch et al. (2020) that depict a 2040

[3]See: pomato.readthedocs.io/en/latest/line_parameters.html
[4]See: transparency.entsoe.eu

fully decarbonized system, the values in this study are obtained for 2030 with the latest ENTSO-E "sustainable transition" scenario as a lower bound for renewable capacity and an upper bound for thermal capacities (ENTSOG and ENTSO-E 2020). The wind and photovoltaik (PV) capacities are distributed based on the FfE potentials. Decommissioning of conventional and fissile generation capacities is based on plant lifetime and national energy and climate plans. However, plant specific commissioning and decommissioning of individual plants proves challenging and therefore the used data-set includes modest changes to the conventional and nuclear capacity and the two target years are mostly defined by the regionalized increase in wind and PV capacities. Table 6.1 shows the decommissioning of lignite, hard coal and nuclear generation capacities between the 2020 and 2030 scenario.

Table 6.1: Decommissioning of lignite, hard coal and nuclear generation capacities in GW per country between 2020 and 2030.

	BE	CH	DE	ES	FR	NL	PL	SE	UK
lignite	0	0	20.6	0.92	0	0	2.78	0	0
hard coal	0	0	8.47	1.96	0.88	1.54	4.58	0.04	3.53
uran	1.78	1.03	10.8	2.27	18.94	0	0	2.86	2.68

The weather year for both 2020 and 2030 was chosen to be 2019. Therefore, 2019 timeseries for load and availability of intermittent generation are used as well as 2019 commercial exchanges used to derive static NTCs and weekly storage levels.

The final data-set is compiled using the complementary PomatoData tool of POMATO (Weinhold 2021) that includes all data processing and documents data origin, thereby provides the required accessibility and compatibility to the data and are published supplementary to the paper.

6.3.2 Parametrization of the flow-based parameters

The aim of this study is to quantify the effect of less restrictive capacity allocation on the resulting congestion management. Therefore the parametrization of the flow-based parameters remains very close to the official documentation (50Hertz et al. 2020) for GSK, CNEC selection and the implementation of the minRAM criterion.

For all scenarios a *Pro-Rata* GSK is used. This GSK weights nodal participation factors based on the scheduled power output of dispatchable generation capacities and is the basis for most GSKs currently in use (50Hertz et al. 2020) and has proven to

be effective (Schönheit, Weinhold, and Dierstein 2020). For the construction of the zonal PTDF, CNEs are selected based on a 5% threshold in the zone-to-zone PTDF, with the exception of one scenario where only cross-border lines are considered critical. Contingencies are selected based on a 20% sensitivity threshold of a contingency towards the CNE, i.e. contingencies are considered if in case of an outage more than 20% of the load is diverted to the respective CNE.

The minRAM criterion is enforced by setting the RAM to $\max(RAM, \overline{f} \cdot \text{minRAM})$ in Equation (6.2) and the model is run for different minRAM values of 20%, 40% and 70%. In addition the 70% is also run with only cross-border lines as CNE indicated as *70% (only CB)* in the following result tables. The effect on the day-ahead capacity allocation is visualized in a flow-based domain for the exchange between Germany-France and Germany-Netherlands in Figure 6.4.

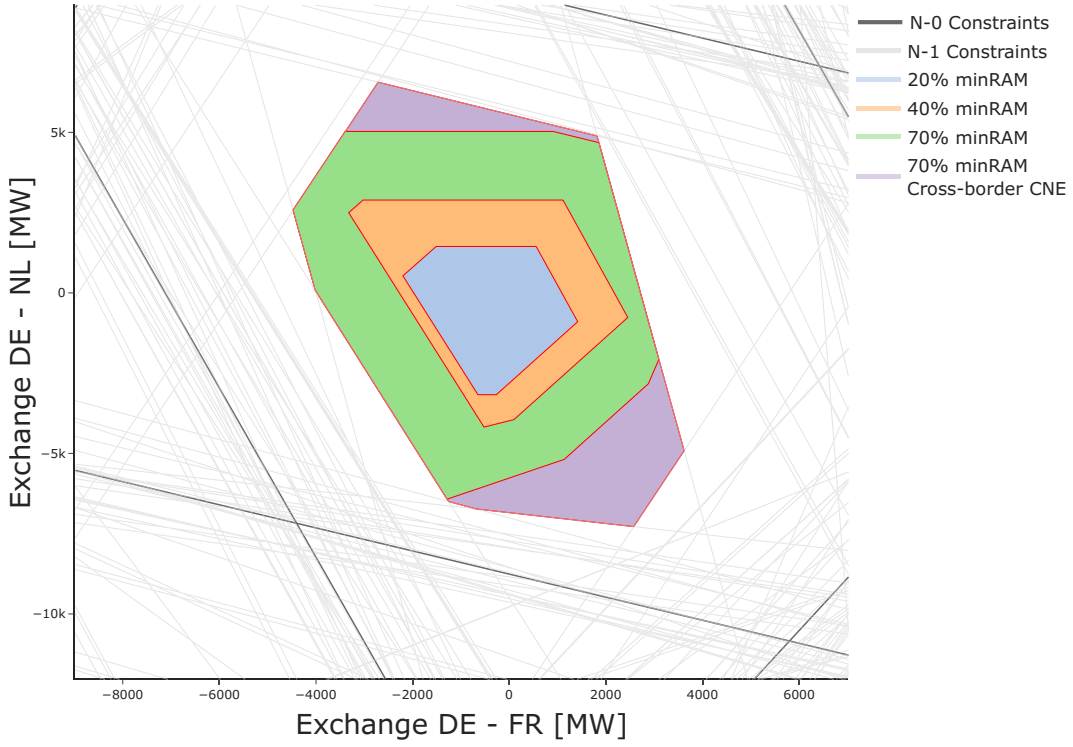

Figure 6.4: Visualization of the day-ahead CA for exchange between Germany-France (x-axis) and Germany-Netherlands (y-axis) depending on the chosen minRAM configuration.

The four configurations differ in the permissiveness of commercial exchange and we can expect higher trading volumes with higher minRAM requirements. Additionally, in order

to further limit the impact of internal congestions on cross-border exchange (European Commission 2019a) the fourth scenario only considers cross-border lines as CNEs, thus further relaxing the commercial exchange domains.

The final 2030 data-set is composed of 5458 generators, that includes 2236 wind/PV plants and 953 storages. The network is made up of 1663 nodes, 3276 lines and 100 HVDC lines. The model size is substantial and to alleviate the computational effort, the model is solved for every 7th week of the year, 8 weeks in total, with the electricity market model POMATO (Weinhold and Mieth 2020b). Therefore the model remains tractable on standard pc hardware, all results are obtained using a AMD Ryzen 7 CPU, 32GB of memory and the Gurobi solver (Gurobi Optimization LLC 2018).

6.4 Model Results

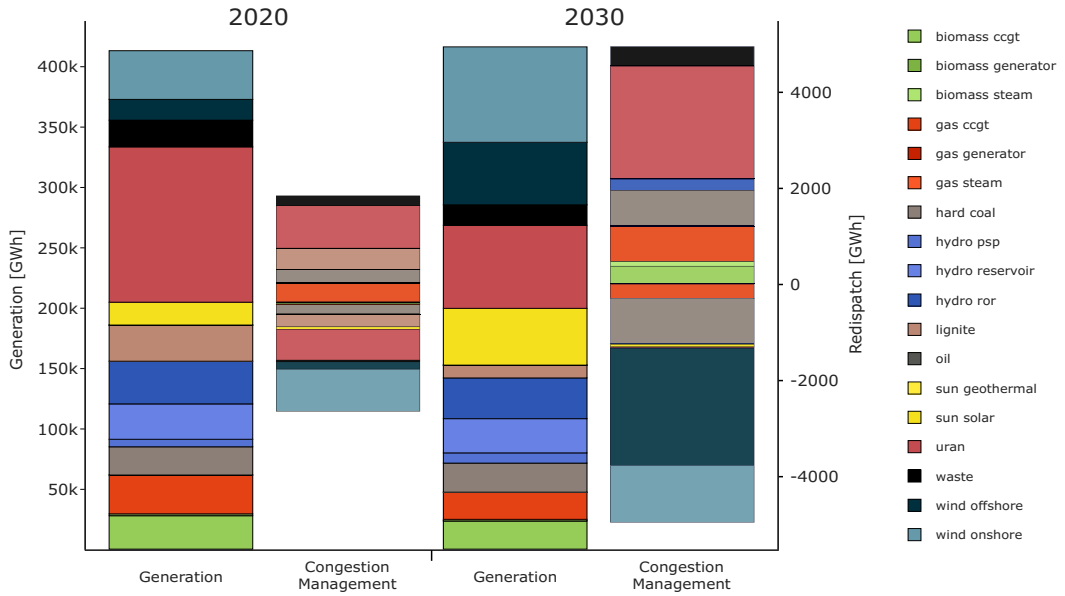

Figure 6.5: Total generation and congestion management by fuel-type for the *70% min-RAM* configuration in 2020 (left) and 2030 (right).

As described in Section 6.3 FBMC is modeled in three dedicated steps. From a basecase the day-ahead market result is obtained using flow-based parameters following the four configurations regarding the permissiveness of the day-ahead trading domain and subsequent congestion management. The model results are evaluated after congestion management and therefore include generation cost from the market- and congestion management

stage, as well as additional cost for redispatch and curtailment. Figure 6.5 presents the resulting dispatch for the *70% minRAM* configuration in 2020 and 2030 and illustrates the overall system states with a renewable share of 43% in 2020 and 66% in 2030 as well as the volumes and composition of congestion management.

As the primary result metric, the system cost indicate the efficiency of the market design and when decomposed into cost for generation, curtailment and redispatch show the relation between capacity allocation and congestion management. Table 6.2 shows lower system cost in 2030 due to an increased share of intermittent renewable generation and decreasing generation cost with more permissive commercial exchange domains. Cost for congestion management are the highest for the *20% minRAM* configuration, indicating overly conservative trading domain and in combination with the least effective use of generation capacities, results in highest total cost. With higher commercial exchange capacities curtailment increases and redispatch quantities decrease. The lowest total cost align with the lowest congestion management volume, depicted in Table 6.3, in the *70% minRAM* configuration for 2020 and the less constraint *70% minRAM (only CB)* configuration in 2030.

Table 6.2: Total cost for generation, curtailment and redispatch in mio. €

		minRAM configuration			
		20%	40%	70%	70% (only CB)
2020	Generation	9,837	9,758	9,718	9,704
	Curtailment	104	108	111	117
	Redispatch	129	94	84	98
	Total	10,070	9,960	9,913	9,919
2030	Generation	6,926	6,905	6,888	6,864
	Curtailment	559	560	567	588
	Redispatch	180	160	155	146
	Total	7,665	7,625	7,610	7,598

Overall, the best configuration in 2020 represents a 1.56% cost reduction and 27.84% reduction in congestion management in comparison to the *20% minRAM* configuration. In 2030 the total cost reduction is 0.87% and congestion management is reduced by 8.34%.

In order to evaluate the impact on congestion management Figure 6.6 shows the difference in congestion management between the *20% minRAM* and *70% minRAM* con-

Table 6.3: Congestion management volumes in TWh

		minRAM configuration			
		20%	40%	70%	70% (only CB)
2020	Curtailment	1.05	1.09	1.11	1.17
	Redispatch	5.2	3.77	3.4	3.94
	Total	6.25	4.86	4.51	5.11
2030	Curtailment	5.6	5.6	5.68	5.89
	Redispatch	7.23	6.43	6.22	5.87
	Total	12.83	12.03	11.9	11.76

figurations for 2020 and 2030. For both years less restricted commercial exchange causes more congestion management along the CWE border region, which is out-weight by less congestion management generally more within the bidding zones. The impact of the substantial increases in offshore wind capacities in the north sea is also clearly visible.

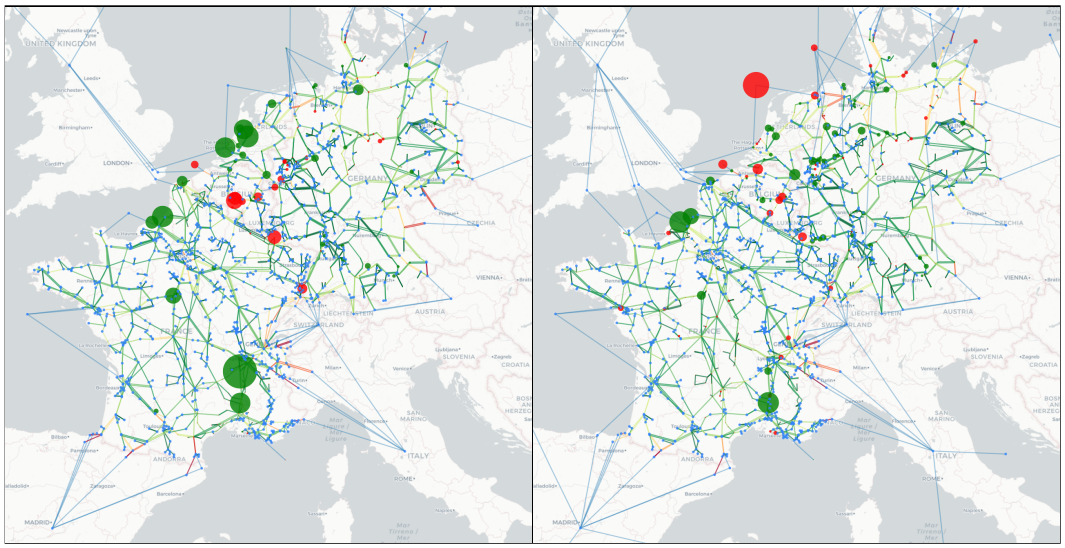

Figure 6.6: Difference in congestion management for 2020 (left) and 2030 (right) between the *20% minRAM* and *70% minRAM* configurations. Increased congestion management with *70% minRAM* is indicated in red and less congestion management in green.

A core metric of the European IEM is price convergence, as it quantifies increased market efficiency and competition that should result in lower prices (European Commission 2019b). Table 6.4 shows different compositions of the model endogenous electricity

prices λ resulting from the dual variable of the energy balances. For the day-ahead (D-1) stage λ is the average zonal price for the CWE bidding zones and $\Delta\lambda$ the average difference in zonal price between the CWE bidding zones. For congestion management (D-0), with nodal restrictions present, nodal marginal prices in congestion management λ are averaged. The marginal in congestion management indicates the additional nodal cost after congestion management, meaning after network feasibility is achieved.

Table 6.4: Average price λ and price differences $\Delta\lambda$ in- and between CWE bidding zones in terms of year and minRAM configuration.

		20%		40%		70%		70% (only CB)	
		λ	$\Delta\lambda$	λ	$\Delta\lambda$	λ	$\Delta\lambda$	λ	$\Delta\lambda$
2020	D-1	50.02	24.41	44.68	22.4	41.61	21.23	39.08	17.06
	D-0	47.18		48.13		48.46		47.88	
2030	D-1	43.47	31.73	42.02	24.62	41.3	22.49	37.58	19.46
	D-0	54.39		55.48		56.32		57.67	

Similar to the system cost results in Table 6.2, average prices decrease between 2020 and 2030 due to the influx of low cost generation. For both 2020 and 2030 the average prices decrease with less restricted commercial exchange domains. Additionally, price differences decrease with more exchange capacities with 2030 showing, on average, price differences at lower average prices.

Results of the average marginal cost for electricity after congestion management show generally higher values in 2030, reflecting the increased congestion management volumes. This is visualized in Figure 6.7, that shows the average nodal prices after congestion management by the dual on the energy balances as a contour plot for the modeled region for the *70% minRAM* configuration.

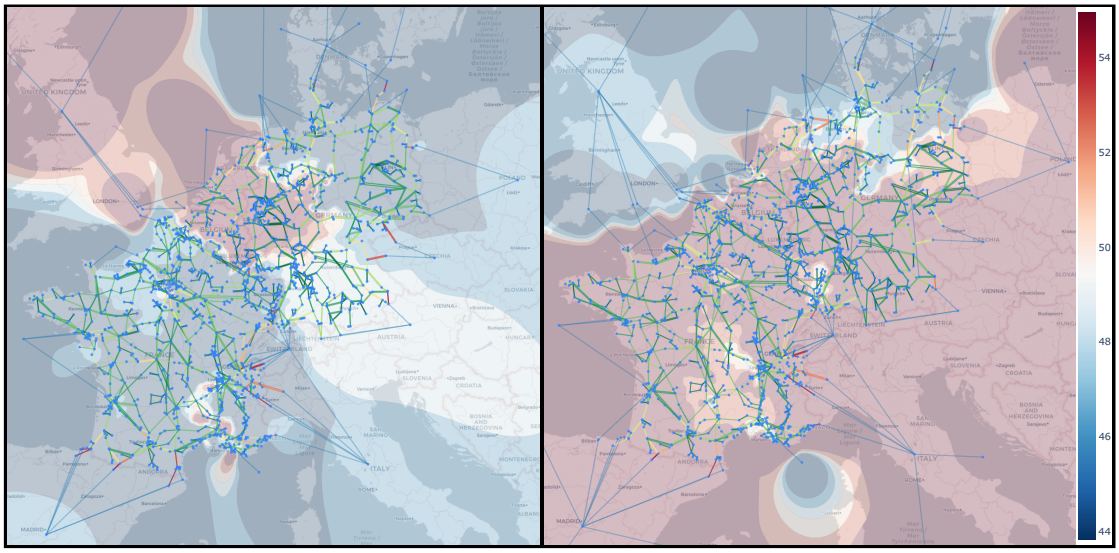

Figure 6.7: Average nodal marginal cost for congestion management in 2020 (left) and 2030 (right) for the *70% minRAM* configuration.

The plot verifies the overall increased congestion management effort in 2030. Also, given the distribution of RES capacities by potential, 2030 shows fairly even contour in the CWE region.

Interestingly, between the FBMC configurations, the values negatively correlate to the congestion management volumes, with higher prices for lower overall volumes. Thereby, higher average price after congestion management indicates that additional nodal load is more often subject to network constraints, or indicate higher average network utility.

6.5 Conclusions

The presented results show the effect of FBMC configurations that, in line with the regulators perspective, provide higher commercial exchange capacities to the market. The modeled configurations are chosen to represent the status-quo and the proposed target by 2030, modeled through different minRAM requirements and choice of critical network elements.

More permissive configurations provide lower generation cost, as the markets are less constrained. For 2020, the trade-off between capacity allocation and congestion management is visible. Here both, too constrained as well as too permissive flow-based parameter configurations lead to higher overall cost. The least cost solution is provided by the *70% minRAM* configuration. For 2030 the most permissive configuration *70% minRAM (only*

CB) provided the least over cost and congestion management.

In terms of price convergence, the results show that indeed more permissive exchange capacities lead to higher levels of price convergence in both 2020 and 2030. However, 2030 shows an overall lower price convergence than 2020 at lower overall price level, indicating higher price volatility in 2030. Analysis of marginal cost in congestion management also reflect the overall higher volumes of congestion management. Additionally, the comparison between the FBMC configurations leads to the conclusion that more permissive flow-based domains lead to a higher network utilization.

This paper provides comprehensive insights into the effect of policy relevant considerations as part of FBMC. This includes the status-quo as well as the mid-term future. Indeed, enforcing larger commercial exchange capacities lead to increased price convergence, however potentially with increased congestion management. The results also indicate that larger commercial exchange domains are favourable in high shares of intermittent renewable generation. However, the 2030 scenario also shows high levels of congestion management, that indicate the systems inability to adequately make use or transport excess intermittent renewable generation. The extensive use of curtailment as part of congestion management, despite the high cost, also indicates that the homogeneous distribution makes curtailment very effective tool for congestion management. The 2030 scenario in this study differs from the status-quo mainly in terms of the renewable capacities and the HVDC projects of the immediate future. Thereby the effect of higher shares of intermittent renewable generation becomes visible.

The methods and data that are used in this research are open and accessible and aim to provide transparency and sustainability to the research and results of this study as well prove useful for future work. The proposed data-set that accompanies the used electricity market model POMATO (Weinhold and Mieth 2020b) allows for detailed and in-depth analysis of large-scale electricity system in respect to market design and the involved policy decisions.

For future studies, the impact of means to reduce excess generation, flatten load and increase system flexibility via sector coupling, prosumage or demand response would provide relevant avenues for extensions. The expected decrease in congestion management as well as additional flexibility in terms of network operation would represent valuable insights.

Part IV

Appendix

Appendix A

Appendix to Chapter 3

A.1 Chapter 3: Description of Used Symbols

Table A.1: Nomenclature for model application in Chapter 3

A. Sets	
$\emptyset$	The empty set
$\mathcal{C}$	Set of contingency scenarios with $C = \lvert\mathcal{C}\rvert$
$\mathcal{F}(B, \overline{f})$	Feasible region of system $(B, \overline{f})$
$\mathcal{G}$	Set of generators with $G = \lvert\mathcal{G}\rvert$
$\mathcal{I}, \mathcal{J}$	Set of indices
$\mathcal{L}$	Set of lines/edges with $L = \lvert\mathcal{L}\rvert$
$\mathcal{L}_c$	Set of failed lines at contingency scenario c, $\mathcal{L}_c \subseteq \mathcal{L}$
$\mathcal{L}_n$	Set of lines connected to node n, $\mathcal{L}_n \subseteq \mathcal{L}$
$\mathcal{N}$	Set of nodes with $N = \lvert\mathcal{N}\rvert$
$\mathcal{T}$	Set of time steps indexed with $T = \lvert\mathcal{T}\rvert$
B. Parameters and Variables	
d_t	Active power demand at t indexed by $d_{t,n}, n \in \mathcal{N}$
f_t	Active power flow at t indexed by $f_{t,l}, l \in \mathcal{L}$
$\overline{f}$	Maximum line capacity indexed by $\overline{f}_l, l \in \mathcal{L}$
g_t	Active power generation at t indexed by $g_{t,i}, i \in \mathcal{G}$
$\underline{g}_t$	Lower generation limit at t indexed by $\underline{g}_{t,i}, i \in \mathcal{G}$
$\overline{g}_t$	Upper generation limit at t indexed by $\overline{g}_{t,i}, i \in \mathcal{G}$
x_t	Nodal injection at t indexed by $x_{t,n}, n \in \mathcal{N}$
$\check{x}, \hat{x}$	Asymmetric bounds on nodal injection
$\underline{x}, \overline{x}$	Symmetric bounds on nodal injection
B	Generalized power transfer distribution matrix
I	Identity matrix of appropriate dimensions
LODF_{lc}	Line outage distribution factor for line l under c
M	Mapping of generators to nodes
η	Impact screening margin
C. Operators	
$\lvert\mathcal{X}\rvert$	Cardinality of set $\mathcal{X}$
$\mathcal{X}^\circ$	Interior of set $\mathcal{X}$

Nomenclature (continued).

$X^\top$	Transpose of matrix X
X_i	Row vector equal to the i-th row of X
X_{ij}	j-th entry in the i-th row of X

A.1.1 PTDF Derivation

Assuming that voltage magnitudes are fixed, phase angle differences between neighbouring nodes are small and reactance dominates resistance on all lines, the active power flow on line l from node s to node r can be written in terms of the phase angle difference between those nodes such that

$$f_{t,l} = (x_{t,l})^{-1}(\theta_{t,s} - \theta_{t,r}), \tag{A.1}$$

where $\theta_{t,n}$ is the voltage angle at node n at time t and we define θ_t to collect all $\theta_{t,n}, n \in \mathcal{N}$. All nodal injections and power flows are balanced such that:

$$x_{t,n} = \sum_{\mathcal{L}_n} f_{t,l}, \tag{A.2}$$

where $\mathcal{L}_n$ is the set of lines connected to node n. Defining incidence matrix $A \in \{-1, 0, 1\}^{L \times N}$ such that all entries are zero except $A_{(l,n)} = 1$ if node n is the sending node of line l and $A_{(l,n)} = -1$ if n is the receiving node of line l (A.1) and (A.2) can be written in their vector forms as

$$f_t = X^{-1}A\theta_t = B^{(f)}\theta_t, \tag{A.3}$$

$$x_t = A^\top X^{-1}A\theta_t = B^{(n)}\theta_t, \tag{A.4}$$

where diagonal matrix $X \in \mathbb{F}^{L \times L}$ collects line reactances such that $X_{(l,l)} = 1/b_l, \forall l \in \mathcal{L}$ and $B^{(f)} \in \mathbb{R}^{L \times N}$, $B^{(n)} \in \mathbb{R}^{N \times N}$ is the line and bus susceptance matrix, respectively. Next, because (A.1) is based on angle *differences*, we define a reference (slack) node with fixed phase angle. Without loss of generality we choose the index of the slack node to be $n_{\text{slack}} = 1$. Then $B^0 \in \mathbb{R}^{L \times N}$ is defined by:

$$B^0 = B^{(f)} \begin{bmatrix} 0 & 0 \\ 0 & \left(\tilde{B}^{(n)}\right)^{-1} \end{bmatrix} =: B^{(f)}\hat{B} \tag{A.5}$$

where $\tilde{B}^{(n)} \in \mathbb{S}^{N-1}$ is the bus susceptance matrix without the row and column associated with the slack bus (first row and first column in our case).

A.1.2 LODF derivation

Given outage scenario c with $\mathcal{L}_c \subseteq \mathcal{L}$ the set of failed lines, $\text{LODF}_{l\mathcal{L}_c} \in \mathbb{R}^{1\times|\mathcal{L}_c|}$ can be calculated as Jiachun et al. 2009, Eq. (3):

$$\text{LODF}_{l\mathcal{L}_c} = (X_{[l]}^{-1} A_l \hat{B} A_{\mathcal{L}_c}^\top)(I - X_{[\mathcal{L}_c]}^{-1} A_{\mathcal{L}_c} \hat{B} A_{\mathcal{L}_c}^\top)^{-1} \tag{A.6}$$

with $\hat{B}$ as defined in (A.5) and $X_{[\mathcal{L}_c]}$ the diagonal matrix composed of the rows and columns of X corresponding to the lines in $\mathcal{L}_c$. Thus, if $\mathcal{L}_c$ is a singleton, then $X_{[\mathcal{L}_c]}$ is a scalar. Matrix $A_{\mathcal{L}_c}$ is the $C \times N$ matrix composed of the rows of A corresponding to the lines in $\mathcal{L}_c$. Thus, if $\mathcal{L}_c$ is a singleton, then $A_{\mathcal{L}_c}$ is a row vector. Therefore, $X_{[l]}$ and A_l are a scalar and a row vector, respectively.

A.1.3 Implementation of RayShoot

Algorithm 2: `RayShoot`$(B, \overline{f}, z, x^*)$

input : System $(B, \overline{f})$
Interior point z
Point on or outside of feasible region x^*
output: Index of first inequality that limits a ray starting at z in the direction of r
begin
  $\mathcal{H} \leftarrow \emptyset$; `// Set of crossed hyperplanes`
  $\epsilon \leftarrow \epsilon^{\text{init}}$; `// Set inital ray increment`
  $r = \frac{x^* - z}{\|x^* - z\|_2}$; `// Set direction of ray`
  while $|\mathcal{H}| \neq 1$ **do**
    $z \leftarrow z + \epsilon r$; `// Add increment to ray`
    $\mathcal{H} \leftarrow \{i \mid B_i z > \overline{f}_i\}$;
    if $|\mathcal{H}| > 1$ **then**
      $z \leftarrow z - \epsilon r$; `// Go back one step`
      $\epsilon \leftarrow \epsilon/10$; `// Reduce step size`
    end
  end
  return $\mathcal{H}$
end

Note that, because x^* is associated with constraint k, see Fig. 3.2, the ray from z to $x*$ will always hit at least k and therefore always return an index. In practical implementation, if step size ϵ reaches floating point precision, `RayShoot` can return any of the indices of the inequalities that limit the ray from z in the direction r.

Appendix B

Appendix to Chapter 4

B.1 Reference Domain: JAO Data

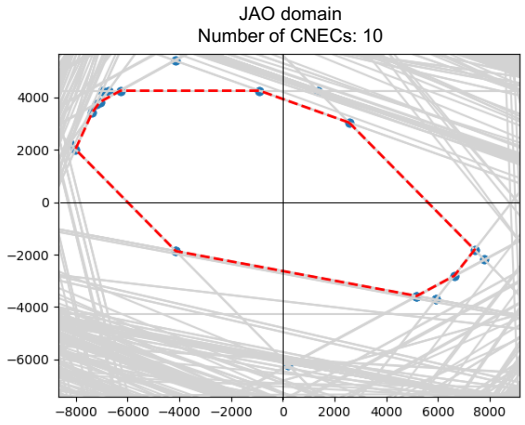

Figure B.1: Two-dimensional Joint Allocation Office (JAO) domain (in MW) for the borders DE-FR (x-axis) and DE-NL (y-axis) for timestamp t134. Positive values express an increasing bilateral net position change, with more export from Germany to the respective importing country. Source: Own figure.

B.2 Model Formulation

B.2.1 Nomenclature

Please note that the model formulation follows the convention of upper case for variables and sets and lower case for parameters and indices. This is not necessarily consistent with the formulation in the paper, where naming coincides with the abbreviation, e.g. NP for net position.

Table B.1: Nomenclature for model application in Chapter 4

A1. Sets and Indices

U	set of units
$TS \subset U$	subset of units with capacity timeseries
$ES \subset U$	subset of electricity storages
T	set of timesteps
Z	set of zones
$CWE \subset Z$	subset of CWE zones
N	set of nodes

Nomenclature (continued).

CNE	set of critical network elements
$CNEC$	set of critical network elements under contingency
$SLACK \subset N$	subset of slack nodes
DC	set of DC lines
A2. Set-Mapping	
N_z	set of nodes in zone z
U_z, U_n	set of units in zone z / at node n
N_s	set of nodes which are balanced through slack s
B1. Variables	
$COST$	total system cost
$INJ_{n,t}$	net injection
$F^{DC}_{dc,t}$	flow in dc line
B2. Positive Variables	
$P_{u,t}$	active power generation
$D^{es}_{es,t}$	electricity demand by electricity storage
$L^{es}_{es,t}$	electricity storage level
$EX_{z,zz,t}$	commercial exchange from z to zz
B3. Parameters	
mc_u	marginal generation costs
eta_s	efficiency for storage charge units in %
g^{max}_u	maximum electricity generation
$ava_{ts,t}$	availability factor
es^{cap}_{es}	electricity storage capacity
$ptdf_{n,cne}$	ptdf - sensitivity node to CNE
$ptdf_{n,cnec}$	ptdf - sensitivity node to CNE under contingency
l^{cap}_{cne}	line capacity
l^{cap}_{cnec}	line capacity under contingency (RAM)
dc^{max}_{dc}	DC line capacity
$inc^{DC}_{dc,n}$	incidence matrix for DC connections
$d^{el}_{n,t}$	electricity demand

Nomenclature (continued).

$nex_{z,t}$	net position
$export_{z,t}$	net export injection

The model formulation follows the common approach of an economic dispatch model. Its objective function (B.1) minimizes total generation cost subject to capacity constraints (B.2) for all generation units, storage constraints (B.3), transport constraints (B.4), which consist of upper and lower bounds on AC and DC lines, energy balances (B.5) on a nodal and zonal level and constraints (B.6) regarding the base case representation.

Objective function:

$$COST = \min \sum_{u \in U, t \in T} P_{u,t} \cdot mc_u \tag{B.1}$$

Generation capacity constraints:

$$P_{u,t} \leq g_u^{max} \qquad \forall t \in T, u \in U \backslash_{TS} \tag{B.2a}$$

$$P_{ts,t} \leq ava_{ts,t} \cdot g_{ts}^{max} \qquad \forall t \in T, ts \in TS \tag{B.2b}$$

Generation variables are positive and upper bound by the installed capacity g_u^{max}. If the generation unit has a time dependant capacity factor, e.g. renewable generation, it is part of the subset TS and has an availability factor multiplied by its capacity.

Storage Constraints:

$$L_{es,t}^{es} = L_{es,t-1}^{es} - P_{es,t} + \eta_{es} D_{es,t}^{es} \qquad \forall t \in T, es \in ES \tag{B.3a}$$

$$L_{es,t}^{es} \leq es_{es}^{cap} \qquad \forall t \in T, es \in ES \tag{B.3b}$$

$$D_{es,t}^{es} \leq d_{es}^{max} \qquad \forall t \in T, es \in ES \tag{B.3c}$$

Electricity storages are modeled by tracking storage levels over the model horizon in Equation (B.3a). The storage generation is upper bound by (B.2a) and therefore storage level and charge receive an upper bound in (B.3b) and (B.3c).

Transport Constraints:

$$\sum_{n \in N} ptdf_{cnec,n} \cdot INJ_{n,t} \leq l^{cap}_{cbco} \qquad \forall t \in T, cnec \in CNEC \tag{B.4a}$$

$$\sum_{n \in N} ptdf_{cnec,n} \cdot INJ_{n,t} \geq -l^{cap}_{cbco} \qquad \forall t \in T, cnec \in CNEC \tag{B.4b}$$

$$\sum_{n \in N_{slack}} INJ_{n,t} = 0 \qquad \forall t \in T, slack \in SLACK \tag{B.4c}$$

The line flows are implemented with a DC load flow formulation with upper and lower bounds in (B.4a) and (B.4b) and nodal injections balanced through a slack or reference node. Equation (B.4c) allows to balance a group of nodes through a specific slack, which is necessary for disconnected networks. The set $CNEC$ consist of the CNEs which are derived from the matched list described in Section 4.4.3 and outages with an load outage distribution factor (LODF) of more than 5%.

$$F^{DC}_{dc,t} \leq dc^{max}_{dc} \qquad \forall t \in T, dc \in DC \tag{B.4d}$$

$$F^{DC}_{dc,t} \geq -dc^{max}_{dc} \qquad \forall t \in T, dc \in DC \tag{B.4e}$$

Equations (B.4d) and (B.4e) set bounds on flows of DC lines.

Energy Balances:

$$d^{el}_{n,t} = \sum_{co \in CO_n} P_{co,t} - \sum_{es \in ES_n} D^{es}_{es,t} + export_{n,t} - \sum_{dc \in DC} F^{DC}_{dc,t} \cdot inc^{DC}_{dc,n} + INJ_{n,t} \quad \forall t \in T, n \in N \tag{B.5a}$$

$$\sum_{n \in N_z} d^{el}_{n,t} = \sum_{co \in CO_z} P_{co,t} - \sum_{es \in ES_z} D^{es}_{es,t} + \sum_{n \in N_z} export_{n,t} + \sum_{zz \in Z} (EX_{zz,z,t} - EX_{z,zz,t}) \quad \forall t \in T, z \in Z \tag{B.5b}$$

The energy balance is enforced through Equations (B.5b) and (B.5a). The nodal energy balance accounts for all nodal injections which are restricted by line flows. Injections from DC lines are mapped to the start and end nodes by the incidence parameter $inc^{DC}_{dc,n}$. The zonal energy balance accounts for all generation and demand on a zonal level thereby setting the net position, potentially restricted through NTCs or through the following constraints regarding the base case calculation. Countries that are not part of CWE and therefore have no power plants or grid representation are included with a net export timeseries on the respective nodes.

Base Case Constraints:

$$\sum_{zz \in Z} (EX_{zz,z,t} - EX_{z,zz,t}) = nex_{z,t} \qquad \forall t \in T, z \in CWE \tag{B.6a}$$

$$\sum_{n \in N} ptdf_{cb,n} \cdot INJ_{n,t} = f^{ref}_{cb,t} \qquad \forall t \in T, cb \in CNE \tag{B.6b}$$

Equations (B.6a) and (B.6b) are used to calibrate the economic dispatch to historical data published by JAO Joint Allocation Office 2019. This is done by enforcing historical net positions for countries in CWE and reference flows for lines, which are matched to the data set used in this analysis. The reference flows are labeled by JAO as "N-State" or "Basecase", which is why flows under no contingency are enforced. Therefore, this constraint is enforced for all CNE and not $CNEC$.

Appendix C

Appendix to Chapter 5

C.1 Chapter 5: Description of Used Symbols

Table C.1: Nomenclature for model application in Chapter 5

A. Sets	
$\mathcal{T}$	Set of time steps within the model horizon.
$\mathcal{G}$	Set of generators.
$\mathcal{R}$	Subset $\mathcal{R} \subset \mathcal{G}$ of intermittent generators.
$\mathcal{N}$	Set of network nodes.
CNEC	Set of critical network elements and contingencies.
$\mathcal{Z}$	Set of bidding zones.
B. Variables	
G_t	Active power generation at $t \in \mathcal{T}$ indexed by $G_{g,t}, g \in \mathcal{G}$
C_t	Curtailment $t \in \mathcal{T}$.
I_t	Active nodal power injection at $t \in \mathcal{T}$.
NP_t	Zonal net-positions at $t \in \mathcal{T}$.
EX_t	Bilateral exchange at $t \in \mathcal{T}$ indexed by $EX_{t,z,z'}, z, z' \in \mathcal{Z}$
G_t^{red}	Active power redispatch at $t \in \mathcal{T}$.
α_t	Generator response at $t \in \mathcal{T}$ indexed by $\alpha_{g,t}, g \in \mathcal{G}$
$T_{j,t}$	Standard deviation of the flow $t \in \mathcal{T}$ on $j \in$ CNEC.
C. Parameters	
d_t	Nodal load at $t \in \mathcal{T}$.
r_t	Available intermittent generation at $t \in \mathcal{T}$
m	Mapping of generators/load (subscript) to nodes/zones (superscript).
$\overline{g}$	Upper generation limit.
$\overline{f}$	Line capacity of CNEC indexed as $\overline{f}_j, j \in$ CNEC
$f_{j,t}^{ref}$	Reference flow on $j \in$ CNEC at $t \in \mathcal{T}$.
ntc	Net-transfer capacity indexed by $ntc_{z,zz}, z, z' \in \mathcal{Z}$
g^{da}	Day-ahead scheduled generation at $t \in \mathcal{T}$.
c^{da}	Day-ahead scheduled curtailment at $t \in \mathcal{T}$.
ω_t	Real-time deviation on intermittent generation r_t at $t \in \mathcal{T}$.
Ω	Uncertainty space $\omega \in \Omega$
ϵ	Risk-level

Nomenclature (continued).

Φ	Cumulative distribution function of the standard normal distribution
Σ_t	Variance-Covariance matrix of ω at $t \in \mathcal{T}$.

Appendix D

Appendix to Chapter 6

D.1 Nomenclature

Table D.1: Nomenclature for model application in Chapter 6

A. Sets	
$\mathcal{T}$	Set of time steps within the model horizon.
$\mathcal{G}$	Set of generators.
$\mathcal{R}$	Subset $\mathcal{R} \subset \mathcal{P}$ of intermittent generators.
$\mathcal{N}$	Set of network nodes.
CNEC	Set of critical network elements and contingencies.
$\mathcal{Z}$	Set of bidding zones.
B. Variables	
G_t	Active power generation at $t \in \mathcal{T}$ indexed by $G_{g,t}, g \in \mathcal{G}$
C_t	Curtailment $t \in \mathcal{T}$.
I_t	Active nodal power injection at $t \in \mathcal{T}$.
NP_t	Zonal net-positions at $t \in \mathcal{T}$.
F_t^{dc}	Flow on HVDC lines at $t \in \mathcal{T}$.
EX_t	Bilateral exchange at $t \in \mathcal{T}$ indexed by $EX_{t,z,z'}, z, z' \in \mathcal{Z}$
L_t	Storage level at $t \in \mathcal{T}$ indexed by $L_{t,s}, s \in \mathcal{ES}$
D_t	Storage demand/charging at $t \in \mathcal{T}$ indexed by $D_{t,s}, s \in \mathcal{ES}$
G_t^{red}	Active power redispatch at $t \in \mathcal{T}$.
C. Parameters	
d_t	Nodal load at $t \in \mathcal{T}$.
r_t	Available intermittent generation at $t \in \mathcal{T}$
m	Mapping of generators/load (subscript) to nodes/zones (superscript).
$\overline{g}$	Upper generation limit.
$\overline{d}$	Upper storage charging limit indexed by $\overline{d}_{t,s}, s \in \mathcal{ES}$
η	Storage charging efficiency indexed by $\eta_s, s \in \mathcal{ES}$
$\overline{l}$	Upper storage capacity indexed by $\overline{l}_{t,es}, es \in \mathcal{ES}$
$\overline{f}$	Maximum line flow.
$\overline{f^{dc}}$	Maximum dc-line flow.
ntc	Net-transfer capacity indexed by $ntc_{z,zz}, z, z' \in \mathcal{Z}$
g^{da}	Day-ahead scheduled generation at $t \in \mathcal{T}$.

Nomenclature (continued).

c^{da}	Day-ahead scheduled curtailment at $t \in \mathcal{T}$.

D.2 Model Formulation

Equations D.1 formulate the economic dispatch problem that finds the least cost dispatch to satisfy demand for each timestep $t \in \mathcal{T}$.

$$\min \quad \sum_{t \in \mathcal{T}} c(G_t) + c(C_t) \tag{D.1a}$$

$$\text{s.t.} \quad 0 \leq G_t \leq \overline{g} \qquad \forall t \in \mathcal{T} \tag{D.1b}$$

$$0 \leq C_t \leq r_t \qquad \forall t \in \mathcal{T} \tag{D.1c}$$

$$L_{t,s} = L_{t-1,s} - G_{t,s} + \eta_s D_{t,s} \qquad \forall s \in \mathcal{ES}, t \in \mathcal{T} \tag{D.1d}$$

$$0 \leq D_t \leq \overline{d} \qquad \forall t \in \mathcal{T} \tag{D.1e}$$

$$0 \leq L_t \leq \overline{l} \qquad \forall t \in \mathcal{T}, \tag{D.1f}$$

$$-\overline{f^{dc}} \leq F_t^{dc} \leq \overline{f^{dc}} \qquad \forall t \in \mathcal{T}, \tag{D.1g}$$

$$\mathrm{m}_g^n G_t + \mathrm{m}_r^n (r_t - C_t) - \mathrm{m}_g^n D_t + A^{dc} \cdot F_t^{dc} - d_t = I_t \qquad \forall t \in \mathcal{T} \tag{D.1h}$$

$$\mathrm{m}_g^z G_t + \mathrm{m}_r^z (r_t - C_t) - \mathrm{m}_g^z D_t - m_d^z d_t = NP_t \qquad \forall t \in \mathcal{T} \tag{D.1i}$$

$$NP_{t,z} = \sum_{z' \in \mathcal{Z}} \mathrm{EX}_{t,z,z'} - \mathrm{EX}_{t,z',z} \qquad \forall t \in \mathcal{T}, \forall z \in \mathcal{Z} \tag{D.1j}$$

$$e^T I_t = 0 \qquad \forall t \in \mathcal{T} \tag{D.1k}$$

The objective function (D.1a) minimizes generation costs, given by a costs function $c(\cdot)$ and the vector of hourly generation levels G_t and curtailment C_t. Equations (D.1b) and (D.1c) provide bounds to generation and curtailment based on the installed capacity $\overline{g}$ and available capacity r_t.

Storages are modeled using a storage balance (D.1d) and bounds on storage charging (D.1e) and storage level (D.1f). Note, the storage balance requires parametrization of start- and end levels for feasibility. In the application in this study, weekly historic storage levels are used for this purpose.

Generation and load are balanced in nodal injections for each node in (D.1h) and zonal net-positions for each zones in (D.1i). The net-position can be expressed as the sum of bilateral exchanges for each zone as per (D.1j). The positive variable EX captures bilateral exchange but requires physical connection between zones, otherwise it is fixed to zero.

HVDC lines, as active network elements are always part of the economic dispatch problem. Flow on HVDC lines F^{dc} is bounds by line's capacity $\overline{f^{dc}}$ in (D.1g) and included in the nodal energy balance with an incidence matrix A^{dc} that maps flows to start- and end nodes.

The entire system is balanced with constraint (D.1k).

D.2.1 Network Constraints

As discussed in Section 6.3, problem (D.1) can be subject to transport constraints to model the different FBMC steps.

$$I_t \in \mathcal{F}^n \coloneqq \{x : \mathrm{PTDF}^n\, x \leq \overline{f}\} \qquad \forall t \in \mathcal{T}. \tag{D.2}$$

$$NP_t \in \mathcal{F}^z \coloneqq \{x : \mathrm{PTDF}_t^z\, x \leq RAM_t\} \qquad \forall t \in \mathcal{T}, \tag{D.3}$$

$$EX_t \in \mathcal{F}^{ntc} \coloneqq \{x : 0 \leq x \leq ntc\} \qquad \forall t \in \mathcal{T}. \tag{D.4}$$

Equation (D.2) defines the feasible region for nodal net-injections using the nodal PTDF matrix and line capacities $\overline{f}$. Equation (D.3) constrains the zonal net-positions with the flow-based parameters, as described in Section 6.2. Equation (D.4) defines bounds on bilateral commercial exchange.

D.2.2 Congestion management

Congestion management finds the least cost deviation from day-ahead generation schedule g_t^{da} and c_t^{da} that are the decisions on G_t and C_t from the previous market clearing stage while creating network feasibility as per (D.2).

$$C(G^{red}) = c^{red} \sum_{t \in \mathcal{T}} |G_t^{red}| \tag{D.5a}$$

$$G_t - g_t^{da} = G_t^{red} \qquad \forall t \in \mathcal{T} \tag{D.5b}$$

$$C_t \geq c^{da} \qquad \forall t \in \mathcal{T}, \tag{D.5c}$$

Equation (D.5a) captures the additional costs that occur for changing the day-ahead generation schedule. Constraints (D.5b) and (D.5c) bound the allowed deviation from day-ahead schedule for generation and curtailment.

The dispatch problem for congestion management is therefore:

$$\min \quad \text{(D.1a)} + \text{(D.5a)} \tag{D.6}$$

$$\text{s.t.} \ \text{(D.1b)} - \text{(D.1k)} \tag{D.7}$$

$$\text{(D.5b)} + \text{(D.5c)} \tag{D.8}$$

Bibliography

50Hertz, Amprion, APG, Creos, ČEPS, ELES, Elia, HOPS, MAVIR, PSE, RTE, SEPS, TenneT, Transelectrica, and TransnetBW. 2017. *Explanatory Note DA FB CC Methodology for Core CCR: For Public Consultation.* Technical Report.

50Hertz, Amprion, APG, Creos, Elia, Rte, TenneT, and TransnetBW. 2020. *Documentation of the CWE FB MC Solution - Version 5.0.* Technical Report.

ACER. 2011. *Framework Guidelines on Capacity Allocation and Congestion Management for Electricity.* Report FG-2011-E-002.

———. 2016. *Decision of the Agency for the Cooperation of Energy Regulators No 06/2016 of 17 November 2016: On the Electricity Transmission System Operators' Proposal for the Determination of Capacity Calculation Regions.*

ACER and CEER. 2018. *Annual Report on the Results of Monitoring the Internal Electricity and Natural Gas Markets in 2017 - Electricity Wholesale Markets Volume.* Report.

———. 2020. *Annual Report on the Results of Monitoring the Internal Electricity and Natural Gas Markets in 2019.* Report.

Aguado, M, R. Bourgeois, J. Bourmaud, J. Van Casteren, M. Ceratto, M. Jakel, B. Malfiet, C. Mestdag, P. Noury, M. Pool, W. Van Den Reek, M. Rohleder, P.H. Schavemaker, S. Scolari, O. Weis, and J. Wolpert. 2012. *Flow-Based Market Coupling in the Central Western European Region: On the Eve of Implementation.* C5-204. Cigré.

Alsac, Ongun, and Brian Stott. 1974. "Optimal Load Flow with Steady-State Security." *IEEE Transactions on Power Apparatus and Systems* PAS-93 (3): 745–751.

Amprion. 2019. *Amprion Market Report 2019 - Flow Based Market Coupling: Development of the Market and Grid Situation 2015-2018.* Report.

Amprion, APX, Belpex, Creos, Elia, EPEX Spot, RTE, TenneT, and TransnetBW. 2014. *Documentation of the CWE FB MC Solution: As Basis for the Formal Approval-Request.* Technical Report.

Amprion, APX-ENDEX, Belpex, Creos, Elia, EnBW, EPEX SPOT, RTE, and TenneT. 2011. *CWE Enhanced Flow-Based MC Feasibility Report.* Technical Report.

Antonopoulos, Georgios, Silvia Vitiello, Gianluca Fulli, and Marcelo Masera. 2020. *Nodal Pricing in the European Internal Electricity Market.* JRC Technica Reports JRC119977. European Commission, Joint Research Centre.

Aravena, Ignacio, Quentin Lété, Anthony Papavasiliou, and Yves Smeers. 2021. "Transmission Capacity Allocation in Zonal Electricity Markets." *Operations Research* 69 (4): 1240–1255.

Aravena, Ignacio, and Anthony Papavasiliou. 2016. "Renewable Energy Integration in Zonal Markets." *IEEE Transactions on Power Systems* 32 (2): 1334–1349.

Ardakani, Ali Jahanbani, and François Bouffard. 2013. "Identification of Umbrella Constraints in DC-based Security-Constrained Optimal Power Flow." *IEEE Transactions on Power Systems* 28 (4): 3924–3934.

———. 2018. "Prediction of Umbrella Constraints." In *2018 Power Systems Computation Conference,* 1–7.

Ardakani, Ali Jahanbani, and Francois Bouffard. 2015. "Acceleration of Umbrella Constraint Discovery in Generation Scheduling Problems." *IEEE Transactions on Power Systems* 30 (4): 2100–2109.

Bezanson, Jeff, Alan Edelman, Stefan Karpinski, and Viral B Shah. 2017. "Julia: A Fresh Approach to Numerical Computing." *SIAM Review* 59 (1): 65–98.

Bienstock, Daniel. 2015. *Electrical Transmission System Cascades and Vulnerability: An Operations Research Viewpoint.* Philadelphia, PA: SIAM.

Bienstock, Daniel, Michael Chertkov, and Sean Harnett. 2014. "Chance-Constrained Optimal Power Flow: Risk-Aware Network Control under Uncertainty." *SIAM Review* 56 (3): 461–495.

Birchfield, Adam B., Ti Xu, Kathleen M. Gegner, Komal S. Shetye, and Thomas J. Overbye. 2017. "Grid Structural Characteristics as Validation Criteria for Synthetic Networks." *IEEE Transactions on Power Systems* 32 (4): 3258–3265.

Bjørndal, Mette, and Kurt Jørnsten. 2001. "Zonal Pricing in a Deregulated Electricity Market." *The Energy Journal* 22 (1): 51–73.

Boisseleau, Francois. 2004. "The Role of Power Exchanges for the Creation of a Single European Electricity Market: Market Design and Market Regulation." PhD diss., TU Delft Technology, Policy and Management.

Bouffard, François, Francisco D Galiana, and José M Arroyo. 2005. "Umbrella Contingencies in Security-Constrained Optimal Power Flow." In *15th Power Systems Computation Conference.*

Boury, Jonas. 2015. "Methods for the Determination of Flow-Based Capacity Parameters: Description, Evaluation and Improvements." Master's thesis, KU Leuven.

Brandwajn, Vladimir. 1988. "Efficient Bounding Method for Linear Contingency Analysis." *IEEE Transactions on Power Systems* 3 (1): 38–43.

Brunekreeft, Gert, Karsten Neuhoff, and David Newbery. 2005. "Electricity Transmission: An Overview of the Current Debate." *Utilities Policy* 13 (2): 73–93.

Bundesnetzagentur. 2018. *Genehmigung des Szenariorahmens 2019-2030.*

Bundesnetzagentur and Bundeskartellamt. 2019. *Monitoring Report 2019.* Report.

Byers, Conleigh, and Gabriela Hug. 2020. "Modeling Flow-Based Market Coupling: Base Case, Redispatch, and Unit Commitment Matter." In *2020 17th International Conference on the European Energy Market,* 1–6.

Capitanescu, Florin, JL Martinez Ramos, Patrick Panciatici, Daniel S. Kirschen, A Marano Marcolini, Ludovic Platbrood, and Louis Wehenkel. 2011. "State-of-the-Art, Challenges, and Future Trends in Security Constrained Optimal Power Flow." *Electric Power Systems Research* 81 (8): 1731–1741.

Capitanescu, Florin, and Louis Wehenkel. 2008. "A New Iterative Approach to the Corrective Security-Constrained Optimal Power Flow Problem." *IEEE Transactions on Power Systems* 23 (4): 1533–1541.

Chakrabarti, Sambuddha, and Ross Baldick. 2020. "Look-Ahead SCOPF (LASCOPF) for Tracking Demand Variation via Auxiliary Proximal Message Passing (APMP) Algorithm." *International Journal of Electrical Power & Energy Systems* 116:105533.

Chakrabarti, Sambuddha, Matt Kraning, Eric Chu, Ross Baldick, and Stephen Boyd. 2014. "Security Constrained Optimal Power Flow via Proximal Message Passing." In *2014 Clemson University Power Systems Conference,* 1–8.

Christie, Richard D, Bruce F Wollenberg, and Ivar Wangensteen. 2000. "Transmission Management in the Deregulated Environment." *Proceedings of the IEEE* 88 (2): 170–195.

Christie, Richard D. 2019. *IEEE PES Power Grid Library - Optimal Power Flow.* Dataset v19.01. github.com/power-grid-lib/.

Clarkson, Kenneth L. 1994. "More Output-Sensitive Geometric Algorithms." In *Proceedings 35th Annual Symposium on Foundations of Computer Science,* 695–702.

Consentec. 2007. *Towards a Common Co-Ordinated Regional Congestion Management Method in Europe.* Report.

———. 2012. *Begleitstudie zur Optimierung der Methodik zur Bestimmung von Generation Shift Keys zur Modellierung des Einspeiseverhaltens von Erzeugungseinheiten im Übertragungsnetz.* Report.

Consentec and Frontier Economics. 2004. *Analysis of Cross-Border Congestion Management Methods for the EU Internal Electricity Market.* Report.

Consentec and Institute of Power Systems and Power Economics of Aachen University of Technology. 2001. *Analysis of Electricity Network Capacities and Identification of Congestion.* Report.

CREG. 2017. *Functioning and Design of the Central West European Day-Ahead Flow Based Market Coupling for Electricity: Impact of TSOs Discretionary Actions.* Study (F)1687.

Dantzig, George. 1963. *Linear Programming and Extensions.* RAND Corporation.

De Jonghe, C., L. Meeus, and R. Belmans. 2008. "Power Exchange Price Volatility Analysis after One Year of Trilateral Market Coupling." In *2008 5th International Conference on the European Electricity Market,* 1–6.

Dierstein, Constantin. 2017. "Impact of Generation Shift Key Determination on Flow Based Market Coupling." In *2017 14th International Conference on the European Energy Market,* 1–7.

Directorate General for Energy. 2019. *Clean Energy for All Europeans.* White Paper. European Commision.

Dowle, Matt, and Arun Srinivasan. 2017. *Data.Table: Extension of 'data.Frame'.* Software.

Dufour, Aurélie. 2007. "Capacity Allocation Using the Flow-Based Method." Master's thesis, KTH Electrical Engineering.

Dunning, Iain, Joey Huchette, and Miles Lubin. 2017. "JuMP: A Modeling Language for Mathematical Optimization." *SIAM Review* 59 (2): 295–320.

Dvorkin, Yury. 2020. "A Chance-Constrained Stochastic Electricity Market." *IEEE Transactions on Power Systems* 35 (4): 2993–3003.

Dvorkin, Yury, Pierre Henneaux, Daniel S. Kirschen, and Hrvoje Pandžić. 2016a. "Optimizing Primary Response in Preventive Security-Constrained Optimal Power Flow." *IEEE Systems Journal* 12 (1): 414–423.

Dvorkin, Yury, Miles Lubin, Scott Backhaus, and Michael Chertkov. 2016b. "Uncertainty Sets for Wind Power Generation." *IEEE Transactions on Power Systems* 31 (4): 3326–3327.

Ebner, Michael, Claudia Fiedler, Fabian Jetter, and Tobias Schmid. 2019. "Regionalized Potential Assessment of Variable Renewable Energy Sources in Europe." In *2019 16th International Conference on the European Energy Market,* 1–5.

Egerer, Jonas, Clemens Gerbaulet, Richard Ihlenburg, Friedrich Kunz, Benjamin Reinhard, Christian von Hirschhausen, Alexander Weber, and Jens Weibezahn. 2014. *Electricity Sector Data for Policy-Relevant Modeling: Data Documentation and Applications to the German and European Electricity Markets.* DIW Data Documentation 72. DIW Berlin.

Ehrenmann, Andreas, and Yves Smeers. 2005. "Inefficiencies in European Congestion Management Proposals." *Utilities Policy* 13 (2): 135–152.

Energinet, Svenska Kraftnät, Fingrid, and Statnett SF. 2014. *Methodology and Concepts for the Nordic Flow-Based Market Coupling Approach.* Technical Report.

ENTSO-E. 2018. *First Edition of the Bidding Zone Review – Final Report.* Report.

———. 2019. *Power Facts Europe 2019.* Report.

ENTSOG and ENTSO-E. 2020. *TYNDP 2020: Scenario Report.* Report.

ETSO. 2000. *Net Transfer Capacities (NTC) and Available Transfer Capacities (ATC) in the Internal Market of Electricity in Europe (IEM): Information for User.* Technical Report.

———. 2001a. *Co-Ordinated Auctioning: A Market-Based Method for Transmission Capacity Allocation in Meshed Networks.* Technical Report.

———. 2001b. *Co-Ordinated Use of Power Exchanges for Congestion Management.* Technical Report.

———. 2001c. *Procedures for Cross-Border Transmission Capacity Assessments.* Technical Report.

ETSO and EuroPEX. 2004. *Flow-Based Market Coupling: A Joint ETSO-EuroPEX Proposal for Cross-Border Congestion Management and Integration of Electricity Markets in Europe.* Technical Report.

European Commission. 1997. *Directive 96/92/EC Concerning Common Rules for the Internal Market in Electricity.*

———. 2009a. *Directive 2009/72/EC Concerning Common Rules for the Internal Market in Electricity.*

———. 2009b. *Regulation (EC) No 714/2009 on Conditions for Access to the Network for Cross-Border Exchanges in Electricity.*

———. 2015. *Commission Regulation (EU) 2015/1222: Establishing a Guideline on Capacity Allocation and Congestion Management.*

———. 2016. *Commission Staff Working Document: Impact Assesment. Proposal for a Directive of the European Parliament and of the Council on Common Rules for the Internal Market in Electricity (Recast).* Working Document.

———. 2018. *Commission Staff Working Document: On the Development of Single Day-Ahead and Intraday Coupling in the Member States and the Development of Competition between NEMOs in Accordance with Article 5(3) of Commission Regulation 2015/1222 (CACM).* Working Document.

———. 2019a. *Commission Regulation (EU) 2019/943 on the Internal Market for Electricity.*

———. 2019b. *Directive (EU) 2019/944 on Common Rules for the Internal Market for Electricity.*

European Parliament. 2020. *Internal Energy Market.* Fact Sheets on the European Union.

European Parliamentary Research Service. 2019. *Briefing: EU Legislation Process: Internal Market for Electricity.* Briefing. European Commission.

Felice, Matteo De, Giuseppe Peronato, and Konstantinos Kavvadias. 2021. *JRC Hydropower Database.* Dataset Release v8.

Felling, Tim, Björn Felten, Paul Osinski, and Christoph Weber. 2019. *Flow-Based Market Coupling Revised - Part II: Assessing Improved Price Zones in Central Western Europe.* HEMF Working Paper No. 07/2019. University of Duisburg-Essen, House of Energy Markets & Finance.

Felten, Björn, Tim Felling, Paul Osinski, and Christoph Weber. 2019. *Flow-Based Market Coupling Revised - Part I: Analyses of Small- and Large-Scale Systems.* HEMF Working Paper 06/2019. Essen: University of Duisburg-Essen, House of Energy Markets & Finance.

Felten, Björn, Paul Osinski, Tim Felling, and Christoph Weber. 2021. "The Flow-Based Market Coupling Domain - Why We Can't Get It Right." *Utilities Policy* 70:101136.

Finck, Rafael, Armin Ardone, and Wolf Fichtner. 2018. "Impact of Flow-Based Market Coupling on Generator Dispatch in CEE Region." In *2018 15th International Conference on the European Energy Market,* 1–5.

Fliscounakis, Stéphane, Patrick Panciatici, Florin Capitanescu, and Louis Wehenkel. 2013. "Contingency Ranking with Respect to Overloads in Very Large Power Systems Taking into Account Uncertainty, Preventive, and Corrective Actions." *IEEE Transactions on Power Systems* 28 (4): 4909–4917.

Fuchs, Alexander, Marc Scherer, and Göran Andersson. 2015. *Polyhedral Computation Based Transfer Capacities in Multi-Area Power Systems.* ArXiv preprint 1511.00435.

Fukuda, Komei. 2016. *Lecture: Polyhedral Computation, Spring 2016.* Institute for Operations Research and Institute of Theoretical Computer Science, ETH Zürich.

Gebrekiros, Yonas, Gerard Doorman, Traian Preda, and Arild Helseth. 2015. "Assessment of PTDF Based Power System Aggregation Schemes." In *2015 IEEE Electrical Power and Energy Conference,* 358–363.

Glachant, Jean-Michel. 2010. *The Achievement of the EU Electricity Internal Market through Market Coupling.* EUI Working Papers RSCAS 2010/87. Florence School of Regulation.

Glachant, Jean-Michel, and François Lévêque. 2006. *Electricity Internal Market in the European Union: What to Do Next?* Cambridge Working Papers in Economics CWPE 0623 and EPRG 0605. University of Paris-Sud and Ecole des Mines de Paris.

Göke, Leonard. 2021. "A Graph-Based Formulation for Modeling Macro-Energy Systems." *Applied Energy* 301:117377.

Göke, Leonard, Mario Kendziorski, Claudia Kemfert, and Christian von Hirschhausen. 2021. *Accounting for Spatiality of Renewables and Storage in Transmission Planning.* ArXiv preprint 2108.04863.

Gurobi Optimization LLC. 2018. *Gurobi Optimizer Reference Manual.* Documentation.

Hainsch, Karlo, Hanna Brauers, Thorsten Burandt, Leonard Göke, Christian von Hirschhausen, Claudia Kemfert, Mario Kendziorski, Konstantin Löffler, Pao-Yu Oei, Fabian Präger, and Ben Wealer. 2020. *Make the European Green Deal Real: Combining Climate Neutrality and Economic Recovery.* Politikberatung kompakt 153. DIW Berlin.

Halilbašić, Lejla, Florian Thams, Andreas Venzke, Spyros Chatzivasileiadis, and Pierre Pinson. 2018. "Data-Driven Security-Constrained AC-OPF for Operations and Markets." In *2018 Power Systems Computation Conference,* 1–7.

Hauschild, Richard. 2019. "Flow-Based Market Coupling – Terms and Methodologies: Determination of the Base Case Using a Grid and Market Model." Master's thesis, Technische Universität Berlin.

Hirth, Lion, Ingmar Schlecht, and Jonathan Mühlenpfordt. 2018. *Open Data for Electricity Modeling: Report on Behalf of the Federal Ministry for Economic Affairs and Energy.* White Paper. German Federal Ministry of Economic Affairs and Energy.

Hofmann, Fabian, Johannes Hampp, Fabian Neumann, Tom Brown, and Jonas Hörsch. 2021. "Atlite: A Lightweight Python Package for Calculating Renewable Power Potentials and Time Series." *Journal of Open Source Software* 6 (62): 3294.

Hörsch, Jonas, Henrik Ronellenfitsch, Dirk Witthaut, and Tom Brown. 2018. "Linear Optimal Power Flow Using Cycle Flows." *Electric Power Systems Research* 158:126–135.

Hua, Bowen, Zhaohong Bie, Cong Liu, Gengfeng Li, and Xifan Wang. 2013. "Eliminating Redundant Line Flow Constraints in Composite System Reliability Evaluation." *IEEE Transactions on Power Systems* 28 (3): 3490–3498.

Jegleim, Birgit. 2015. "Flow Based Market Coupling." Master's thesis, Norwegian University of Science and Technology.

Jiachun, Guo, Fu Yong, Li Zuyi, and M. Shahidehpour. 2009. "Direct Calculation of Line Outage Distribution Factors." *IEEE Transactions on Power Systems* 24 (3): 1633–1634.

Joint Allocation Office. 2017. *CWE Market Coupling - Publication Handbook.* JAO.

———. 2019. *Joint Allocation Office, Utility Tool.*

Karangelos, Efthymios, and Louis Wehenkel. 2019. "An Iterative AC-SCOPF Approach Managing the Contingency and Corrective Control Failure Uncertainties with a Probabilistic Guarantee." *IEEE Transactions on Power Systems* 34 (5): 3780–3790.

Kendziorski, Mario, Leonard Göke, Claudia Kemfert, Christian von Hirschhausen, Elmar Zozmann, Fabian Präger, Citlali Rodriguez, Christoph Weyhing, and Johanna Winkler. 2021. *100% erneuerbare Energie für Deutschland unter besonderer Berücksichtigung von Dezentralität und räumlicher Verbrauchsnähe Potenziale, Szenarien und Auswirkungen auf Netzinfrastrukturen.* Politikberatung kompakt 167. DIW Berlin.

Kirschen, Daniel S., and Goran Strbac. 2004. *Fundamentals of Power System Economics.* Chichester, West Sussex, England ; Hoboken, NJ: John Wiley & Sons.

Klaar, Dennis, and Patrick Panciatici. 2004. *Collaboration between European Transmission System Operators for Day Ahead Congestion Forecast.* C2-306. Cigré.

Kunz, Friedrich, Mario Kendziorski, Wolf-Peter Schill, Jens Weibezahn, Jan Zepter, Christian von Hirschhausen, Philipp Hauser, Matthias Zech, Dominik Möst, Sina Heidari, Jörg Felten, and Christoph Weber. 2017. *Electricity, Heat and Gas Sector Data for Modelling the German System.* Data Documentation 92. DIW Berlin.

Lang, Lukas Maximilian, Bettina Dallinger, and Georg Lettner. 2020. "The Meaning of Flow-Based Market Coupling on Redispatch Measures in Austria." *Energy Policy* 136:111061.

Lehner, Bernhard, and Günther Grill. 2013. "Global River Hydrography and Network Routing: Baseline Data and New Approaches to Study the World's Large River Systems." *Hydrological Processes* 27 (15): 2171–2186.

Leuthold, Florian U., Hannes Weigt, and Christian von Hirschhausen. 2008. *ELMOD - A Model of the European Electricity Market.* Munich Personal RePEc Archive MPRA Paper No. 65660.

———. 2012. "A Large-Scale Spatial Optimization Model of the European Electricity Market." *Networks and Spatial Economics* 12 (1): 75–107.

Li, Yuan, and James D McCalley. 2008. "Decomposed SCOPF for Improving Efficiency." *IEEE Transactions on Power Systems* 24 (1): 494–495.

Liu, Hailiang, Gorm Bruun Andresen, Tom Brown, and Martin Greiner. 2019. "A High-Resolution Hydro Power Time-Series Model for Energy Systems Analysis: Validated with Chinese Hydro Reservoirs." *MethodsX* 6:1370–1378.

Logarithmo and E-Bridge. 2017. *CWE Flow Factor Competition Study Part III: Fairness Assessment.* Report.

Luenberger, David G., and Yinyu Ye. 2008. *Linear and Nonlinear Programming.* 3rd ed. International Series in Operations Research and Management Science. New York, NY: Springer.

Madani, Ramtin, Javad Lavaei, and Ross Baldick. 2016. "Constraint Screening for Security Analysis of Power Networks." *IEEE Transactions on Power Systems* 32 (3): 1828–1838.

Marien, Alain, Patrick Luickx, Andreas Tirez, and Dominique Woitrin. 2013. "Importance of Design Parameters on Flowbased Market Coupling Implementation." In *10th International Conference on the European Energy Market,* 1–8.

Marjanovic, I., D. vom Stein, N. van Bracht, and A. Moser. 2018. "Impact of an Enlargement of the Flow Based Region in Continental Europe." In *2018 15th International Conference on the European Energy Market,* 1–5.

Matthes, Bjorn, Christopher Spieker, Dennis Klein, and Christian Rehtanz. 2019. "Impact of a Minimum Remaining Available Margin Adjustment in Flow-Based Market Coupling." In *2019 IEEE Milan PowerTech,* 1–6.

Matthes, Bjorn, Christopher Spieker, and Christian Rehtanz. 2017. "Flow-Based Parameter Determination in Large-Scale Electric Power Transmission Systems." In *2017 IEEE Manchester PowerTech,* 1–6.

Meeus, L., L. Vandezande, S. Cole, and R. Belmans. 2009. "Market Coupling and the Importance of Price Coordination between Power Exchanges." *Energy* 34 (3): 228–234.

Meeus, Leonardo, and Ronnie Belmans. 2008. "Electricity Market Integration in Europe." In *16th Power Systems Computation Conference 2008,* 1505.

Meeus, Leonardo, Konrad Purchala, and Ronnie Belmans. 2005. "Development of the Internal Electricity Market in Europe." *The Electricity Journal* 18 (6): 25–35.

Mieth, Robert. 2021. "Risk-Aware Control, Dispatch and Coordination in Sustainable Power Systems." PhD diss., Technische Universität Berlin.

Mieth, Robert, Jip Kim, and Yury Dvorkin. 2020. "Risk- and Variance-Aware Electricity Pricing." *Electric Power Systems Research* 189:106804.

Mieth, Robert, Richard Weinhold, Clemens Gerbaulet, Christian von Hirschhausen, and Claudia Kemfert. 2015. "Electricity Grids and Climate Targets: New Approaches to Grid Planning." *DIW Economic Bulletin* 5 (6): 75–80.

Morin, Thomas. 2016. "Statistical Study and Clustering of Thecritical Branches Defining the Marketcoupling in the Central West Europezone." Master's thesis, KTH Royal Institute of Technology.

MOSEK ApS. 2021. *MOSEK Modeling Cookbook.* Documentation Release 3.2.3.

Neuhoff, Karsten, Julian Barquin, Janusz W. Bialek, Rodney Boyd, Chris J. Dent, Francisco Echavarren, Thilo Grau, Christian von Hirschhausen, Benjamin F. Hobbs, Friedrich Kunz, Christian Nabe, Georgios Papaefthymiou, Christoph Weber, and Hannes Weigt. 2013. "Renewable Electric Energy Integration: Quantifying the Value of Design of Markets for International Transmission Capacity." *Energy Economics* 40:760–772.

Neuhoff, Karsten, Benjamin F. Hobbs, and David Newbery. 2011. *Congestion Management in European Power Networks: Criteria to Assess the Available Options,* Discussion Papers 1161. DIW Berlin.

Overbye, Thomas J, Xu Cheng, and Yan Sun. 2004. "A Comparison of the AC and DC Power Flow Models for LMP Calculations." In *Proceedings of the 37th Hawaii International Conference on System Sciences,* 1–9. IEEE.

Pena, Ivonne, Carlo Brancucci Martinez-Anido, and Bri-Mathias Hodge. 2017. "An Extended IEEE 118-Bus Test System with High Renewable Penetration." *IEEE Transactions on Power Systems* 33 (1): 281–289.

Phan, Dzung, and Jayant Kalagnanam. 2013. "Some Efficient Optimization Methods for Solving the Security-Constrained Optimal Power Flow Problem." *IEEE Transactions on Power Systems* 29 (2): 863–872.

Pineda, S., J. M. Morales, and A. Jimenez-Cordero. 2020. "Data-Driven Screening of Network Constraints for Unit Commitment." *IEEE Transactions on Power Systems* 35 (5): 1–1.

Plancke, Glenn, Kristof De Vos, Cedric De Jonghe, and Ronnie Belmans. 2016. "Efficient Use of Transmission Capacity for Cross-Border Trading: Available Transfer Capacity versus Flow-Based Approach." In *2016 IEEE International Energy Conference,* 1–5.

Poplavskaya, Ksenia, Gerhard Totschnig, Fabian Leimgruber, Gerard Doorman, Gilles Etienne, and Laurens de Vries. 2020. "Integration of Day-Ahead Market and Redispatch to Increase Cross-Border Exchanges in the European Electricity Market." *Applied Energy* 278:115669.

R Core Team. 2018. *R: A Language and Environment for Statistical Computing.* Vienna, Austria: R Foundation for Statistical Computing.

Rangoni, Bernardo. 2016. "Uncertainty and Experimentalist Policymaking in Internal Market Regulation by the European Commission: Cases on Electricity and Gas Policy." PhD diss., London School of Economics.

Roald, Line, Frauke Oldewurtel, Bart Van Parys, and Göran Andersson. 2015. *Security Constrained Optimal Power Flow with Distributionally Robust Chance Constraints.* ArXiv preprint 1508.06061.

Roald, Line A., and Daniel K. Molzahn. 2019. "Implied Constraint Satisfaction in Power System Optimization: The Impacts of Load Variations." In *2019 57th Annual Allerton Conference on Communication, Control, and Computing,* 308–315.

Rte, Amprion, Creos, Elia, TenneT, and TransnetBW. 2015. *CWE Flow Based Market Coupling Project: Parallel Run Performance Report.* Technical Report.

Schavemaker, Pieter, A. Croes, R. Otmani, Jean-Yves Bourmaud, U. Zimmermann, J. Wolpert, F. Reyer, O. Weis, and C. Druet. 2008. *Flow-Based Allocation in the Central Western European Region.* C5-307. Cigré.

Schlecht, Ingmar. 2018. *OPSD Data Package: Renewable Power Plants.* Dataset Version: 2018-03-08.

Schönheit, David. 2019. "An Improved Statistical Approach to Generation Shift Keys: Lessons Learned from an Analysis of the Austrian Control Zone." *Zeitschrift für Energiewirtschaft* 43 (3): 193–212.

Schönheit, David, Kenneth Bruninx, Michiel Kenis, and Dominik Möst. 2021a. *Improved Selection of Critical Network Elements for Flow-Based Market Coupling Based on Congestion Patterns.* ZBW – Leibniz Information Centre for Economics.

Schönheit, David, Constantin Dierstein, and Dominik Möst. 2021. "Do Minimum Trading Capacities for the Cross-Zonal Exchange of Electricity Lead to Welfare Losses?" *Energy Policy* 149:112030.

Schönheit, David, Dirk Hladik, Hannes Hobbie, and Dominik Möst. 2020a. *ELMOD Documentation: Modeling of Flow-Based Market Coupling and Congestion Management.* Working paper of the Chair of Energy Economics. TU Dresden.

Schönheit, David, Michiel Kenis, Lisa Lorenz, Dominik Möst, Erik Delarue, and Kenneth Bruninx. 2021b. "Toward a Fundamental Understanding of Flow-Based Market Coupling for Cross-Border Electricity Trading." *Advances in Applied Energy* 2:100027.

Schönheit, David, Michiel Kenis, Lisa Lorenz, Dominik Möst, Erik Delarue, and Kenneth Brunix. 2020b. *Toward Understanding Flow-Based Market Coupling: An Open-Access Model.* Energy Systems Integration & Modeling Group Working Paper Series No. ESIM2020-23. KU Leuven.

Schönheit, David, and Roman Sikora. 2018. "A Statistical Approach to Generation Shift Keys." In *2018 15th International Conference on the European Energy Market,* 1–6.

Schönheit, David, Richard Weinhold, and Constantin Dierstein. 2020. "The Impact of Different Strategies for Generation Shift Keys (GSKs) on the Flow-Based Market Coupling Domain: A Model-Based Analysis of Central Western Europe." *Applied Energy* 258:114067.

Schröder, Andreas, Friedrich Kunz, Jan Meiß, R. Mendelevitch, and Christian von Hirschhausen. 2013. *Current and Prospective Costs of Electricity Generation until 2050.* DIW Data Documentation 68. DIW Berlin.

Spieker, Christopher, Dennis Klein, Volker Liebenau, Jan Teuwsen, and Christian Rehtanz. 2016. "European Electricity Market and Network Simulation for Energy System Analysis." In *2016 IEEE International Energy Conference,* 1–6.

Stott, Brian, and Eric Hobson. 1978. "Power System Security Control Calculations Using Linear Programming, Part I & II." *IEEE Transactions on Power Apparatus and Systems* PAS-97 (5): 1713–1720.

Svarstad, Vegard Bremerthun. 2016. "Flow Based Market Clearing - GSK Strategies." Master's thesis, Norwegian University of Science and Technology.

Szedlak, May. 2017. "Redundancy in Linear Systems: Combinatorics, Algorithms and Analysis." PhD diss., ETH Zürich.

Tennet. 2015. *Determining Securely Available Cross-Border Transmission Capacity within Flow-based.* Technical Report.

Thams, Florian, Spyros Chatzivasileiadis, Pierre Pinson, and Robert Eriksson. 2017. "Data-Driven Security-Constrained Opf." In *10th Bulk Power Systems Dynamics and Control Symposium.*

Van den Bergh, Kenneth, Jonas Boury, and Erik Delarue. 2016. "The Flow-Based Market Coupling in Central Western Europe: Concepts and Definitions." *The Electricity Journal* 29 (1): 24–29.

Van den Bergh, Kenneth, and Erik Delarue. 2016. "An Improved Method to Calculate Injection Shift Keys." *Electric Power Systems Research* 134:197–204.

Van den Bergh, Kenneth, Erik Delarue, and William D'haeseleer. 2014. *DC Power Flow in Unit Commitment Models.* TME Working Paper - Energy and Environment WP EN2014-12. KU Leuven.

Van Hertem, D. 2006. "Usefulness of DC Power Flow for Active Power Flow Analysis with Flow Controlling Devices." In *8th IEE International Conference on AC and DC Power Transmission,* 2006:58–62.

Van Stiphout, Femia. 2016. "Approximating the Flow-Based Transport Capacity Constraints for the Day-Ahead Power Market." Master's thesis, University of Twente.

Vattenfall Europe Transmission GmbH. 2009. *Das lastflussbasierte Modell zur Berechnung von Übertragungskapazitäten in der CEE-Region.* Technical Report.

Velloso, Alexandre, Pascal Van Hentenryck, and Emma S Johnson. 2019. *An Exact and Scalable Problem Decomposition for Security-Constrained Optimal Power Flow.* ArXiv preprint 1910.03685.

Ventosa, Mariano, Álvaro Baìllo, Andrés Ramos, and Michel Rivier. 2005. "Electricity Market Modeling Trends." *Energy Policy* 33 (7): 897–913.

Voswinkel, Simon, Björn Felten, Tim Felling, and Christoph Weber. 2019. *Flow-Based Market Coupling – What Drives Welfare in Europe's Electricity Market Design?* HEMF Working Paper No. 08/2019. University of Duisburg-Essen, House of Energy Markets & Finance.

Weber, Alexander, Dietmar Graeber, and Andreas Semmig. 2010. "Market Coupling and the CWE Project." *Zeitschrift für Energiewirtschaft* 34 (4): 303–309.

Weibezahn, Jens, and Mario Kendziorski. 2019. "Illustrating the Benefits of Openness: A Large-Scale Spatial Economic Dispatch Model Using the Julia Language." *Energies* 12 (6): 1153.

Weibezahn, Jens, Richard Weinhold, Clemens Gerbaulet, and Friedrich Kunz. 2018. *OPSD Data Package: Conventional Power Plants.* Dataset Version: 2018-12-20.

Weigt, Hannes. 2009. "A Review of Liberalization and Modeling of Electricity Markets." *SSRN Electronic Journal.*

Weinhold, Richard. 2020a. "Pomato - Documentation." pomato.readthedocs.io/.

———. 2020b. "Pomato - GitHub Repository." github.com/richard-weinhold/pomato.

———. 2021. "PomatoData - GitHub Repository." github.com/richard-weinhold/PomatoData.

Weinhold, Richard, and Robert Mieth. 2020a. "Fast Security-Constrained Optimal Power Flow Through Low-Impact and Redundancy Screening." *IEEE Transactions on Power Systems* 35 (6): 4574–4584.

———. 2020b. *Power Market Tool (POMATO) for the Analysis of Zonal Electricity Markets.* ArXiv preprint 2011.11594v1.

———. 2021. "Power Market Tool (POMATO) for the Analysis of Zonal Electricity Markets." *SoftwareX* 16:100870.

Wickham, Hadley. 2009. *Ggplot2: Elegant Graphics for Data Analysis.* Springer-Verlag New York.

———. 2011. "The Split-Apply-Combine Strategy for Data Analysis." *Journal of Statistical Software* 40 (1): 1–29.

Wiegmans, Bart. 2016. *Gridkit Extract Of Entso-E Interactive Map.* Dataset. Zenodo.

Wood, Allen J, and Bruce F Wollenberg. 1996. *Power Generation, Operation, and Control.* John Wiley & Sons.

Wyrwoll, Lothar, Andreas Blank, Christoph Müller, and Ralf Puffer. 2019. "Determination of Preloading of Transmission Lines for Flow-Based Market Coupling." In *2019 16th International Conference on the European Energy Market,* 1–6.

Wyrwoll, Lothar, Katharina Kollenda, Christoph Müller, and Armin Schnettler. 2018. "Impact of Flow-Based Market Coupling Parameters on European Electricity Markets." In *53rd International Universities Power Engineering Conference,* 1–6.

Zad, Bashir Bakhshideh, Jean-François Toubeau, Behzad Vatandoust, Kenneth Bruninx, Zacharie De Grève, and François Vallée. 2021. "Enhanced Integration of Flow-Based Market Coupling in Short-Term Adequacy Assessment." *Electric Power Systems Research* 201:107507.

Zhai, Qiaozhu, Xiaohong Guan, Jinghui Cheng, and Hongyu Wu. 2010. "Fast Identification of Inactive Security Constraints in SCUC Problems." *IEEE Transactions on Power Systems* 25 (4): 1946–1954.

Zhang, Shubo, Hongxing Ye, Fengyu Wang, Yonghong Chen, Stephen Rose, and Yaming Ma. 2019. "A Data-aided Security Constraint Prescreening Technique and Application to Real-world System." In *2019 North American Power Symposium,* 1–6.

Zimmerman, Ray Daniel, Carlos Edmundo Murillo-Sánchez, and Robert John Thomas. 2011. "MATPOWER: Steady-State Operations, Planning, and Analysis Tools for Power Systems Research and Education." *IEEE Transactions on Power Systems* 26 (1): 12–19.